TRANSPORTATION RESEARCH RECORD 684

Tunneling and Underground Structures

TRANSPORTATION RESEARCH BOARD

COMMISSION ON SOCIOTECHNICAL SYSTEMS
NATIONAL RESEARCH COUNCIL

NATIONAL ACADEMY OF SCIENCES
WASHINGTON, D.C. 1978

Transportation Research Record 684
Price $3.00

modes
1 highway transportation
3 rail transportation

subject areas
21 facilities design
25 structures design and performance
33 construction
63 soil and rock mechanics

Transportation Research Board publications are available by ordering directly from the board. They may also be obtained on a regular basis through organizational or individual supporting membership in the board; members or library subscribers are eligible for substantial discounts. For further information, write to the Transportation Research Board, National Academy of Sciences, 2101 Constitution Avenue, N.W., Washington, DC 20418.

Library of Congress Cataloging in Publication Data
National Research Council. Transportation Research Board.
Tunneling and underground structures.

(Transportation research record; 684)
Includes bibliographical references. 1. Tunneling–Congresses. 2. Underground construction–Congresses. I. Title. II. Series.
TE7.H5 no. 684 [TA800] 380.5'08s [624'.19] 79-15352
ISBN 0-309-02829-9

Sponsorship of the Papers in This Transportation Research Record

GROUP 2–DESIGN AND CONSTRUCTION OF TRANSPORTATION FACILITIES
Eldon J. Yoder, Purdue University, chairman

Structures Section
Ivan M. Viest, Bethlehem Steel Corporation, chairman

Committee on Design of Underground Transportation Structures
Don A. Linger, Federal Highway Administration, chairman
Robert B. Begin, O. H. Bentzen, James Birkmyer, Gilbert L. Butler, G. Wayne Clough, R. Kenneth Dodds, Philip Egilsrud, Eugene L. Foster, W. W. Hakala, Delon Hampton, A. J. Hendron, Jr., Frank P. Hurka, Jerome S. B. Iffland, J. Donovan Jacobs, Robert S. Mayo, Russell K. McFarland, Phillip R. Mcollough, Ikuo Nagai, Forrest H. Stairs, Jr., Donald N. Tanner, Samuel Taradash, James D. Washington

Construction Section
David S. Gedney, Federal Highway Administration, chairman

Committee on Tunnel Construction
Ellis L. Armstrong, Armstrong Associates, chairman
Vinton W. Bacon, J. Barry Cooke, Edward J. Cording, Frank E. Dalton, Edward D. Graf, J. Donovan Jacobs, Robert G. Lenz, William C. Maurer, Robert S. Mayo, Phillip R. Mcollough, Norman A. Nadel, E. Donald Phinney, Pierrepont E. Sperry, Victor L. Stevens, Roger B. Stevenson, Samuel Taradash, Lyman D. Wilbur

Lawrence F. Spaine and William G. Gunderman, Transportation Research Board staff

The organizational units and officers and members are as of December 31, 1977.

Contents

Analysis of Nationwide Demand for Urban Transportation Tunnels

M. G. Myers and R. K. Wood, Logistics Management Institute, Washington, D.C.
L. B. Blattenberger, Congressional Budget Office
Armando M. Lago, Ecosometrics, Inc., Bethesda, Maryland

For the purpose of determining estimates of the amount of transportation-related tunneling activity likely to occur to 1990, a methodology was devised whereby the conditions necessary to justify the application of tunnel segments for mass transit facilities were identified and matched against the number of situations in which these conditions are likely to be fulfilled. A corollary outcome of the analysis is an appraisal of factors that affect the preference of one type of mass transit system over others and an understanding of the sensitivity of preferred system choice to these factors. A technical evaluation of supply and demand for alternative types of mass transit systems was conducted to determine the future viability of such systems for cities that do not have them. Results of city-by-city application of the methodology developed revealed that, with current construction costs and property values, three cities currently without mass transit systems—Detroit, Cincinnati, and Denver—would meet necessary conditions for tunneled systems by 1990. At the other extreme, tunnel distance was computed for conditions in which tunnel construction costs in real terms were postulated to fall to 40 percent of today's cost and right-of-way values to rise by 5 percent/year. Other sensitivity results for the preference of tunnels to new right-of-way and for the forecast of nationwide tunnel construction under other assumptions are also reported.

A tunnel is used by transportation planners as a device to bypass obstacles that obstruct or otherwise make more costly the movement of freight and passengers. Justifying the use of this expensive technique to solve transportation problems involves consideration of the direct and indirect benefits and costs unique to the particular obstacle to be bypassed. The intent of this paper is to summarize a research methodology (1) to identify the underlying economic, demographic, and technological forces that jointly influence the decision to tunnel in urban areas and to present estimates of the likely extent of tunneling in the future based on this methodology. Emphasis is placed on tunnels used in conjunction with urban mass transit systems where the major obstacles to be bypassed are centers of high-density activity and where right-of-way costs and system capacity requirements and costs may call for tunneling as a solution.

The following procedure was used in the study:

1. Develop an analytical framework to indicate conditions in terms of ridership, cost for new rights-of-way, facility costs, operating characteristics, and social costs where alternative bus or rail modes with surface and subsurface guideways are preferred.
2. Develop estimates for future values of these variables, and identify the location and extent of justifiable urban transit systems (both bus and rail) with tunnel segments.
3. Base forecasts of future tunneling on alternative assumptions of urban growth for estimates of ridership, cost of new tunnel construction, and cost of new right-of-way for future at-grade systems.

First, ridership forecasts made at various census boundaries emanating from the central city for each of the 35 largest U.S. standard metropolitan statistical areas (SMSAs) are presented. Transit ridership is explained in terms of residential and employment distribution by using statistical regression techniques. The supply side of the analysis is next concerned with establishing, through parametric costing techniques, the conditions by which bus or rail transit is preferred to alternative surface and subsurface guideway options. Finally, the results of the analysis of transit demand and supply are merged with forecasts of urban population growth, construction costs, and costs for new right-of-way to provide a nationwide forecast of warranted system distance for tunneled segments. These results are useful (a) in assisting designers and planners in establishing criteria for system specification under existing and future conditions and (b) in framing the impacts that may result from federal policies toward urban growth patterns and research and development expenditures to alter or reduce costs for new tunnel construction.

FORECASTS OF URBAN TRANSIT RIDERSHIP

Paramount among the factors that influence the choice of preferred urban transit systems is the prospective level of ridership. The level, geographic dispersion, and time distribution of demand must be known to dimension system capacity, which in turn is the basis for costing system capital and operating expenses for each alternative considered. The methodology for demand forecasting is designed to produce estimates of peak-hour, primary-direction transit ridership at each of four geographic boundaries. The estimation procedure is evaluated under two alternative assumptions for the distribution of urban growth: (a) that historic population trends for the central city and the suburbs will continue and (b) that current population distribution will prevail in the future.

The procedure for demand estimation, shown in Figure 1, consists of two components: the determination of daily primary-direction work trips at three outer cordons and the determination of total peak-hour flows at the central business district (CBD) cordon. In the first instance, daily primary-direction work trips are converted into total peak-hour trips and, for both components, total primary-direction, peak-hour trips are converted first into corridor-specific flows and then into transit ridership. The need for separate treatment of CBD traffic flows and flows at other boundaries reflects the unique nature of the CBD as the geographic center of an urban area and the consequent use of the CBD as a conduit for traffic that neither originates nor terminates in the CBD.

Daily work trips crossing the three outer cordons in 1970 (corresponding to the concentric census boundaries called rural and scattered urban, urbanized area, and central city except CBD) can be derived from a recent publication of the U.S. Department of Transportation (2). This publication presents for each of the 35 largest SMSAs 1970 census data for the journey to work in the format of an origin-destination table in which trip origins and terminations correspond to the five concentric census rings. From this data source, primary-direction radial work trips at the other three cordons can easily be found by summing at each outer cordon boundary the number of trips that originate outside the boundary and

Figure 1. Procedure for demand estimation.

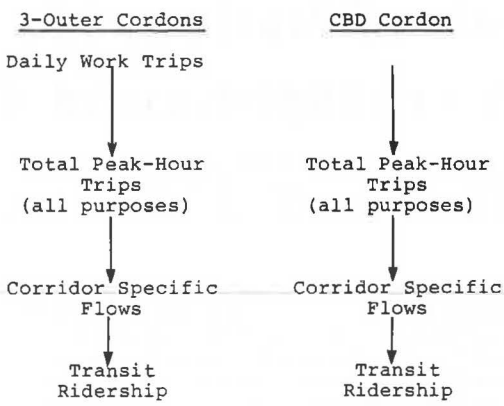

terminate in an inner census ring. A conversion process to translate daily primary-direction radial work trips to peak-hour trips for all purposes was then developed by using two average factors: peak-hour trips as a percentage of total daily work trips (factor 1) and peak-hour work trips as a percentage of total peak-hour trips (factor 2). These adjustment factors, applied to daily work-trip flows, provide peak-hour trips for all purposes. These two factors, which cover a total of six cities, are (a) factor 1, 21.87 percent (standard deviation 2.77); and (b) factor 2, 73.35 percent (standard deviation 3.48) (3, 4).

For the critical CBD cordon, a more involved procedure was used since it is well known that a significant fraction of CBD traffic neither originates nor terminates in the CBD. Meyer, Kain, and Wohl (5) cite pre-1960 data for a small sample of cities that suggest that from 30 to 70 percent of CBD traffic is of this nature. A statistical procedure was developed to provide a relation for estimating total peak-hour CBD cordon crossings based on the total number of work-trip terminations in the CBD, the number of intraring work trips in rings adjacent to the CBD, and the distance of these intraring trips.

Data for peak-hour CBD cordon crossings were assembled for 19 out of the 35 largest SMSAs together with values for the city-specific explanatory variables listed above. In many instances, data for CBD cordon crossings were for other than census years; interpolation was thus required to provide consistent data observations.

Regression equations were computed in linear and log-linear form by using the following as explanatory variables: CBD workers, intraring work trips in rings adjacent to the CBD starting with the nearest adjacent ring and adding more distant rings, and the radial distance from midpoint to midpoint of the adjacent rings. The theory being tested was that traffic across the CBD was explained by both CBD attraction and through-trip generation and that the greater intraring traffic is and the shorter the distance represented by radial trips through the CBD is, the more CBD trips occur.

Preliminary results that used CBD workers as the single explanatory variable indicated that the inclusion of New York City in the data set was unduly affecting the results (New York City had a peak-hour flow nearly as large as the combined values of 15 out of 19 remaining cities) and, consequently, this data point was dropped from further regressions. Furthermore, these preliminary results indicated that CBD workers explain a large fraction of the variability of peak-hour CBD cordon crossings; the dependent variable appeared to be elastic with respect to CBD workers. Larger cities show a higher elasticity, which indicates that peak-hour traffic increases more than proportionally to the number of CBD workers as the city becomes larger and probably reflects a greater proportion of white-collar employment. A final statistical check was used to test whether the error term was systematically increasing with increasing values of the dependent variable since large variability of the independent variables is present in the sample. A ratio test that compared the sum of squared residuals for separate regressions fit to large and small values of the dependent variables revealed the presence of heteroscedasticity for the linear specification but not for the log-linear formulation. Consequently, a log-linear specification was selected.

Regressions that use first intraring trips and radial distance for the closest ring adjacent to the CBD and then the next adjacent ring were then computed. Only trips within the closest adjacent ring (central city) proved to be statistically significant, so the process was stopped at this point. The regression results, which consider first CBD workers and then add the closest intraring and corresponding radial distances, are given below (t-statistics in parentheses):

$$\log(Y) = \underset{}{-0.187} + \underset{(6.89)}{1.044}\log(X_1) \qquad R^2 = 0.736 \tag{1}$$

$$\log(Y) = \underset{}{-0.135} + \underset{(5.63)}{0.934}\log(X_1) + \underset{(2.89)}{0.437}\log X_2 - \underset{(-4.05)}{1.013}\log D_2 \qquad R^2 = 0.876 \tag{2}$$

$$\log(Y) = \underset{}{-0.546} + \underset{(5.31)}{0.999}\log(X_1) + \underset{(3.0)}{0.534}\log X_2 - \underset{(-2.43)}{1.624}\log D_2 - \underset{(-1.16)}{0.197}\log X_3 + \underset{(0.84)}{0.779}\log D_3 \qquad R^2 = 0.888 \tag{3}$$

where

- Y = peak-hour CBD cordon flow,
- X_1 = CBD workers,
- X_2 = trips that originate and terminate in the central-city ring,
- D_2 = radial distance from midpoint to midpoint of the central-city ring,
- X_3 = trips that originate and terminate in the urbanized area, and
- D_3 = radial distance from midpoint to midpoint of the urbanized area.

On the basis of statistical properties, the second regression equation was used for forecasting purposes. The results of this equation suggest that peak-hour CBD cordon flows increase nearly in proportion to increases in CBD workers, that work trips within the ring adjacent to the CBD have a positive but less than proportionate

effect on peak-hour CBD cordon crossings, and that the impact of through traffic is directly proportional to the radial distance across the next adjacent ring to the CBD. Nearly 88 percent of the variability of CBD peak-hour crossing is explained by this relation.

The peak-hour cordon flows developed above can be used to generate estimates of future traffic flows once residential and employment patterns—the explanatory variables—are themselves projected. Historic trends reveal that an increasing share of the U.S. population resided in metropolitan areas until 1970, at which point relative growth rates for urban and rural areas equalized. Within metropolitan areas, central-city populations have declined on a relative basis. After 1970, absolute declines in central-city populations were observed. Employment trends generally follow the same pattern. A universal tendency for population to reside close to the place of employment was observed. In the five largest SMSAs, between 61 and 67 percent of workers reside and work in the same census ring. In the five smallest SMSAs, the comparable percentages range from 53 to 58 percent. The average for the entire 35-city sample is 55 percent.

To forecast employment and residential levels and distribution, we first projected employment by census ring and assumed that the probability of a worker residing in ring i, given that that worker is employed in ring j, remains unchanged from the probability of 1970. Levels and distribution of employment are thus assumed to determine residential decisions; employment levels are forecast by using the assumption that historic rates of growth among census rings remain unchanged:

$$E = E_1 + E_2 \quad (4)$$

$$\Delta E/E = (E_1/E)(\Delta E_1/E_1) + (E_2/E)(\Delta E_2/E_2) \quad (5)$$

$$(\Delta E_1/E_1)/(\Delta E_2/E_2) = \alpha \quad (6)$$

where E is employment and α is historic relative growth rates.

By way of illustration, total metropolitan employment consists of employment in rings 1 and 2 (E_1 and E_2 respectively). Projected overall growth in employment $\Delta E/E$ equals the weighted growth in each ring $\Delta E_i/E_i$ where the weights are base-period shares E_i/E and are found after correction for changes in geographic boundaries attributed to annexation. By using Equations 5 and 6, each ring's growth rate can be found from α, E_i/E, and $\Delta E/E$ for the projected area. The third value was obtained from U.S. Department of Commerce projections (6).

A second forecast was also prepared that assumed uniform growth rates in each census ring or that the distribution of employment remains unchanged. Note that this assumption is equivalent to setting $\alpha = 1$ in Equation 6.

Employment projections that use historic trends show 32 out of 34 cities to have higher suburban employment growth relative to central-city growth. The exceptions—Pittsburgh and San Antonio—will therefore show higher forecasts of traffic flow when trends are used than when the forecast that assumes uniform growth in all census rings is used. Thus, in general, forecasts that assume uniform growth will produce higher CBD and central-city boundary flow rates than the comparable rates obtained by assuming continuing historic relative growth. Two SMSAs—Houston and Dallas—have the highest central-city growth rates and the most balanced growth between the central city and suburban rings. For these two cities, forecasts of traffic flow under the two alternative assumptions can be expected to be similar.

The forecasts of residential and employment levels by SMSA are next substituted into the previously developed peak-hour relations. The distribution of peak-hour primary-direction flows into corridor-specific flows is based on the number of existing corridors in an SMSA and their existing share of traffic. A mode assignment to transit is also based on existing observations that show higher transit shares as the absolute volume of peak-hour traffic increases.

COST ANALYSIS OF URBAN TRANSIT SYSTEMS

A cost analysis was performed to identify critical levels of demand, property values, and tunneling construction costs at which tunneling could compete in cost with the best surface alternative.

A three-step procedure was used:

1. System specifications were prepared to reflect the major competing transit system types under consideration.
2. Cost parameters were obtained for all of these systems.
3. A parametric cost model was used to solve for a locus of property values and tunnel construction costs that define conditions in which tunneling should be used.

Results were obtained by parametrically varying ridership to cover the range encountered in American cities.

Specifications

The systems to be discussed all consist of a line-haul and a CBD component. All would require feeder lines but, since tunneling is improbable for a feeder route, no feeder systems were costed. Bus and rail rapid transit systems, the two major urban transit alternatives currently in use, are compared.

The roadway options included in the study are tunnel, aerial, and three surface options—dedicated lanes, acquisition of new right-of-way, and median strip of an existing roadway. Comparative analysis was eventually limited to new right-of-way versus tunnel. Station spacing was set at an average of 0.5 km (0.33 mile) in the CBD and 2.4 km (1.5 miles) in the line-haul. This spacing approximates that of systems currently under construction.

To normalize for differences in the speed of operations between the modes, bus service is taken as half express and half local whereas rail service is strictly local. Provision of only one track in each direction simplified computations and allowed adequate passenger-carrying capacity for all cities currently without rail transit. Service is provided 20 h/d on weekdays (with two peak hours each morning and evening) and 18 h/d on weekends and holidays. Demand is based on peak-hour major-direction passengers per hour, and secondary directions or off-peak, one-way flows are set at 15 percent of the peak flow. Minimum service frequency is 15 trains or buses/h at the peak and 6 at the off-peak. A train has a maximum of eight 23-m (75-ft) cars in married pairs or 182 m (600 ft) of length.

Although bus and rail systems were required to provide similar performance for purposes of cost comparisons, it did not seem realistic to make seating standards or speeds identical. The purpose of the analysis is to predict tunnel construction based on systems that will actually be in use in the next decade or two. Instead, the number of seats per length of railcar was equated to standards of a 12-m (40-ft) bus or 50 seats/bus and 94 seats/railcar. At peak, some standing is allowed for railcars (30 percent of seating) and local buses (20 per-

cent of seating since there is less standing room in the narrower bus) but not for express buses, which remain full for the entire route. Average speeds for buses vary from 19 km/h (12 mph) in the CBD on dedicated lanes to 61 km/h (38 mph) on the line-haul for an express bus on a special busway. Rail speeds average 60 km/h (37 mph) on the line-haul and 32 km/h (20 mph) in the CBD.

Bus and rail differ in two other respects that do not affect service but do affect costs. First, bus stations may be larger (i.e., have more platforms) in the CBD than in the line-haul where fewer buses may be stopping provided the minimum service frequency is met. However, rail stations must always accommodate one train at the platform; station costs have therefore been based on 182 m of length. Second, buses on special busways can make the return trip on local streets by using excess local street capacity so that only one-way capacity is required, whereas rail always has one track in each direction.

Costs

System costs, like system specifications, are intended to be representative rather than specific to any one city. Operating and capital costs were derived from the past experience of existing systems and modified by expected future trends in technology and prices. Other costs—externalities to nonusers, travel time, accidents, damage to property during construction, and property values—cannot easily be documented and were either estimated or treated as parameters for sensitivity analysis.

Operating costs were based on the American Transit Association (ATA) reports of bus and rail transit companies (7). Costs were divided into costs per vehicle mile, costs per vehicle hour (chiefly drivers' wages), and maintenance costs per vehicle, per station, or per lane mile.

Costs of operation and maintenance of underground busway and rail or bus stations were not available from ATA reports. The major cost element for operation of underground busways is ventilation; lighting, washing, and signaling also contribute to the total. A rough estimate of $0.12/bus-km ($0.20/bus-mile) was used to cover these costs.

Station operating costs were derived from a report prepared for the Washington, D.C., Metro system (8). For underground stations, almost half the cost of operation is for electricity, and about half of that is for lighting. Underground stations are twice as expensive to operate as surface stations.

Costs of construction of vehicles, roadway, and stations were also obtained from the current experience of several systems. Bus stations were included in bus systems to make them comparable to rail but, since there is little current cost experience with bus stations for local urban transit, it was necessary to estimate bus platform costs at a tenth of the cost of a rail station per platform. The factor of one-tenth was based on both the physical size of the platform and passenger use.

All capital costs were annualized by using a discount rate of 10 percent and lifetimes similar to those used by other authors (5, 9). The lifetimes are given below:

Item	Life (years)	
	Rail	Bus
Line		
Surface	50	35
Underground	50	50
Stations	50	50
Yards	50	40
Vehicles	30	12
Land	∞	∞

Tunnel costs were obtained for three types of tunnels: earth (soft), rock (hard), and cut-and-cover. In reality, an infinite variety of tunneling conditions can be encountered, and these three types were intended to be representative of the relevant ranges. Since Washington, D.C., and San Francisco have conducted a great deal of recent tunneling construction, the cost figures relied heavily on data from these two systems. Supplemental data were, however, obtained from other cities (10, 11, 12).

The final figures cited below include all extras and all stages of construction—engineering, administration and contingencies, track, signaling, and ventilation for bus tunnels as well as all other categories—in 1975 prices (1 km = 0.62 mile):

Tunnel Type	Cost ($000 000)			
	Per Rail-Line-km	Per Bus-Line-km	Per Rail Station	Per Bus Station Platform
Cut-and-cover				
CBD	29	36	17	1.4
Line-haul	27	34	15	1.1
Earth				
CBD	21	23		
Line-haul	20	22		
Rock				
CBD	14	15	22	2.0
Line-haul	13	15	22	1.6

The table compares costs of three kinds of tunnels and underground stations for bus and rail systems. Bus and rail route costs are given for double-track (lane) kilometers; rail station costs are per station, and bus station costs are per platform (a station may have many platforms). A total cost comparison is therefore possible only by using this table with estimates of the level of passenger demand. No earth stations are listed since stations are generally cut-and-cover in soft conditions. Note that, although cut-and-cover line is more expensive than other alternatives, the stations are cheaper so that station frequency will determine which alternative provides the lowest cost.

The following table (10, 11, 14, 15) shows the percentage breakdown of tunneling costs by various components:

Category	Cut-and-Cover Tunnels (%)	Round Tunnels (%)
Route construction	88-92	86-90
Mobilization	3-7	2-10
Excavation and mucking	24-36	40-66
Utility relocation	4-16	0-5
Underpinning of buildings	4-16	0-5
Traffic maintenance and street decking	4-16	0
Lining and structures	30-50	24-40
Backfill and restoration	4-8	0
Guideway	2-3	3-4
Signaling	2-7	3-8
Electrification	2-3	3-4

The distribution of costs for the different categories is only illustrative and may vary substantially in different tunneled segments. Bus terminals have an additional cost component of $4 to $9 million/km ($6 to $14 million/mile) for ventilation (13). The smaller number is for round tunnels (earth or rock), which are able to use part of the tunnel cross section above and below the roadway for transverse ventilation structures. Ventilation of cut-and-cover tunnels requires construction of additional ducts and is more costly given present technology.

Total costs were adjusted for accidents, damage to property during construction, and noise-shielding devices. These costs generally do not account for more

than 6 percent of total costs. They therefore do not play a decisive role in preferences of one mode over another. The value of passenger time, on the other hand, can be a major cost component. Time was valued at $1.94/h at the peak and $0.97/h at the off-peak. The peak figure is 40 percent of the average hourly wage for 1975 and is typical of time values found by other researchers (8). When costs of travel time are included in improved evaluation of systems on a more comparable basis, they account for as much as half of total costs depending on which system alternative is specified.

Parametric cost analysis was used to find the critical property value at which tunneling becomes feasible. Tunneling should proceed from the center of the city out to the point where estimated property values drop below this critical value. A gradient of land values was consequently estimated for each city.

Unfortunately, little evidence is available about patterns of land values in American cities. Data on the assessed value of land and improvements were collected from city assessment directories for 85 properties each in Washington, D.C., and Baltimore. The assessed values were converted to market values according to assessment practices in these cities (the ratio of assessed to market value is 0.55 in Washington and 0.50 in Baltimore). A regression on these data yielded the following coefficients, with t-statistics in parentheses (these equations were formulated in U.S. customary units; therefore, no SI equivalents are given):

$$Y = -683 - \underset{(4.70)}{0.187}\, X_1 - \underset{(10.96)}{0.758}\, X_2 - \underset{(3.25)}{0.126}\, X_3 \qquad R^2 = 0.69 \qquad (7)$$

where

$Y = \log_{10}$ property market value (CBD property value, $/ft^2$);
$X_1 = \log_{10}$ residential density (CBD worker density/ $mile^2$);
$X_2 = \log_{10}$ (distance to CBD, miles); and
X_3 = dummy variable (1 if Baltimore, 0 if Washington).

CBD property values for other cities were calculated as follows. Rental values per unit of area of floor space in many cities were obtained from realtors in each city. Floor space per CBD unit of area was then estimated for each city based on CBD worker density. Next, rental values were capitalized into property values by a conversion based on monthly rent equal to 1 percent of property value. Finally, these CBD property values were used to obtain property-value gradients by applying the regression equation (with the dummy equal to 1 for small cities and 0 for large cities). Property values of $376/m^2 ($35/ft^2), a critical value for tunnel feasibility found from sensitivity analysis with the parametric cost model, would be found at 0.6 km (0.4 mile) from the CBD of small cities and 1.3 km (0.8 mile) from the CBD of large cities. Air rights costs were computed at 75 percent of surface acquisition costs (16).

This method is admittedly crude, but some measure of urban property-value gradients is necessary to gauge tunnel applicability. It should be noted that explicit values for right-of-way acquisition were necessary to produce a definitive tunnel forecast. However, the identification of required right-of-way values by use of the parametric cost model is itself an important planning factor.

Results of Cost Analysis

The cost analysis computed costs of alternative systems for a 16-km (10-mile) line-haul and a 1.2-km (0.75-mile) CBD component for a range of values of capacity ridership, tunnel construction costs, and property values. The comparisons were based on annual totals rather than on peak-hour costs alone, which avoided the issue of proper allocation of capital costs to peak and off-peak users. Tunnel construction costs were a "basic" cost (average of earth, rock, cut-and-cover) of $18.6 million/km ($30 million/mile) of double track and $17 million/rail station. Tunneling costs were, however, treated as a parametric variable that ranged from 0.25 to 1.30 times the base case costs; this represents different geological tunneling conditions encountered across U.S. cities given current technology as well as possible future advances in technology.

Figure 2 shows how CBD system preference depends on the level of demand. All values for this illustration were computed by using a property value of $1076/m^2 ($100/ft^2). Tunneled systems may be competitive for ridership levels greater than 8000 to 10 000 passengers/h depending on tunneling costs. The next best option is rail aerial, but many cities have chosen to exclude this alternative. Note that the sensitivity of system costs to levels of tunnel construction cost is identified by the tunneling cost index, which measures the proportion of base case costs included in those systems that have tunnel components.

The program also computed property values above which tunneling is preferred. First, the cheaper tunnel option (bus or rail) was selected for the particular level of peak-hour ridership. The program then solved for the property value that made the cheaper tunnel option equal in cost to the best (cheapest) surface alternative.

Figures 3 and 4 show these trade-offs for tunnels versus surface systems on new right-of-way. Asterisks are placed at levels of ridership for which rail tunnels are preferred to bus tunnels. In the line-haul, bus tunnels are preferred because bus stations are smaller and only one-way capacity is provided. In the CBD, rail tunnels are preferred for a peak demand of 8000 to 12 000 (or more) passengers/h/corridor. At current construction costs (1.0 in Figures 3 and 4), tunnels compare favorably with surface systems in the CBD when surface systems require new right-of-way that costs more than $1076 to $1184/m^2 ($100 to $110/ft^2). This level of necessary right-of-way costs remains constant for systems that are required to meet peak-hour capacity greater than 8000 passengers/h in a corridor. Further, increases or decreases in tunnel construction costs produce right-of-way values to justify tunnels that rise and fall roughly in proportion to the relative changes in costs. However, dramatic reductions in tunnel construction costs to 40 percent of today's value would make tunnels compare favorably with surface systems in the CBD for a right-of-way value of only $161/m^2 ($15/ft^2). For the line-haul, a comparison between tunnel and surface systems that require new right-of-way shows that tunnels are preferred when right-of-way costs approach $376 to $430/m^2 ($35 to $40/ft^2). Proportionate changes in the costs of tunnel construction appear to produce proportionate changes in the right-of-way value required to favor tunnels.

The major cost categories that affect tunnel competitiveness in the CBD are given in Table 1. It can be seen that the cost of acquisition of new right-of-way dominates the cost of surface systems on new right-of-way and the cost of roadway and stations dominates the cost of underground routes. Stations represent the following fraction of overall (line and station) tunneling costs: line-haul rail, 29 percent; line-haul bus, 11 percent; CBD rail, 75 percent; CBD bus, 41 percent. Thus, a one-third reduction in station costs would reduce overall tunnel construction costs for CBD rail by about 25 percent.

Figure 2. Cost per passenger of CBD transit systems (1975 costs in 1975 dollars).

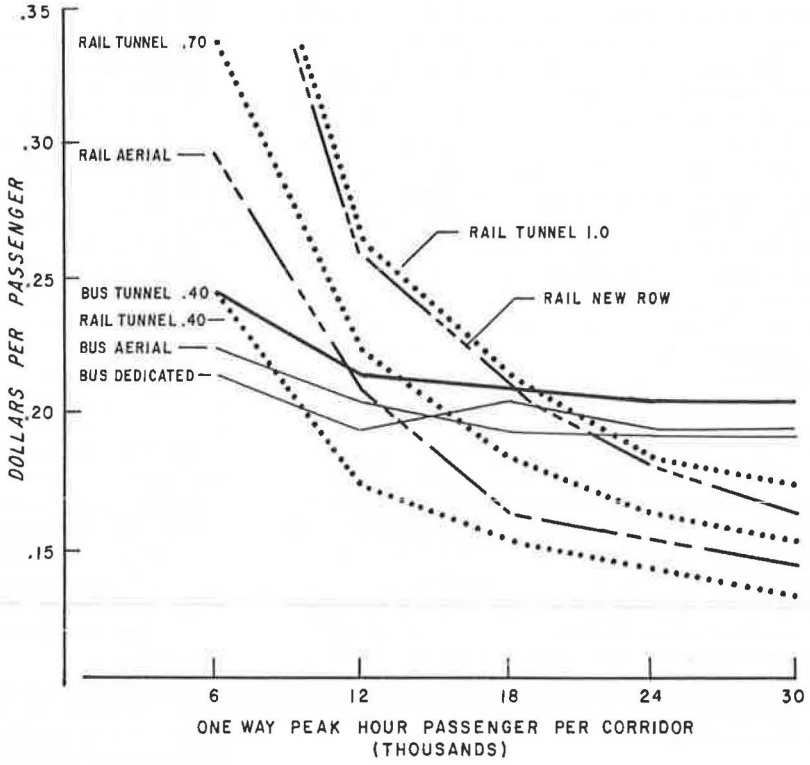

Figure 3. Critical property values: tunnel versus new right-of-way for CBD.

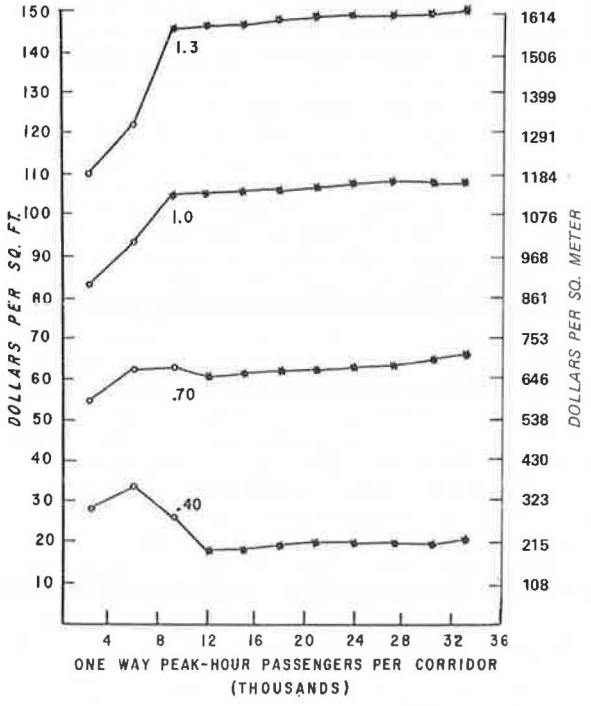

Figure 4. Critical property values: tunnel versus new right-of-way for line-haul.

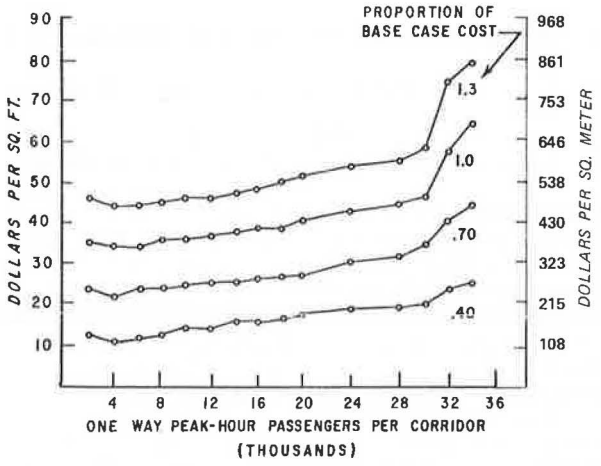

There is a striking difference between the cost of underground roadway for bus and rail in the CBD. This can be accounted for in three ways. First and most important, there will be two lanes in each direction for bus traffic. A lane capacity of 200 buses/h was used in this computation, so the corridor peak demand of 12 000 passengers/h is close to the marginal level of adding an extra lane. In fact, estimates of bus-lane capacities by other writers and from actual experience vary considerably (17). Second, bus tunnels are more expensive. Third, bus stations are off line whereas rail stations are necessarily on line, and two 182-m stations/km (three 600-ft stations/mile) in the CBD means that much less distance is required in the roadway category for rail.

FORECAST OF TUNNELS TO 1990

A procedure was used to integrate the results of the preceding sections to identify (a) where tunneling is a suitable alternative and (b) the extent of tunneled construction activity that is justified under a cost-effectiveness criterion. Projections for three critical factors are used to forecast the 1990 level of justifiable tunnel kilometers: the average level of tunnel construction

costs, the rates of peak-hour transit use in the two heaviest corridors, and property values along corridors as a proxy for surface right-of-way costs.

The method used to integrate these factors for each forecast was to determine from the results of the cost model the minimum necessary or critical property value that must be satisfied to justify either a bus or rail subsurface segment when the least costly tunnel mode is compared with the least costly surface system. Critical property values are found by using the cost model for both CBD and line-haul given the level of transit use (ridership) and the level of tunnel construction cost assumed in the particular scenario. The critical property values are then superimposed on estimated city-specific property value tapers—property values versus distance from the center city, today and after 5 percent annual shifts to 1990—and the amount of justifiable tunnel mileage is identified. This technique is shown in Figure 5.

An identification of justifiable tunneling mileage was conducted across the sample of 35 candidate cities for the following alternative scenarios:

1. A base case that uses current average costs of tunnel construction and the current level of property value estimates developed during the course of this study,
2. A moderate forecast in which average costs of tunnel construction are assumed to fall to 70 percent of the current level because of technological change and right-of-way costs are assumed to increase relative to other cost factors at a rate of 5 percent/year to 1990, and
3. An optimistic scenario in which average costs of tunnel construction are assumed to fall to 40 percent of the current level and right-of-way costs are assumed to increase at a relative rate of 5 percent/year to 1990.

Table 1. Total annual costs in 1975 dollars for 1.2-km (0.75-mile) CBD segment of four possible systems [demand of 12 000 passengers/h/corridor and property values of $1076/m² ($100/ft²)].

Category	Cost for Express Bus ($000)		Cost for Rail Rapid Transit ($000)	
	New Right-of-Way	Underground	New Right-of-Way	Underground
Roadway	597	6 056	506	1 450
Stations	443	3 275	1 212	4 640
Right-of-way	6 704	118	4 323	108
Vehicles	331	331	718	718
Operation	1 188	1 640	657	694
Time	2 444	2 440	1 955	1 955
Noise, accidents, and damages	746	1 015	642	747
Total annual costs	12 453	14 859	10 063	10 312

Results of city-by-city application of this methodology for the two heaviest corridors for the base case revealed that three cities currently without systems would meet necessary conditions for tunneled systems by 1990: Detroit, with 15.5 combined kilometers (9.6 combined miles) of tunnels; Cincinnati, with 7.7 km (4.8 miles); and Denver, with 5.5 km (3.4 miles). This gives a two-corridor total of 29 km (17.8 miles) of tunnels. When these additional system distances are combined with "hard" forecasts of tunnel distance for extensions to existing systems and systems under construction, they produce a total forecast of 223 km (138 miles) of tunnel by 1990. For the moderate scenario, the same procedure produced justifiable tunnel segments for all of the 35 candidate cities except San Jose and Tampa. In the heaviest corridor, all qualifying cities showed tunneled segments for the entire CBD. When it was combined with the line-haul distance, the overall justifiable distance amounted to 223 km of tunnels. In the second heaviest corridor, the overall distance increased slightly because of lower critical property values in certain instances caused by a switch from rail to bus in the comparison between lowest cost tunnel mode and lowest cost surface mode. The aggregate justifiable distance in both corridors amounts to 448 km (278 miles) in 1990. When the hard estimates for extensions and systems under construction are combined, the moderate forecast results in a total of nearly 645 km (400 miles) of tunnels by 1990.

For the optimistic scenario, all candidate cities qualified for some tunneling. This scenario produced a forecast of 976 tunnel km (605 tunnel miles) by 1990.

The table below gives kilometers of nationwide transportation tunneling under each scenario (1 km = 0.62 mile):

Category	Pessimistic Forecast		Moderate Forecast (1990)	Optimistic Forecast (1990)
	1990	If Plans Implemented		
Extensions to existing systems	90	90	90	90

Figure 5. Integration of supply and demand.

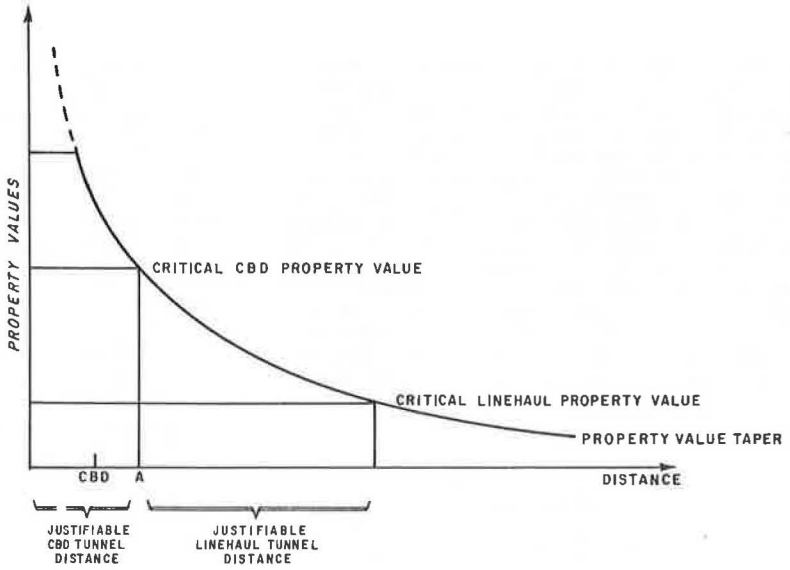

Category	Pessimistic Forecast 1900	Pessimistic Forecast If Plans Implemented	Moderate Forecast (1990)	Optimistic Forecast (1990)
Systems under construction	104	104	104	104
Forecast of additional systems	29	284	449	782
Total	223	478	643	976

Included in this table, under "if plans implemented," are 284 km (175.9 miles) of tunnel construction that would result if cities that have applied for federal grant money or have completed feasibility studies were actually to implement existing plans.

ACKNOWLEDGMENTS

This research was sponsored by the Office of the Secretary, U.S. Department of Transportation. The work was performed for the Transportation Systems Center by SYSTAN, Inc.

REFERENCES

1. M. G. Myers, A. M. Lago, L. B. Blattenberger, and R. K. Wood. Feasibility Analysis of Urban Transit Systems With Special Reference to Tunnels. Transportation Systems Center, Rept. DOT-TSC-OST-77-47, Oct. 1977.
2. Urban Data Book. U.S. Department of Transportation, Rept. DOT-TSC-OST-75-45, Vols. 1 and 2, Nov. 1975.
3. S. B. Chase, ed. Problems in Public Expenditure Analysis. Brookings Institution, Washington, DC, 1968.
4. Patterns of Car Ownership, Trip Generation and Trip Sharing in Urban Areas. Wilbur Smith and Associates, June 1968.
5. J. R. Meyer, J. F. Kain, and M. Wohl. The Urban Transportation Problem. Harvard Univ. Press, 1966.
6. Area Economic Projections 1990. U.S. Department of Commerce, 1974.
7. 1973 Transit Operating Report. American Transit Association, Washington, DC.
8. Traffic, Revenue and Operating Costs. W. C. Gilman and Company, Alan M. Voorhees and Associates, and Washington Metropolitan Area Transit Authority, Feb. 1971.
9. J. Boyd, N. J. Asher, and E. S. Wetzler. Evaluation of Rail Rapid Transit and Express Bus Service in the Urban Commuter Market. U.S. Department of Transportation, S-417, Sept. 1973.
10. Rail Transit Systems Cost Study. T. K. Dyer, Inc., and U.S. Department of Transportation, 1975.
11. T. R. Kuesel. BART Subway Construction: Planning and Costs. Civil Engineering, March 1969.
12. Pricing Guide. Washington, DC, Metropolitan Area Transit Authority, various years.
13. Bus Rapid Transit Options for Densely Developed Areas. Wilbur Smith and Associates and U.S. Department of Transportation, Feb. 1975.
14. Cut-and-Cover Tunneling Techniques: Volume 1—A Study of the State-of-the-Art. Federal Highway Administration, U.S. Department of Transportation, Feb. 1973.
15. W. Van Dyke. Report on Subway Tunneling Needs of 13 Selected U.S. Cities 1971-1975. U.S. Department of Transportation, Transportation Systems Center, Cambridge, MA, Technical Rept., June 1972.
16. P. F. Dienemann and W. W. Smith. Airspace Valuation for Northeast Corridor High-Speed Ground Transportation Systems. Resource Management Corp. and Office of High-Speed Ground Transportation, U.S. Department of Transportation, 1969.
17. Highway Capacity Manual. HRB, Special Rept. 87, 1965.

Fracture Control in Tunnel Blasting

Donald B. Barker, William L. Fourney, and James W. Dally, Department of Mechanical Engineering, University of Maryland

This paper describes a procedure for achieving control of the fracture plane in construction blasting. The conventional drill-and-blast technique is modified in three ways. First, side notches that extend the length of the borehole are used to control the initiation site for the cracks that produce the fracture plane. Second, the pressure in the borehole is maintained between specified limits by using light and cushioned charges. Third, stemming length is increased to avoid venting that could produce premature arrest of the crack that produces the controlled fracture plane. The procedures suggested have been validated by using fracture mechanics computations, two-dimensional experiments in rock and polymeric models, and field tests in large rock boulders. Fracture control in tunnel blasting can reduce the time and equipment required to make the opening cut while increasing the size and improving the quality of the cut. Fracture control can also reduce the cost of contouring the walls and roof of a tunnel and at the same time improve tolerances and reduce structural damage to the remaining rock.

Excavation in hard rock is usually accomplished by a drill-and-blast procedure: A hole is drilled in the rock, packed with high explosive, and stemmed, and the explosive is detonated. The detonation pressures are extremely high, and an extensive amount of energy is dissipated in the process. Very little of this energy is used to create the specified fracture planes required for the excavation. Energy is expended in producing a radially outgoing stress wave that crushes the adjacent rock and in producing a dense radial crack pattern about the hole. These radial cracks arrest quickly and only about 8 to 12 randomly oriented cracks extend any significant distance from the borehole. The stress wave reflects from a free face and initiates an additional set of cracks at the location of flaws in the rock far removed from the borehole (1). The fracture pattern is largely random in this process, and very little control can be exercised in forming the specified fracture plane.

When control of the fracture plane is important, the conventional drill-and-blast process has been modified. Presplitting, postsplitting, and smooth-blasting procedures that offer some degree of control have been developed.

In presplitting, a row of closely spaced and highly

charged holes are detonated simultaneously. The resulting stress waves interact to produce cracking in the region between the holes where the stress waves overlap and double the dynamic stresses. Unfortunately, highly charged holes produce extensive cracking and weaken the wall of an excavation. In addition, simultaneous detonation results in excessively high ground shocks in populated urban areas. Postsplitting is similar except that the holes are fired after the central core of the excavation has been fragmented. Postsplitting is usually used in highly stressed rock where the residual stress system diverts the cracks. Removal of the central core alters the distribution of residual stress, and the cracks can be directed along the contour of the opening. The disadvantages of presplitting also apply to postsplitting.

In smooth blasting where a face is available, the holes are drilled on centers sufficiently close to ensure intercepting radial cracks along the specified fracture plane with cushioned charges. As control is obtained by spacing the holes, delays can be used and the ground shock reduced. Smooth blasting gives satisfactory results when enough holes are drilled and when the charge is properly cushioned; however, the number of holes that must be drilled and loaded increases the cost of the excavation.

This paper describes an alternative procedure in which a high degree of fracture control can be achieved while the ground shock associated with detonation of the charge is minimized. This alternative procedure greatly reduces the number of radial cracks that extend into the wall of the excavation. Reducing these cracks improves the strength and stability of the walls and minimizes the need for auxiliary support from rock bolts, shotcrete, and frames. Precise control of the excavation contour in tunnels will also greatly reduce the costs associated with either overbreak or underbreak.

This paper describes a simple method for achieving control of the fracture plane by using longitudinal grooves at the borehole to direct properly the cracks that form the cut and by using highly cushioned charges to eliminate random parasitic breakage. Analytical results and experimental demonstrations in both the laboratory and the field are presented to illustrate the concept and to define the important operating parameters. Application of the method to a new parallel hole cut and the final contour of a tunnel round are suggested.

FRACTURE CONTROL IN EXCAVATION OF HARD ROCK

Fracture control implies exercising control over all three phases of the fracture process—crack initiation, crack propagation, and crack arrest. Control of crack initiation involves specifying the number of cracks to be initiated and the location of the initiation sites on the wall of the borehole. Control of the propagation phase requires orienting the cracks (usually in the radial direction) and providing a stress field that will produce the strain energy required to maintain the desired crack velocity. Finally, control of crack arrest necessitates maintaining a stress intensity that is sufficiently large to avoid crack arrest until the crack has achieved its specified length. If all three aspects of the fracture process can be controlled, then a blasting round can be designed for optimum performance.

Fracture control can be achieved by using a modified drill-and-blast process in which the borehole is grooved and loaded with a light, cushioned charge. This procedure has been developed from experiments conducted at the University of Maryland over the past few years.

Control of Crack Initiation

The concept of using longitudinal notches on the side of a borehole is not new. Langefors and Kihlstrom (2) indicate that notches can be used to initiate cracks and control the fracture plane. Indeed, notching was described by Foster (3) in 1905 as a method of promoting fracture.

Notching is an effective means for concentrating stress at the borehole and ensuring that cracks initiate at the notch location. However, cracks will start at other locations (4) about the borehole when the detonation pressure is sufficiently high and the beneficial effect of the notch is nullified. A certain pressure range must be achieved to control initiation. If the pressure is too low, the cracks will not initiate even at the notches. When the pressure is too high, cracks will form at the natural flaws on the side of the borehole.

Dally and Fourney (5) have used linear elastic fracture mechanics to determine the range of allowable pressure for control of crack initiation. Three parameters that significantly affect the allowable pressure range include the depth of the groove, the grain size of the rock, and the fracture toughness K_{Ic} of the rock. A typical example of the allowable pressure range for granite with $K_{Ic} = 2.2\ \text{MPa}\sqrt{\text{m}}$ ($2000\ \text{lbf/in}^2\sqrt{\text{in}}$) is given in Table 1.

In theory, the notch or groove serves as a starter crack and should be very sharp and as long as possible to facilitate initiation at the lowest possible pressure. However, in practice the grooves will be cut with a notching tool that will wear so that the sharp point will become rounded. In addition, the cutting forces and the time it takes to notch the borehole are both reduced if relatively shallow notches are used.

Experiments were conducted to determine the effects of the notch geometry on the crack-initiation phase of controlled fracture (6). It was shown that notch depth should be at least $\frac{1}{20}$ the diameter of the borehole to initiate the crack reliably at the specified location on the borehole. However, a deeper groove is suggested for construction blasting to accommodate the taper that occurs in drilling relatively long holes and to compensate for tool wear. A groove depth of 6 mm (0.25 in) is recommended for a 38-mm (1.5-in) borehole as shown in Figure 1. The suggested radius of 1 mm (0.040 in) should be sufficiently sharp for the groove to act as a crack yet large enough to resist rapid wear. The 45° included angle is to enhance gas flow into the crack and to provide for a sufficient shear area on the broaching tool that is used to cut the grooves.

The charge required to initiate the cracks will depend on the fracture toughness of the rock. Preliminary calculations based on scaling the results from the laboratory tests indicate that 330 to 495 grains/m (100 to 150 grains/ft) of primacord (PETN) would be sufficient in granite [$K_{Ic} = 2.2\ \text{MPa}\sqrt{\text{m}}$ ($2000\ \text{lbf/in}^2\sqrt{\text{in}}$)] and that 165 to 247.5 grains/m (50 to 75 grains/ft) of primacord would initiate the control-plane cracks in limestone. These charge densities are preliminary and represent reasonable estimates for the first trial. Adjustments of the charge size should be made after an inspection of the fragmentation pattern that results from a trial charge.

Control of Orientation of Fracture Plane

If the residual stress is small, as is usually the case in near-surface excavations, the cracks will propagate in a radial direction. Control of the crack path along radial lines is achieved if crack branching or forking can be prevented. Crack branching will occur for two reasons. First, if the crack intersects a large flaw in the rock

structure, the flaw can arrest, divert, or bifurcate the crack. Flaws present a serious problem in control of the fracture plane and dictate that the center-to-center distance between holes must be less than the flaw spacing. The second reason for crack branching is overdriving the crack. If the strain energy available is much greater than the minimum strain energy required to propagate a crack, the crack will branch.

The role of small, natural flaws in rock in the control of the fracture plane does not appear to be important if the stress wave is suppressed by using small, highly cushioned charges. In fracture control tests on slabs of a fine pink westerly granite, flaw-induced branching has not been observed (Figures 2 and 3). Field tests in small limestone boulders at Tamaqua, Pennsylvania, showed that the fracture plane could be closely controlled and that branching caused by small, natural flaws could be suppressed. Results obtained in a small limestone boulder are shown in Figure 4.

Branching caused by overdriving the crack has not been observed except when the amount of explosive used was excessive. In these cases, fracture control was not achieved because of excessive borehole pressures that initiated unwanted radial cracks.

Propagation of a crack across a large flaw such as a fault, joint, or bedding plane is a function of the material in the flaw and the angular orientation of the intersecting crack. As it intersects this large flaw, the crack can (a) arrest, (b) pass through the flaw with no change in orientation, (c) pass through and continue in a new direction, or (d) arrest and then turn in the flaw and cleave the rock along the poorly bonded fault plane.

When a running crack intersects a large open fracture or flaw, it will arrest. The crack will also arrest if the

Table 1. Pressure range for controlling crack initiation by means of side grooving.

Rock Grain		Notch		Pressure (MPa)		
Type	Size (mm)	Type	Size (mm)	P_{max}	P_{min}	P_{max}/P_{min}
Very fine	0.025	Deep	5.00	110	7.6	14.5
Fine	0.050	Medium	2.50	76	11.0	6.9
Medium	0.125	Medium	2.50	48	11.0	4.4
Coarse	0.250	Shallow	1.25	34	15.9	2.2

Note: 1 mm = 0.039 in; 1 MPa = 145 lbf/in^2.

Figure 1. Suggested dimensions for grooves to control crack initiation.

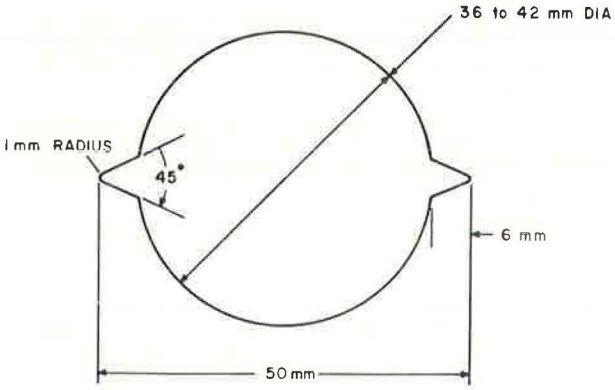

Figure 2. High-speed photographs showing development of fracture control plane in pink westerly granite.

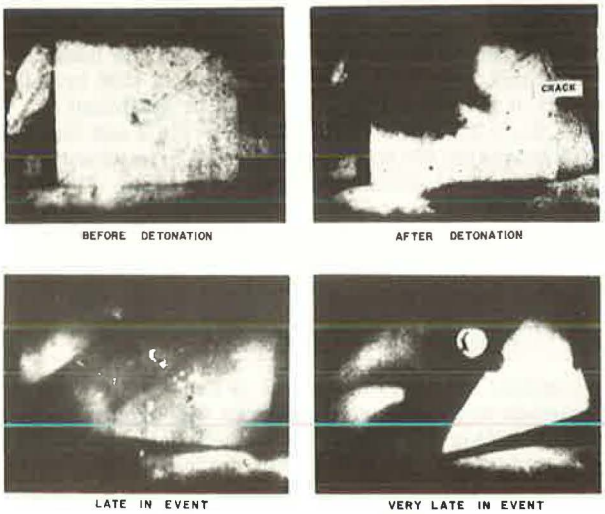

Figure 3. Result of fracture control test in pink westerly granite.

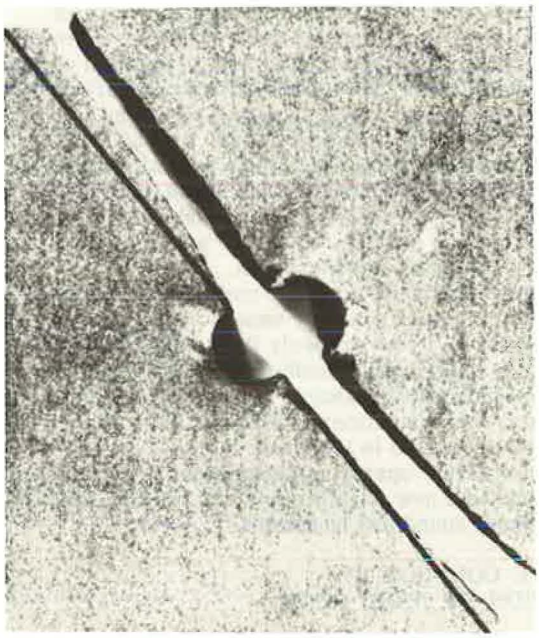

Figure 4. Field test of control of fracture plane in limestone boulders indicating that branching caused by natural flaws can be suppressed.

Figure 5. Field test of control of fracture plane in sandstone boulder.

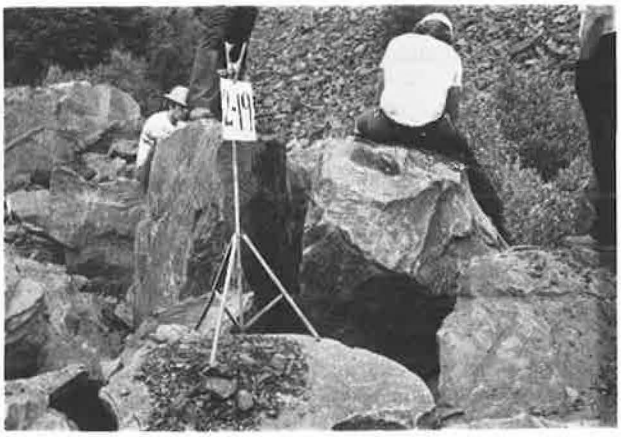

material that fills the flaw is of appreciable thickness and has a greater fracture toughness than the surrounding material. In such a case, two boreholes must be used—one on either side of the flaw—with fracture control planes that intersect at the large flaw.

If the material that fills the flaw is very thin and has a reasonable fracture toughness, the crack will pass through the flaw with no change in orientation. If the material is thick and sufficient stress intensity is driving the crack, the crack can bifurcate in the flaw. When the crack reinitiates in the material on the other side of the flaw, there is only sufficient strain energy to drive one branch. Thus, the crack will continue but in a slightly different orientation. A large flaw can also trap the propagating crack, especially if the angular orientation between the two is less than about 45°. In this case, the crack will turn, propagate in mixed mode, and cleave the rock along the poorly bonded fault plane.

The behavior described above has been observed in polymeric models in which an adhesive was used to simulate a poorly bonded joint plane. The significance of these comments is that large flaws such as joints, faults, and bedding planes do not always adversely affect control of the orientation of the fracture plane.

Large, open fracture planes or flaws affect the conventional techniques of presplitting or postsplitting and smooth blasting to an even greater extent. The drill-and-notch technique is superior for the simple reason that less charge is required and unwanted radial cracks are suppressed. All techniques require that a borehole be placed on opposite sides of a large, open flaw.

Control of Crack Length

Crack length is controlled by maintaining the stress intensity factor at the crack tip above a critical arrest toughness K_{Im} (7). If the explosive gas is confined to the borehole, the stress intensity factor K decreases with increasing crack length until $K < K_{Im}$ and the crack arrests. However, if the gas flows into the opening crack and pressurizes the fracture surface, the stress intensity at the crack tip increases with increasing crack length, and there is no reason for cracks to arrest except that the gas supply is depleted because of the increase in the volume of the cavity.

Experimentally, the maximum propagation distance of a crack has not been determined because the models have been too small. In one test on a sheet of a brittle polymeric material, the ratio of crack length to borehole diameter (s/D) was 25, and the cracks did not arrest. If $s/D \geq 25$ can be achieved in planar models 12 mm (0.47 in) thick where the gases from the explosive are free to vent from the crack at both surfaces, it appears that $25 < s/D < 50$ can be achieved in a well-stemmed tunnel or bench round that will not vent. A crack extension of $s/D = 50$ has been obtained by Plewman (8) in excavating an underground chamber with notched boreholes. These results imply that gas will flow into the crack, maintaining its velocity and extending the fracture plane over very long distances (50D), if the wall of the hole is not crushed by too much pressure during detonation of the explosive.

The gas pressure must be maintained over the period of crack propagation. The time of confinement of the gas pressure is short (of the order of a millisecond). Since the crack velocities are very high, pressure reduction because of thermal losses will be small. Dally and Fourney (7) have shown that the pressure reduction caused by the cavity expansion that results from extension of two diametrically opposed cracks will not cause crack arrest.

If gas flows into the crack, the length that can be achieved before arrest will be limited by the loss of pressure caused by venting. Venting occurs with the loss of the stemming or when the cracks intersect the free surface of the rock. The time required to blow the stemming from a borehole can easily be controlled by adjusting the length l of the stemming column. For instance, with a borehole pressure of 69 MPa (10 000 lbf/in^2), which is about as high as would be used in controlled blasting, a stemming column of 0.3 cm (12 in) provides 2 ms of propagation time.

Venting by intersection of the cracks with the face is more likely to occur. As the cracks are driven from the boreholes, they grow in both the radial and longitudinal directions. By following the crack fronts at intervals of time during the dynamic event, it can be shown that surface venting will occur before complete formation of the fracture plane unless the stemming length l is half the borehole spacing s. For a spacing of s = 50D, the stemming length will be 25D, which is much longer than that required to avoid loss of gas from the hole because of loss of stemming.

DEMONSTRATION OF FRACTURE CONTROL

An experimental program that was instrumental in developing a controlled blasting technique used small, two-dimensional polymeric and rock models and high-speed photography for visualizing the dynamic fracture process. After mechanisms of failure were established and concepts for fracture control were explored in many low-cost laboratory tests, a few of the most promising techniques were tested in the field. In these field tests, methods of fracture control were evaluated on boulders of limestone and sandstone (Figure 5).

Dynamic photoelasticity is an optical method of stress analysis that permits full-field visualization of the state of stress associated with explosive loading and the simultaneous observation of the initiation and propagation of cracks. A two-dimensional photoelastic model is fabricated from a brittle, transparent, polymeric material and loaded with a small explosive charge. The photoelastic fringe pattern that represents the explosive-induced stress waves is photographed with a Cranz-Schardin multiple-spark camera (9). This camera can record 16 frames of dynamic information at rates that can be varied from 30 000 to 800 000 frames/s.

The polymeric material used in the model is known commercially as Homalite 100 and is available from G&L Industries in Wilmington, Delaware. The dynamic fracture characteristics of this material have been de-

termined by Kobayashi and Dally (7), and the initiation toughness K_{Ic}, arrest toughness K_{Im}, and branching toughness K_{Ib} are known. It is interesting to note that the K_{Ic} of Homalite 100 is less than that of Salem limestone (10). Thus, the polymeric material is actually more brittle than one of the most commonly quarried rocks.

A demonstration of fracture control in a two-dimensional Homalite 100 model is given by the sequence of high-speed photographs shown in Figure 6. Four of the 16 frames shown cover a period of 615 μs after detonation of 60 mg of PETN. The dark, circular central section in frame 3 is a pressure-retaining cap held over the borehole by a through bolt. The dark, diagonal line indicates the fracture control plane. In this frame, the dilitational or P type of stress wave has propagated into the model and the shear or S wave is following behind. No cracks are evident yet.

Because of the problems associated with placement of metal inserts in boreholes, it was decided to use grooves cut into the borehole wall to introduce the stress concentrations required for control of the fracture plane.

Field tests are being conducted in Bethesda, Maryland, in granite boulders. The 44-mm (1.7-in) boreholes are being notched by driving into the hole a sharpened tool bit fastened onto the end of a drill rod.

FRACTURE CONTROL APPLIED TO TUNNELING

Tunnel construction is one of the more difficult applications of fracture control, but the potential benefits are tremendous because of the high costs and difficulties encountered in tunneling in urban areas. Fracture control can be applied in two different operations to improve the tunneling process: first, to reduce the time and equipment required to make the opening cut while increasing the size of this cut and improving its quality; second, to reduce the cost of contouring the walls and roof of the tunnel while improving the tolerances that can be achieved and reducing the structural damage to the remaining rock.

Parallel Hole Cuts

In subterranean drill-and-blast construction, the most difficult step in driving any heading is to make the initial opening into the solid rock. The first boreholes detonated create an opening, called a "cut," and produce a free face toward which the rest of the rock is successively blasted. The amount of advance per round is dependent on the type, depth, and success of the first cut. Care exercised in drilling a precise borehole pattern for the cut often means the difference between breaking a full round or obtaining only a small part of the specified advance.

The most common parallel hole cut used in modern tunnel blasting is the cylinder cut. In this cut, the random cracks produced by detonating a live hole are directed toward a single but large-diameter dummy hole. As the charges in the first, second, and subsequent live holes detonate, the rock between the live hole and the dummy hole is broken and ejected through the conduit provided by the large-diameter dummy hole. The dummy hole is successively and uniformly (cylindrically) enlarged over its entire length. The depth of the cut is restricted only by the deviation of the drilled holes since close control over the spacing of the hole pattern must be maintained.

Barker and Fourney (11), in an experimental investigation of the detailed mechanism of the fracture process in a cylinder cut, concluded that driving cracks from the live hole to the dummy hole was a difficult process to control. Since the crack orientation from the live hole is random, failure of the cracks to properly clear the area between the charged and dummy holes can be anticipated.

It appears that a better approach—one that uses control of the fracture plane—would be to isolate a hexagonal block of rock that is then fragmented and ejected. The concept shown in Figure 7 involves initiation of cracks from each of the three triangularly spaced outer holes at an included angle of 120°. The six controlled fracture planes form a hexagonal block of rock that extends into the face that is isolated. The central borehole is highly loaded to fragment the hexagonal block and eject it from the opening. Since the hexagonal block is isolated from the surrounding rock by smooth fracture planes, there is little tendency for the fragments to jam before ejection.

The concept of isolating and then fragmenting the hexagonal region was demonstrated in the laboratory. The results shown in Figure 7 show that the hexagonal region is isolated by fracture control planes in spite of significant crack deviations. The delayed detonation of the highly loaded center charge produces a dense, radial crack pattern that intersects the bounding fracture control planes in many locations.

Although the work described here pertains only to laboratory models, it is believed that the hexagonal cut can be used effectively in tunneling. There appear to be several advantages of the hexagonal cut:

1. In comparison with the double spiral cut, which requires six holes plus the expensive and time-consuming large-diameter hole, the hexagonal cut requires only four small-diameter holes. This should reduce both drilling time and cost.
2. The success of the cylinder cuts depends on very close tolerance drilling. The hexagonal cut does not require the same degree of precision in drilling the pattern. The hexagonal cut should be insensitive to errors in location and inclination of the holes if the hexagonal area does not increase with depth.
3. The isolation of the hexagonal area is accomplished by means of light decoupled charges. This conserves explosives and reduces ground vibration. The isolation reduces the passage of the stress waves to the surrounding area by the concentrated charge used to fragment the cylindrical core, which again minimizes ground vibration.
4. The walls of the hexagonal conduit are relatively smooth, and velocity of radial fragments is low. Both of these features should promote clean ejection of the fragmented hexagonal area.

Tunnel Contouring

Excavation for underground facilities requires close control over the contour of the opening and retention of the strength in the rock walls and ceiling. Obviously, any cracks directed into the remaining walls will weaken the structure and may require auxiliary support from rock bolts, shotcrete, and frames. The drill-and-notch technique of controlled blasting essentially eliminates these cracks that can damage the remaining walls.

In the contouring operation, a series of holes are drilled to outline the desired opening; the ratio of borehole spacing to borehole diameter (s/D) approaches 50. The boreholes are grooved so as to trace the tunnel outline with the fracture control planes. Corners or sharp curvatures can also be cut because the grooves in the boreholes do not need to be diametrically opposed. The resulting tunnel contour will be composed of smooth, flat sections that extend from each borehole to the inter-

Figure 6. Sequence of dynamic photoelastic fringe patterns showing stress wave and crack propagation.

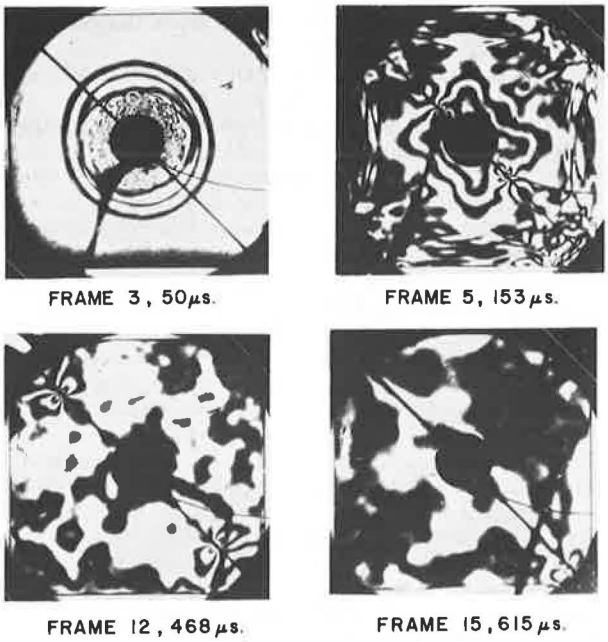

Figure 7. Hexagonal cut using control of fracture plane.

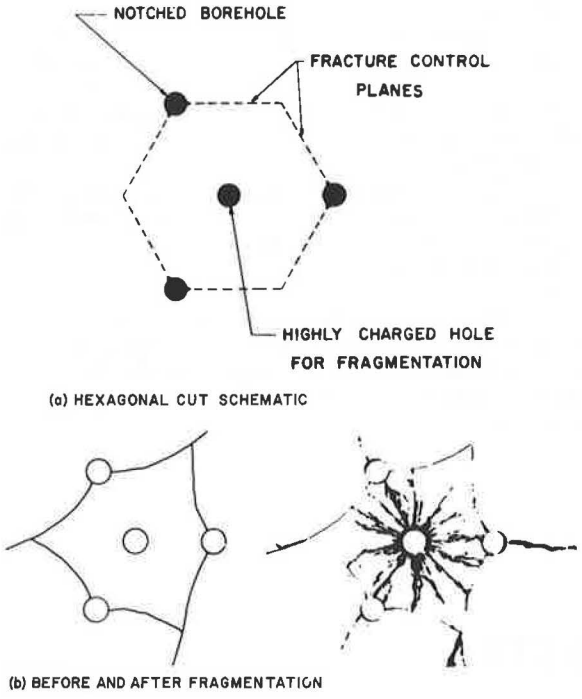

section of the fracture control plane from the adjoining borehole. Few if any cracks will extend into the remaining rock walls at the boreholes as with conventional techniques.

Current controlled blasting techniques of presplitting, postsplitting, and smooth blasting outline the contour of an excavation with holes spaced on s/D ratios of 8 to 16. Thus, if the drill-and-notch technique is used, the number of boreholes required on the contour is reduced by a factor of 3 to 6.

Experience has indicated that it is possible to control the location of the fracture control plane to well within ±5° of the notch location. The notch can be located within the borehole well within ±2°. For boreholes on 50D centers, the resulting overbreak or underbreak would be less than 0.12D; e.g., 50-mm (2-in) boreholes on 1.25-m (50-in) centers will give a maximum deviation from the control plane of only 153 mm (6 in).

If the tunnel is located any appreciable distance below ground level, stresses are present because of the weight of the overburden. This "residual stress" makes it more difficult to control the fracture control planes. Dally and Fourney (5) have examined the static solution of a pressurized borehole in the presence of a uniaxial confining stress and have found that the path of the crack is affected by the confining stress field.

In blasting at depths of 30 m (100 ft) with carefully cushioned charges, crack curvature caused by confining stress can become an important consideration. In these situations, the curvature can be taken into account either by limiting the length of the path of the crack (shorter distance between holes) or by accommodating the effect of curvature by adjusting the location of the groove on the borehole wall. By rotating the initiation plane relative to the fracture control plane, a curved fracture surface can be produced that does not deviate significantly from the control plane.

If the confining stresses are large, as is the case in deep excavations, contours are easily formed by postsplitting. In postsplitting, the central region of the excavation is removed before the contour cut. The cavity formed is roughly the shape of the contour, and the confining stresses are redistributed so that they are parallel to the contour of the excavation. This state of stress is such that any tendency for crack curvature out of the fracture control plane is eliminated.

Plewman (8) has used this postsplitting process successfully in a deep underground mine in South Africa.

SUMMARY

Control of the fracture plane can be achieved by using a modified drill-and-blast process in which the borehole is notched and loaded with a very light and cushioned charge. Notching makes it possible to control the initiation site of the cracks that produce the specified fracture plane and reduces the borehole pressures required for initiation.

Concepts of fracture mechanics that use crack initiation toughness indicate that the borehole pressures required to initiate cracks at notches range from about 7 to 35 MPa (1000 to 5000 lbf/in^2) for most common types of rock. Higher pressures are possible, but pressures in excess of 35 to 175 MPa (5000 to 15 000 lbf/in^2) will cause crack initiation at small, natural flaws on the borehole wall.

The fracture plane is produced by radially outgoing cracks that will not branch provided the pressure in the borehole is not excessive and the branching toughness of the rock material is not exceeded. Field experience indicates that small, natural flaws will not produce branching; however, large flaws can cause the cracks to deviate from the control plane or arrest. Crack curvature caused by confining pressures can be significant whenever the ratio of $p/\sigma_0 < 500$. In tunneling with postsplitting techniques, the confining stresses act to improve control of the direction of the fracture plane.

The fracture plane can be extended over a considerable distance (s = 50D) provided the gas flows into the cracks. Crack arrest occurs because of venting of the pressure when the cracks intersect the surface. Premature arrest can be avoided by using stemming columns of length l = s/2 = 25D.

The drill-and-notch procedure has several advantages in blasting the contour of a tunnel:

1. Drilling costs should be reduced. Langefors and Kihlstrom (2) recommend s/D ratios of 16 and 8 for smooth blasting and presplitting respectively. Increasing the s/D ratio to, say, 50 will reduce the number of boreholes required on the contour by factors of 3 and 6 respectively.
2. Relatively few cracks will be produced in the wall that remains after excavation. This should improve its strength and stability and thus minimize the need for auxiliary support such as rock bolts, shotcrete, and frames.
3. Control of the fracture plane should reduce the possibility of overbreak and underbreak. Thus, the costs associated with scaling forms and concrete should be greatly reduced.
4. There will be a cost savings since the relatively low-density charges of 0.03 kg/m for 3.8-cm diameter (0.02 lb/ft for 1.5-in diameter) specified for use with notched boreholes require less explosive than the more highly loaded 0.12 kg/m for 3.8-cm diameter (0.08 lb/ft for 1.5-in diameter), smooth-blasting rounds. In addition, since low explosives may be used instead of high explosives, further cost reductions for explosives may be achieved.
5. Fracture control used in the hexagonal opening cut reduces the time required for opening the heading. The major advantage is the elimination of the very expensive, large-diameter dummy hole. In addition, the number of smaller holes is reduced, and the tolerance on the drilling pattern can be relaxed.
6. Finally, in both contouring and opening, using reduced and highly cushioned charges will greatly reduce ground vibration and thus reduce the number and frequency of complaints about blasting in heavily populated urban areas.

ACKNOWLEDGMENTS

We would like to express our thanks to the National Science Foundation and W. W. Hakala for supporting this research work.

REFERENCES

1. J. W. Dally and W. L. Fourney. The Influence of Flaws on Fragmentation. Sixth International Colloquium on Gasdynamics of Explosions and Reactive Systems, Stockholm, Aug. 1977.
2. U. Langefors and B. Kihlstrom. Rock Blasting. Wiley, 1963, pp. 300-301.
3. C. L. Foster. A Treatise of Ore and Stone Mining. Charles Griffin and Co., 6th Ed., 1905.
4. J. W. Dally, W. L. Fourney, and P. A. Ladegaard. A Dynamic Photoelastic Evaluation of Some Current Practices in Smooth Wall Blasting. Society of Mining Engineering, Feb. 1978, pp. 184-189.
5. J. W. Dally and W. L. Fourney. Fracture Control in Construction Blasting. Proc., 18th Rock Mechanics Symposium, Keystone, CO; National Science Foundation, Research Applied to National Needs Rept., June 22-24, 1977.
6. W. L. Fourney and J. W. Dally. Grooved Boreholes for Fracture Plane Control in Blasting. National Science Foundation, Research Applied to National Needs Rept. 770216, June 1977.
7. T. Kobayashi and J. W. Dally. The Relation Between Crack Velocity and Stress Intensity Factor in Birefringent Polymers. Symposium on Fast Fracture and Crack Arrest, ASTM STP 627, 1977.
8. R. P. Plewman. An Exercise in Post-Splitting at Vlakfaitem Gold Mining Co. Ltd. Papers and Discussion of Association of Mine Managers of South Africa, 1968-1969, pp. 62-81.
9. W. F. Riley and J. W. Dally. Recording Dynamic Fringe Patterns With a Cranz-Schardin Camera. Experimental Mechanics, Vol. 9, No. 8, Aug. 1969, pp. 27-33.
10. R. A. Schmidt. Fracture Toughness Testing of Limestone. Experimental Mechanics, Vol. 16, No. 5, 1976, pp. 161-167.
11. D. B. Barker and W. L. Fourney. Fracture Control in Parallel Hole Cuts. Tunnels and Tunnelling, Vol. 10, No. 3, 1978.
12. W. L. Fourney and J. W. Dally. Controlled Blasting Using a Ligamented Tube as a Charge Containing Device. National Science Foundation, Research Applied to National Needs Rept. T-75-066, Dec. 1975.
13. W. L. Fourney and J. W. Dally. Further Evaluation of a Ligamented Split-Tube for Fracture Control in Blasting. National Science Foundation, Research Applied to National Needs Rept. 760091, April 1976.

Improvement of Ground-Support Performance by Full Consideration of Ground Displacements

C. W. Schwartz and H. H. Einstein, Department of Civil Engineering, Massachusetts Institute of Technology

A conceptual description of the ground behavior around a tunnel and a quantitative analysis of the effects of the more important factors that influence tunnel support loads are presented. Axisymmetric finite element models of the advancing tunnel were used for the quantitative analysis. The variables considered in the investigation were the relative stiffness of the ground and the support, the constitutive behavior of the ground, and the delay of support installation. The conclusions of the study are that decreasing the relative stiffness of the support or increas-

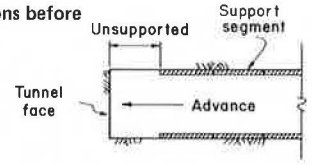

Figure 1. Tunnel conditions before excavation.

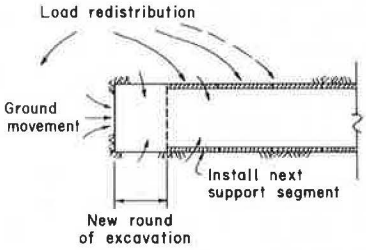

Figure 2. Ground movement and load redistribution resulting from tunnel excavation.

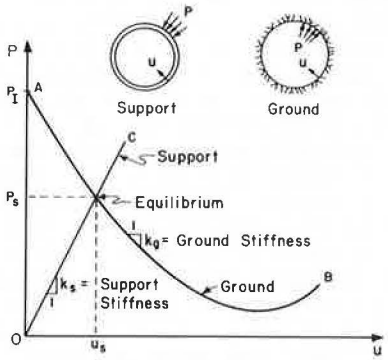

Figure 3. Ground and support characteristic curves.

ing the delay of the support installation generally reduces the forces in the tunnel support but at the same time may induce greater amounts of detrimental yielding in the ground mass. Comments on the optimization or minimization of tunnel support loads are also included.

Tunneling excavation creates a complex pattern of movements in the ground mass around the tunnel. These displacements, a significant portion of which occur in the region ahead of the advancing tunnel face, cause the shearing resistance of the ground to be mobilized and can result in substantially reduced support loads. Unfortunately, however, the exact magnitude of the ground movements near the face and the quantitative effect that these movements have on support loads are generally unknown. Because the relations between ground characteristics, near-face movements, and resulting support loads have not been adequately established by field measurements and analytical studies, no rational model of the mobilization of ground resistance or of corresponding support loads is possible.

The purpose of this paper is to improve the understanding of this ground-support interaction by investigating the effects of several ground and support parameters on tunnel performance, i.e., on ground displacements and support loads. Three major variables were considered in the investigation: (a) the unsupported length between the face of the tunnel and the point of support installation, (b) the ground behavior around the tunnel (elastic and inelastic), and (c) the relative stiffness of the support to the ground. Analytical finite element models were used in these studies since they permit one to examine easily and inexpensively a range of ground and support parameters. The results of these finite element analyses are not intended to represent the behavior of any particular real tunnel but can be used as guidelines for improving the efficiency of tunnel supports.

QUALITATIVE BEHAVIOR OF GROUND AND SUPPORT

The behavior of the ground around a tunnel as it interacts with the support is extremely complex; loading and unloading, fracture and plastic yielding, postfailure strength and stiffness deterioration, seepage, creep, consolidation, or swelling can all occur around a tunnel. Many of the factors that influence the behavior are interrelated, and separating their effects is difficult. However, the conceptual description presented in this section will provide a better understanding of this behavior and the various factors that affect it and will form a basis for the interpretation of the results of the quantitative analytical study.

Only those aspects of interaction behavior that are relevant to this analytical study are described here. A more complete treatment of this topic is given by Einstein and others (4).

Ground-Structure Interaction

A good overview of the patterns of stress changes and ground movements that occur around an advancing tunnel may be gained by considering a typical cycle in the tunnel construction sequence. Figure 1 shows the conditions that exist in the tunnel immediately before a new round of excavation. The tunnel support has been installed up to a point a short distance behind the face. (The exact details of the support conditions at the face depend, of course, on the ground type and on the details of the construction procedure.) The changes that occur after an advance are shown in Figure 2. The removal of ground at the face induces a change in the stress field or a redistribution of load around the tunnel. Most of the redistributed load is transferred to the tunnel support—both to the support already in place and to the newly installed segment—but a significant portion is also transferred to the unexcavated ground ahead of the face. Concurrently, this redistribution of load causes a pattern of movements within the ground mass. Behind the face, predominantly radial deformations toward the tunnel occur around the excavated section while, in the region immediately ahead of the face, the combination of the increase in stress caused by redistribution of load and the removal of lateral support (the excavated ground) up to the new face results in both longitudinal and radial ground displacements. The radial displacements ahead of the face are particularly significant since they may be a sizable fraction (20 to 30 percent or more) of the eventual total radial ground movement around the tunnel.

The load redistribution around an advancing tunnel will produce failure in the ground mass when the shear stresses that result from the excavation exceed the shear strength of the material. In other words, failure occurs when the difference between the major and minor principal stresses exceeds some maximum allowable value. In an unlined tunnel, the largest difference in principal stresses occurs at the tunnel wall where the radial stresses approach zero.

The primary purpose of the tunnel support is to provide a counterstress to the ground mass around the tunnel to maintain the stability of the opening at an acceptable level of deformation. The unloading of the ground mass that follows excavation results in the loading of the tunnel support; this relation can be seen most easily by using the conceptual tool of characteristic curves. Figure 3 shows the characteristic curves for both the ground

Figure 4. Effect of support delay on support loads.

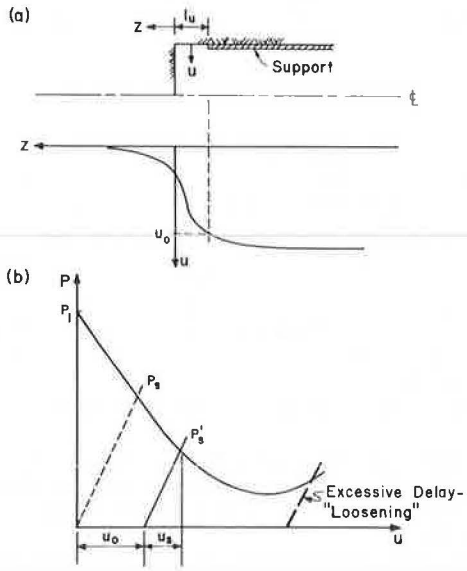

Figure 5. Effect of ground yielding on support loads.

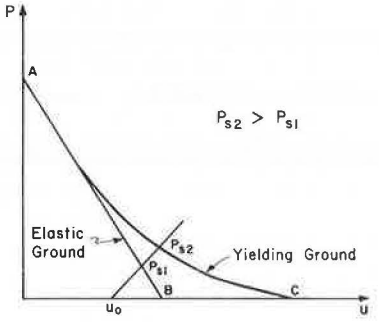

Figure 6. Minimization of support loads.

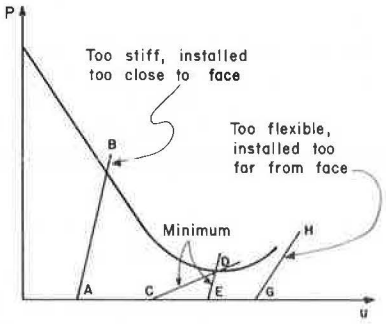

and the support. In this highly idealized situation, the excavation of the ground corresponds to a decrease of the internal tunnel pressure along curve AB. The support is assumed to be in place before any excavation starts, and thus any excavation (i.e., unloading of the ground) immediately results in a loading of the support along curve OC. The intersection of the two curves is the equilibrium point: P_s is the tunnel support load and u_s is the corresponding inward radial displacement at equilibrium. Of course, the support characteristic curves need not have the idealized linear shape shown in the figure; the curves should represent the actual load-displacement characteristics of the support [Lombardi (5) gives examples of nonlinear support systems].

The development of support forces as the support deforms with the ground and the concurrent restraining effects these forces have on further ground movement is the ground-structure interaction around the tunnel. The essential feature of this interaction phenomenon is that the support and the ground mass are in contact and deform together. This can happen in two ways: (a) The support is installed so close to the face that further advances of the tunnel result in additional ground movements and support deformations, and (b) the ground and support movements continue after the support has been installed because of a variation in the ground properties with time. In reality, both types of interaction often occur simultaneously as soon as the in situ state of stress in the ground has been altered by the excavation. However, for the purposes of the present discussion, only the time-independent, or instantaneous, interaction is considered.

The instantaneous ground-structure interaction is greatly affected by any ground movements that occur before the support is constructed. The magnitude of these ground movements depends to a large extent on exactly how far behind the face the support is installed. If the support is installed right at the face, the presupport ground movements will be very small, substantial additional movements will take place as the excavation proceeds, and the eventual support loads will be relatively large. On the other hand, if the support is installed farther behind the face, more ground movements will have already occurred, less interaction will take place between the ground and the support, and consequently smaller support loads will develop (provided no detrimental ground loosening occurs).

The effects of support delay (the spatial lag of support installation behind the face) on the ground-structure interaction and on the resulting tunnel support loads are shown in Figure 4. As shown in the upper part of the figure, the radial ground movements begin at approximately one to two tunnel radii ahead of the face and increase very rapidly near the face. By the time the support is constructed, the ground has already deformed by an amount u_o. This movement corresponds to a partial unloading of the ground mass before support; any further movement of the ground will cause deformations and internal forces in the tunnel support. Preexcavation support of the tunnel (i.e., the support is somehow installed before excavation) would give an equilibrium support pressure equal to P_s; the one-radius support delay would result in the reduced equilibrium pressure P_s' (6). In general, increasing the support delay decreases the support loads if the support delay is not too large. An excessively large delay allows the ground to loosen and leads to larger support loads (Figure 4).

In addition to the delay of support installation, another factor that has an extremely important effect on ground-structure interaction and the resultant support loads is the relative stiffness of the ground mass and the support. This can be seen conceptually by considering the ground-structure interaction as a sharing of load by two dissimilar but intimately connected structural elements much in the same way as load is shared between steel and concrete in a reinforced concrete column. The stiffer element (the steel in the reinforced concrete column) carries a proportionately larger share of the load; increasing the stiffness further increases the load on the element. Similarly, increasing the stiffness of the tunnel support relative to the ground mass results in larger support loads if all other factors are held constant. As Figure 3 shows, the stiffness of the ground and the support are directly related to the slopes of their characteristic curves (6).

The effect on the tunnel support loads of ground yielding or failure is shown in Figure 5. The straight line AB represents the elastic ground behavior, and curve AC is the ground characteristic curve when yielding occurs.

Table 1. Cases analyzed.

Case	Description of Ground	Ground Properties[a]				Support Properties[b]			
		E/P	ν	ϕ	c/P	E_ℓ/P	ν_ℓ	t/R	C*[c]
1A	Dense sand, badly fractured rock	180	0.30	35°	0.0012	37 440	0.30	0.0358	0.134
2A	Undrained clay	60	0.48	0	0.200	37 440	0.30	0.0358	0.052
2B	Loose sand, drained silty clay, very badly fractured rock	60	0.30	25°	0.0012	37 440	0.30	0.0358	0.044
SS	Massive soft rock (e.g., sandstone)	24 000	0.30	-	-	37 440	0.30	0.0358	17.9
LLE[d]	Drained soft ground	60	0.40	-	-	24 000	0.15	0.1	0.028
LEP1[d]	Drained soft ground	60	0.40	30°	0.168	24 000	0.15	0.1	0.028
LEP2[d]	Undrained soft ground	60	0.40	0°	0.168	24 000	0.15	0.1	0.028

[a] In situ ground stresses: $\sigma_v = \sigma_h$ = 575 kPa (12 000 lbf/ft^2); corresponds to a depth of approximately 30 m (100 ft).
[b] R = 3 m (10 ft) in all cases.
[c] $C^* = [ER(1 - \nu_\ell^2)]/[E_\ell t(1 - \nu^2)]$ = measure of stiffness of ground relative to support.
[d] From Ranken and Ghaboussi (7).

Table 2. Summary of analysis results.

Case	Type of Analysis	Support Delay (lu/R)	Finite Element			Closed Form
			u/R	T/PR	Z_p/R[a]	(T/PR)
1A	Elastic	0	0.001 1	0.77	-	0.91
1A	Elastic	0.5	0.002 2	0.51	-	0.91
1A	Elastoplastic (ϕ = 35°, c/P = 0.0012)	0	0.001 1	0.75	0.25	0.91
1A	Elastoplastic (ϕ = 35°, c/P = 0.0012)	0.5	0.002 2	0.50	0.25	0.91
2A	Elastic	0	0.003 8	0.84	-	0.97
2A	Elastic	0.5	0.006 2	0.61	-	0.97
2A	Elastic	1.0	0.015	0.25	-	0.97
2A	Elastoplastic (ϕ = 0, c/P = 0.200)	0	0.009 4	0.65	1.75	0.97
2A	Elastoplastic (ϕ = 0, c/P = 0.200)	0.5	0.014	0.45	2.0	0.97
2A	Elastoplastic (ϕ = 0, c/P = 0.200)	1.0	0.029	0.35	2.0	0.97
2B	Elastic	0	0.002 6	0.83	-	0.97
2B	Elastic	0.5	0.004 6	0.58	-	0.97
2B	Elastoplastic (ϕ = 25°, c/P = 0.0012)	0	0.002 8	0.81	0.75	0.97
2B	Elastoplastic (ϕ = 25°, c/P = 0.0012)	0.5	0.004 9	0.64	0.50	0.97
SS	Elastic	0	0.000 048	0.054	-	0.074
SS	Elastic	0.5	0.000 051	0.030	-	0.074
LLE[b]	Elastic	0	0.002 8	0.88	-	0.98
LLE[b]	Elastic	1.0	0.015 3	0.29	-	0.98
LEP1[b]	Elastoplastic (ϕ = 30°, c/P = 0.168)	0	0.002 8	0.88	0.50	0.98
LEP1[b]	Elastoplastic (ϕ = 30°, c/P = 0.168)	1.0	0.017 7	0.30	0.60	0.98
LEP2[b]	Elastoplastic (ϕ = 0, c/P = 0.168)	0	0.004 1	0.80	1.5	0.98
LEP2[b]	Elastoplastic (ϕ = 0, c/P = 0.168)	1.0	0.018 8	0.45	1.8	0.98

[a] Z_p = extent of yielded zone ahead of face. [b] From Ranken and Ghaboussi (7).

The same support system (stiffness, strength, installation delay) is used in both cases, but in the case of ground yielding the equilibrium support pressure and displacements increase. This increase may be viewed conceptually by considering the effective stiffness of the ground in the two cases. As yielding occurs, the ground within the failed zone becomes plastic and considerably less stiff. The stiffness may even become negative (at least theoretically) in severely strain-softening materials. This decrease in stiffness in the failure zone in turn causes a reduction of the effective stiffness of the ground mass as a whole or, in other words, a decrease in the stiffness of the ground relative to the support. The support loads must, as a consequence, increase.

Minimization of Support Loads

It has been shown that the load sustained by the support in a tunnel is not a fixed quantity. The support pressure can be varied over a moderate range by suitably adjusting factors such as support stiffness and delay of installation. Obviously, then, these factors should be adjusted in such a way as to minimize the support loads or, stated in another way, to mobilize the maximum strength of the ground mass without exceeding maximum admissible displacements from the viewpoint of stability or operation.

Minimizing the support load is conceptually nothing more than an attempt to intersect the ground characteristic curve at its lowest point. Figure 6 shows this minimum and some typical nonminimum cases (curves AB and GH); it also shows that more than one support system can produce the minimum support load for any given tunneling situation (curves CD and ED). This conceptual framework puts the following analytical study of the factors that influence the ground-support interaction into its proper context.

ANALYTICAL STUDIES OF GROUND-SUPPORT INTERACTION

Purpose

Some of the factors that most influence ground-support behavior around a tunnel—ground properties (strength and deformability), the relative stiffness of the support and the ground, and the delay of the support installation—have already been described conceptually. It has also been shown to be possible, at least qualitatively, to adjust these factors to yield a minimum support load. However, in practical tunnel design it is necessary to assign quantitative values to these factors, and that is the purpose of this analytical study. In this study, the major factors are varied to investigate which ranges of their values are most important in optimizing the design of tunnel support. However, the investigation is not intended to be a detailed parametric study.

Two sets of analytical studies were used. The first set consists of the finite element analyses reported in the literature by Ranken and Ghaboussi (7), who used the GEOSYS program (1). The studies in the second set are the finite element analyses that we conducted under the

Figure 7. Analysis results for undrained clay (case 2A).

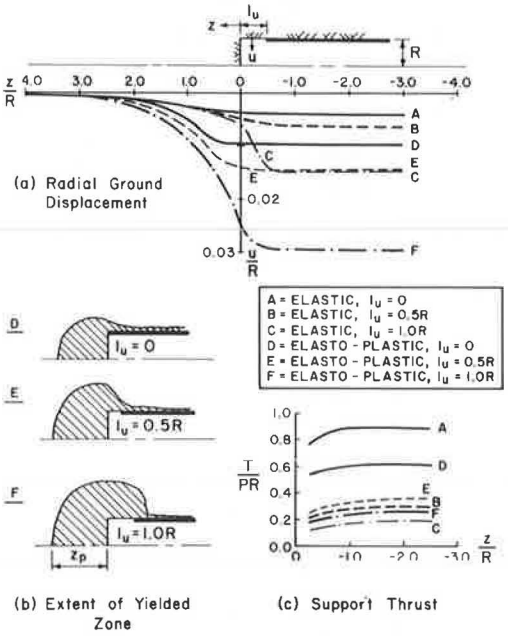

sponsorship of the U.S. Department of Transportation. The computer program ADINA (2, 3) was used in these analyses. Details of these studies are given below.

Description

The analytical studies were conducted to study the effects of three major factors that influence ground-support interaction: (a) the delay of the support installation (it should be recalled that delay refers to a lag in space rather than time)—installation of the support either right at the face, half a tunnel radius behind the face, or one full radius behind the face; (b) the ground behavior—either linearly elastic, frictional elastic and perfectly plastic ($\phi \neq 0$), or purely cohesive elastic and perfectly plastic ($\phi = 0$); and, to a lesser extent, (c) the relative stiffness of the support and the ground. The idealized tunnels are all 6 m (20 ft) in diameter at a centerline depth of 30 m (100 ft). The in situ vertical and horizontal ground stresses are both 575 kPa (12 000 lbf/ft^2), i.e., K = 1. In nearly all cases, the ground properties are characteristic of soft ground—either soil or badly fractured or shattered rock. One intact rock case was analyzed to determine better the effects of the relative stiffness of the ground and the support. The support properties in the cases we analyzed were based on typical dimensions for precast concrete liner segments; the support properties used in the analyses performed by Ranken and Ghaboussi correspond to 30-cm (1-ft) thick concrete liner. Complete details of all of the cases, including those of Ranken and Ghaboussi, are given in Table 1 (E = modulus of elasticity, c = cohesion, and C* = compressibility ratio).

Because of the assumption of uniform in situ ground stresses (i.e., K = 1), two-dimensional axisymmetric finite elements can be used to analyze the behavior near the tunnel face. Sequential excavation of the initially stressed ground and the installation of the liner elements are simulated by deactivating or activating elements at appropriate stages of the calculations. Fourteen excavation-installation steps were used in most of the analyses that we performed.

The details of the finite element analyses performed by Ranken and Ghaboussi are described in their original report (7).

Results

The pertinent data from the analyses performed for this study are summarized in Table 2. The results of most interest are u/R, the normalized radial ground displacements at the tunnel wall, and T/PR, the normalized support thrust (P = overburden pressure and R = tunnel radius). Also given in the table is Z_p, the extent of the plastic zone ahead of the tunnel face, and a reference value for the normalized support thrust obtained from a closed-form elastic plane strain solution (4).

Some important trends can already be discerned in the data presented in Table 2. All of the cases except SS (the intact rock case) have roughly similar values for T/PR independent of the ground type or the ground strength parameters. Only the delay of the support installation has an important influence. When the support is installed right at the face ($l_u = 0$), T/PR varies between 0.6 and 0.9 (and in most cases between 0.75 and 0.88); when the support is delayed (l_u = 0.5R or 1.0R), T/PR ranges from 0.25 to 0.65.

If the intact rock case SS is compared to the other cases, the effect of the relative stiffness of the ground to the support loads becomes apparent. The compressibility ratio C* (defined in Table 1) varies between the narrow limits of 0.028 and 0.134 for all cases except case SS. In contrast, case SS has a compressibility ratio two to three orders of magnitude higher (C = 17.9) and a much lower thrust coefficient (T/PR = 0.054 for $l_u = 0$). Thus, the intact rock, which is much stiffer than the soft ground of the other cases, carries a proportionately larger share of the load around the tunnel, which leaves little to be sustained by the tunnel supports. This is exactly the result predicted qualitatively earlier.

The variation of ground displacements and support thrusts with distance from the tunnel face is shown in Figure 7 for case 2A, a purely cohesive soft ground ($\phi = 0$) (the data for the other cases are not presented but are similar in nature). The results for both elastic and elastoplastic fully supported and partially supported (support installed at a distance l_u behind the face) analyses are presented. In all of the cases, the radial ground movements begin approximately three to four tunnel radii ahead of the face. Nearly all of the ground displacement around these partially or fully supported tunnels occurs ahead of the face; the installation of the support and the rapid development of the support thrust quickly arrest further ground movement. Plane strain equilibrium conditions for both the displacements and the support thrusts are reached one to two radii behind the face in all cases.

The extent of the yielded zone for the elastoplastic analyses of case 2A is also shown in Figure 7. Yielding occurs principally in the region immediately ahead of the face, and the partially supported cases (l_u = 0.5R - 1.0R) generally exhibit more yielding than the fully supported cases ($l_u = 0$). The counterstresses applied to the ground mass by the tunnel support reduce the extent of the yielded zone around the support in the plane strain region. This "collapse" of the plastic zone, which was found in all of the cases we analyzed, is somewhat different from the findings obtained by Ranken and Ghaboussi (7); in their elastoplastic analyses, installation of the support prevented any further increases in the extent of the yielded zone but did not reduce its size in the region of plane strain. From conceptual considerations, however, a decrease in the extent of the yielded zone would be expected after the support is installed. Excavation causes a radial unloading and tangential loading of the ground

Figure 8. Effect of support delay on final radial ground displacement.

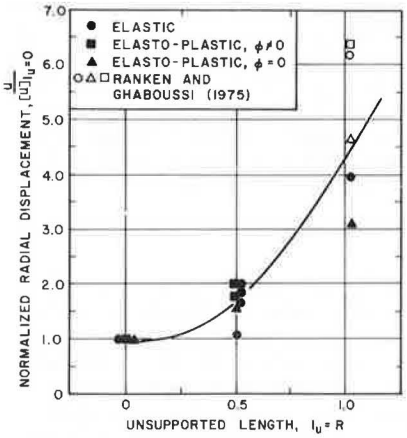

Figure 9. Effect of support delay on support thrust.

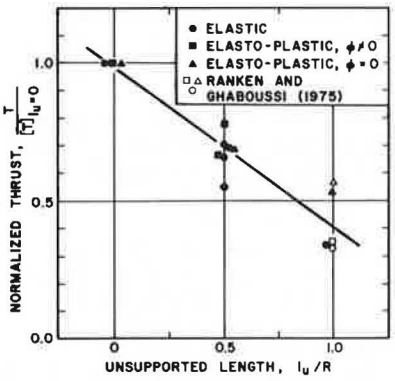

Figure 10. Effect of ground yielding on final radial ground displacement.

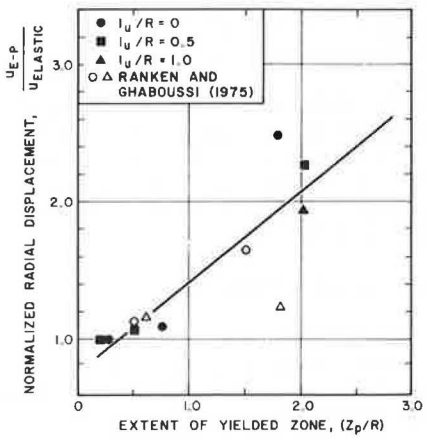

Figure 11. Effect of ground yielding on support thrust.

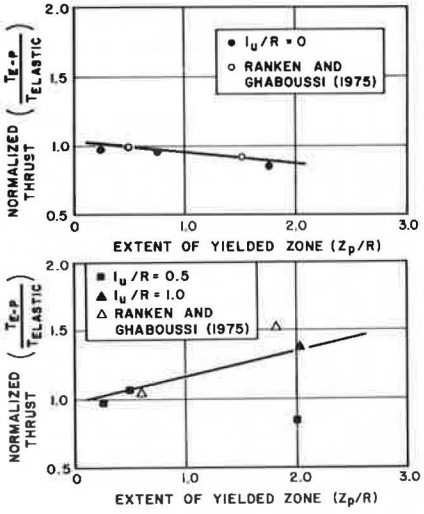

near the tunnel wall; interaction with the support reverses the sense of this loading and should therefore cause a partial return to elastic behavior.

The effect that the delay of the support installation has on radial displacements is shown in Figure 8. The final radial ground displacements have been normalized by dividing by the equivalent displacements for the fully supported cases ($l_u = 0$); thus, the figure shows the percentage increase in ground displacements that results only from the support delay. A delay of 0.5R yielded a 70 percent average increase in radial ground displacements; further increasing the delay to 1.0R increased the ground movements 350 percent above the fully supported cases. Whereas the elastic and frictional ($\phi \neq 0$) elastoplastic analyses yielded similar percentage increases in ground movements, the increases for the purely cohesive ($\phi = 0$) elastoplastic analyses were smaller, possibly because of the absence of postfailure dilatancy in the $\phi = 0$ analyses.

Figure 9 shows the corresponding effect that support delay has on support thrust. In this figure, the support thrusts obtained from the finite element analyses have been normalized by using the thrusts calculated from the closed-form, plane strain solution (Table 2). As expected, based on the qualitative behavior described earlier and on Figure 4, delaying the support installation substantially reduces the support forces: A delay of 0.5R yielded a decrease in thrust of about 30 percent. Further increasing the support delay to 1.0R had a variable effect on support thrust. The increase in delay reduced the support thrust for the elastic cases by another 30 percent; however, in the elastoplastic cases the thrust decreased only slightly as the delay was increased from 0.5R to 1.0R. The additional yielding in these elastoplastic cases appears to have counteracted any benefits of the longer support delay.

The last factor considered in this study was the effect of failure in the ground mass on ground displacements and support forces. As expected, based on the earlier qualitative prediction and on Figure 5, ground yielding or failure should increase ground displacements and support forces. Figure 10 shows the increase in ground displacements obtained from the analyses. The vertical axis represents the final radial displacements in the elastoplastic cases divided by the equivalent elastic displacements, and the horizontal axis represents the amount of ground yielding measured by the extent of the plastic zone ahead of the face (Z_p). There is considerable scatter in the data, but the general trend is an increase in displacements with increased yielding.

The effect of ground yielding on support forces was inconclusive. As shown in Figure 11, increased ground yielding in the fully supported cases ($l_u = 0$) slightly decreased support thrusts. In the partially supported cases ($l_u = 0.5$R and 1.0R), however, increased yielding in the ground mass did increase support forces but by

an unexpectedly small amount. An interaction appears to take place in which the detrimental aspects of ground yielding are counteracted by the beneficial effects of support delay. Yielding of the ground mass increases the distance between the tunnel support and the unyielded, stiffer ground regions ahead of the face and results in what might be called an increase in the effective unsupported length. In some instances, this effect might lead to a net reduction in the support thrusts. This is one possible explanation for the slight decrease in support thrust that occurred in the fully supported tunnels as the extent of the yielded zone increased.

CONCLUSIONS AND RECOMMENDATIONS

This study has attempted to show the following effects that support delay, ground yielding, and relative support stiffness have on the ground displacements around a tunnel and on tunnel support loads:

1. Support delay—Out of the three major variables considered in this study, delay in the support installation had the most dramatic effect on tunnel performance. Delaying the support installation to a point one tunnel radius behind the face increased the average radial ground movements by 350 percent and decreased the average support thrust by 60 percent. These findings agree well with the qualitative predictions.
2. Ground behavior (yielding or nonyielding)—The results of the finite element analyses were inconclusive on this point. Yielding in the ground mass increased radial ground movements in all cases, but it decreased the support thrusts in the fully supported cases (support installed at the face) and increased the thrust in the partially supported tunnels (support installed one-half to one radius behind the face). Qualitatively, ground yielding should increase both ground displacements and support thrusts in all cases. There appeared to be some interaction between the detrimental aspects of ground yielding and the beneficial effects of support delay. In some cases, ground yielding might be considered to increase the total distance between the support and the stiff, unyielded ground ahead of the face or, in other words, to increase the effective support delay.
3. Relative stiffness of ground and support—Increasing relative stiffness (as measured by the compressibility ratio) by over two orders of magnitude reduced support thrusts by nearly 1700 percent. However, radial ground movements depended primarily on the absolute ground stiffness rather than the stiffness of the ground relative to the support.

The forces in the tunnel support can be reduced by delaying the support installation or by decreasing the stiffness of the support relative to the ground. However, this reduction may be offset by the accompanying increase in ground yielding (especially if the ground is strain-softening). The radial movements of the ground increase with increasing support delay and decrease with increasing ground and support stiffness. The optimum combination of support delay and support stiffness that minimizes the support loads depends also on the amount of yielding in the ground mass. Although further investigations are required to assess the full effect of ground yielding (particularly for strain-softening ground behavior, which was not considered in this study), this study does show the beneficial effect of small support delays (unsupported length = 0.5 to 1.0 radius) and moderate reductions in support stiffness on tunnel support loads.

ACKNOWLEDGMENTS

The research in which the conceptual studies and, in particular, the analytical studies were performed was sponsored by the University Research Program of the U.S. Department of Transportation. R. K. McFarland, Office of the Secretary, was technical monitor. A. Azzouz and K. J. Bathe made important contributions to the analytical study. A part of the conceptual study was based on a master's thesis by E. Steinhauer (8).

REFERENCES

1. Analytic Modeling of Rock-Structure Interaction. Agbabian Associates and Advanced Research Projects Agency, U.S. Bureau of Mines, 1973; NTIS, Springfield, VA, AD-761 648.
2. K. J. Bathe. ADINA—A Finite Element Program for Automatic Dynamic Incremental Nonlinear Analysis. Acoustics and Vibration Laboratory, Mechanical Engineering Department, Massachusetts Institute of Technology, Rept. 82448-1, 1976.
3. K. J. Bathe. Static and Dynamic Geometric and Material Nonlinear Analysis Using ADINA. Acoustics and Vibration Laboratory, Mechanical Engineering Department, Massachusetts Institute of Technology, Rept. 82448-2, 1976.
4. H. H. Einstein, C. W. Schwartz, W. Steiner, M. M. Baligh, and R. E. Levitt. Improved Design for Tunnel Supports. U.S. Department of Transportation, final draft rept., June 1977.
5. G. Lombardi. Dimensioning of Tunnel Linings With Regard to Construction Procedures. Tunnels and Tunneling, Vol. 5, No. 4, July-Aug. 1973, pp. 340-351.
6. R. B. Peck. Deep Excavations and Tunneling in Soft Ground. Seventh International Conference on Soil Mechanics and Foundation Engineering, Mexico City, State-of-the-Art Volume, 1969, pp. 225-290.
7. R. E. Ranken and J. Ghaboussi. Tunnel Design Considerations: Analysis of Stresses and Displacements Around Advancing Tunnels. Federal Railroad Administration, U.S. Department of Transportation, Rept. FRA-ORD 75-84, 1975.
8. E. R. Steinhauer. Effects of Ground Behavior on Tunnel Supports. Massachusetts Institute of Technology, MSc thesis, 1976.

Tunnel-Boring Penetration Rate and Machine Design

F. D. Wang and Levent Ozdemir, Colorado School of Mines

The experimental and theoretical findings of an ongoing research program on tunnel borability at the Colorado School of Mines are presented. A theoretical approach has been used to formulate predictor equations to calculate the forces involved in rock cutting with sharp and dull disc cutters. Concurrent with the theoretical analysis, extensive laboratory testing was undertaken with both sharp and artificially dulled disc cutters. These tests were carried out in three rock types and with full-size field cutters. Penetration, spacing, and edge angle, in that order, were found to affect cutting forces to a large extent whereas cutter diameter was found to be a variable of small significance. The effect of cutter wear on cutter forces was found to depend on the spacing of cuts and to decrease with increased spacing. It was concluded that wear is more detrimental to cutter performance at closer spacing of cuts. Predicted cutter forces were found to agree very well with those measured in laboratory cutting experiments. The theoretical behavior of dull cutter forces confirmed experimental observations in that the closer cuts were spaced the greater was the reduction in cutting efficiency of a disc cutter because of wear. Field boring data from a Jarva machine currently in operation in Chicago were procured and compared with predicted values, and agreement was very good. This represents an initial success in the application of the predictor equations to boring cases in the field.

The need for more efficient, faster underground excavation techniques has been well expounded in the literature in recent years. Mechanical tunnel boring offers a great potential for meeting the requirements of efficient underground excavation although its application to hard rock boring is yet to become widely accepted. Among other factors, inaccurate predictions of borability have been the major cause of many failures experienced in the application of mechanical tunnel boring to hard rocks.

This study is concerned with establishing a theoretical approach to predicting field boring performance. Because of its simple geometry and wide use in mechanical tunneling, the theoretical analysis has centered on the disc roller type of cutter. Based on the geometry of cutting and some fundamental assumptions, predictor equations have been developed to predict disc cutting forces.

This paper gives a brief account of the steps followed in deriving the predictor equations. A detailed description of these equations and an in-depth discussion of laboratory cutting tests performed concurrently with the theoretical analysis are given elsewhere (3).

THEORETICAL ANALYSIS OF DISC CUTTER-ROCK INTERACTION

Figure 1 shows an idealized representation of a system of disc cutter-rock interaction together with the parameters involved. Essentially, these parameters can be grouped in two main categories: those that describe the geometry of the disc cutter (edge angle and diameter) and those that pertain to the geometry of the cutting (cutter penetration and spacing).

Several predictor equations for disc-cutter performance are offered in the literature, but these analyses relate to a single, independent cut and therefore cannot be used to predict field borability because the effects of spacing are not known.

To formulate a predictor equation that includes the effect of spacing and other effects, a comprehensive understanding of cutter-force behavior with varying levels of spacing must be established. Miller (1) and Ozdemir (2), by using two different scales of laboratory rock-cutting devices, obtained extensive laboratory cutting data that enabled them to observe the effect of spacing on disc cutting forces. Figure 2, which shows some of their findings, shows the influence of an increase in the spacing of cuts on the vertical force required to obtain a fixed penetration. Regardless of cutter geometry and rock type, the vertical force on the cutter required to achieve a given penetration shows a continual increase as spacing increases because of the larger volume of rock that needs to be broken by each cut.

What is important, however, is the particular trend the force curve follows. As shown in Figure 3, the overall force behavior with increasing cut spacing can be divided into three distinct zones. Zone 1 covers the low spacing values that result in extensive crushing of the rock, zone 2 corresponds to those spacing values over which the force increase is nearly linear, and zone 3 includes the spacing values beyond optimum, a point at which the increase in force departs from linearity. When one examines this observed relation between force and spacing, it is not difficult to realize that the relation, especially for zones 1 and 2, can be expressed by means of a linear equation of a certain slope and intercept as shown in Figure 3. The intercept of the predictor behavior is taken as the load on the cutter that results from a series of cuts positioned on a rock surface in a situation such as that shown in Figure 4 so that complete crushing of the rock occurs. This situation exists at a spacing value somewhere within zone 1 and, depending on the exact location of this spacing, the predictor curve will be above or below or will exactly coincide with the observed behavior. Nevertheless, the arrangement of cutters shown in Figure 4 will result in individual cutter forces of

$$F_1 = C \times AC \tag{1}$$

where

F_1 = vertical force on the cutter (i.e., intercept of the predictor curve),
C = rock uniaxial compressive strength, and
AC = area of contact of the cutter with the rock measured at the level rock surface.

The area of contact is represented in Figure 5 by the shaded portion of the boat-shaped area. Note that this area is half the total contact area because the cutter is rolling over the cutter surface and the rock behind the vertical axis of the cutter is already broken and cannot exert any forces on the cutter. The desired area of contact, which can be determined from geometrical considerations, is $R^2(\phi - \sin\phi\cos\phi)\tan\alpha/2$. Thus, the intercept of the predictor curve becomes

$$F_1 = CR^2(\phi - \sin\phi\cos\phi)\tan\alpha/2 \tag{2}$$

To determine the slope of the predictor curve, the exact mechanism of rock failure between two adjacent cuts must be known.

There are two possible means by which a disc cutter can cause rock failure between adjacent cuts. Rock can

fail either by tension or by shear. A combination of these two mechanisms, one succeeding the other, is also probable. In this study, a detailed analysis of rock failure was performed for the purpose of determining which failure mode prevails. To determine the conditions in which a shear failure would be most likely to occur, several types of qualitative observations were made:

1. Analysis of fracture patterns beneath craters produced by disc cutters,
2. Examination of high-speed films of disc cutting action,
3. Microscopic examination of rock failure surfaces, and
4. Extensive observation of rock surface profiles found in laboratory studies that used disc cutters.

How a shear failure of the interlying rock material between two adjacent cuts would occur is shown in Figure 6. The figure shows the geometry of adjacent cuts and the approximate loading of the interlying material by the pressure bulb that surrounds the penetrating edge of the cutter. Finely crushed rock contained in this bulb, which behaves in a near-plastic manner, is in a state of triaxial compression and produces a hydrostatic loading on the surrounding intact rock in a fashion shown by the arrows. This loading configuration then causes a pure shear failure of the rock material that lies between two adjacent cuts. Note that it is said to be a pure shear failure since no normal loading is exerted on the failure plane. It is also believed that the radial tensile cracks formed around the pressure bulb aid in shearing action by creating an initial path for the shear plane to follow.

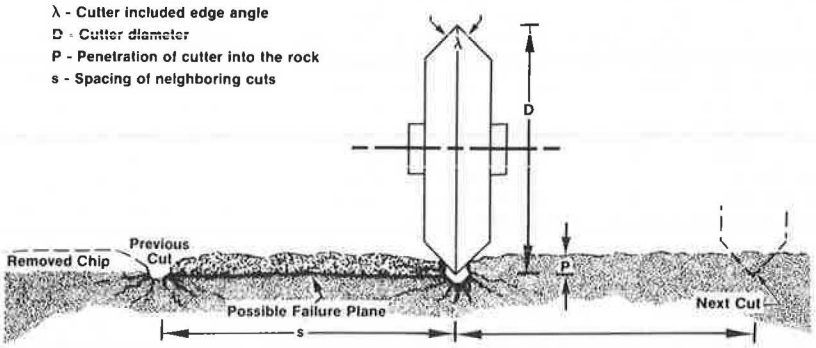

Figure 1. Rock cutting with disc cutter.

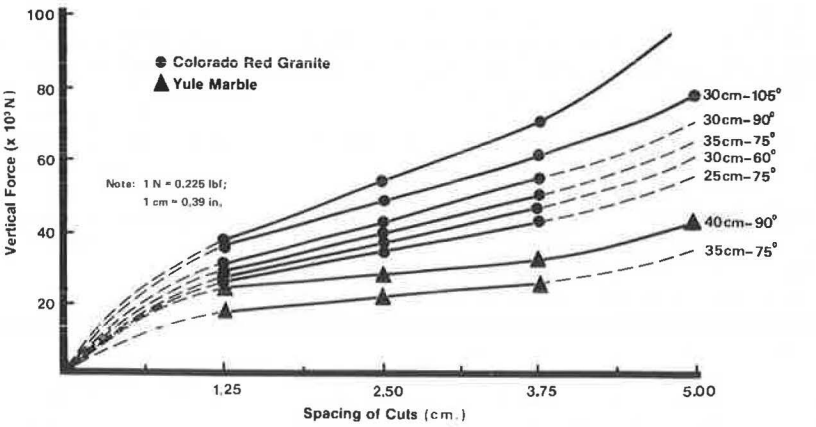

Figure 2. Vertical force versus cut spacing at fixed cutter penetration of 0.25 cm.

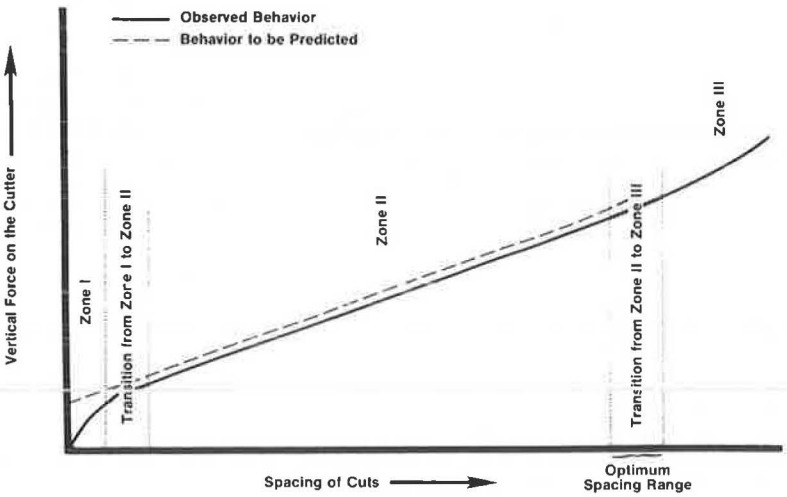

Figure 3. Vertical force versus cut spacing: observed behavior and behavior to be predicted.

Once the occurrence of a shear failure of rock material between two adjacent cuts is determined, the second part of the predictor equation—the part that defines the slope—can easily be obtained by determining the force required to cause this shear failure. Consider the idealized multiple-cut situation shown in Figure 7. The crushed zone was not superimposed in this figure to preserve graphical clarity. To generate a shear failure of rock toward the existing cut or cuts, the side force f_s should be large enough to overcome shearing resistance. That is,

$$f_s = \tau \times SA \quad (3)$$

Figure 4. Limiting condition of interaction of adjacent crushed zones.

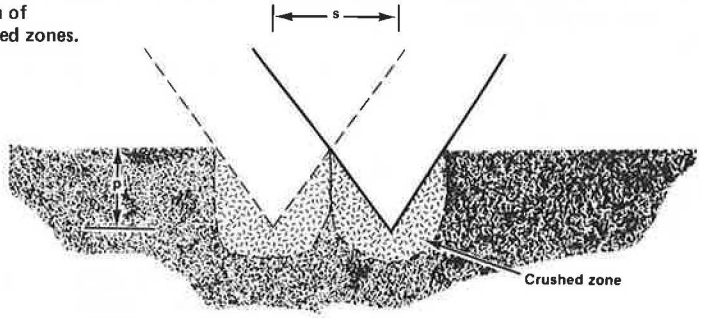

Figure 5. Area of contact of disc cutter with rock.

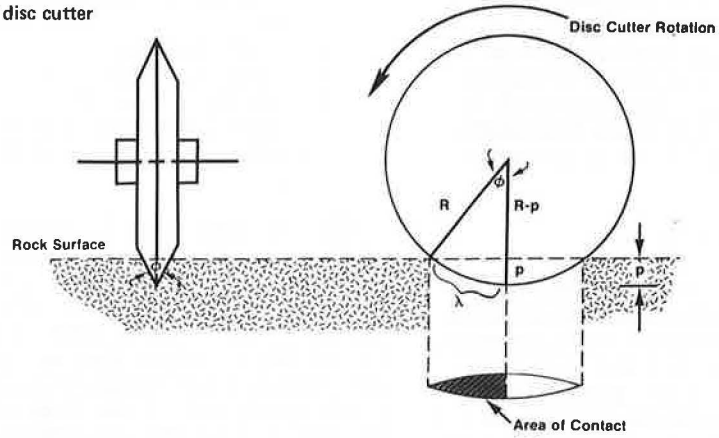

Figure 6. Shear failure of rock between adjacent cuts.

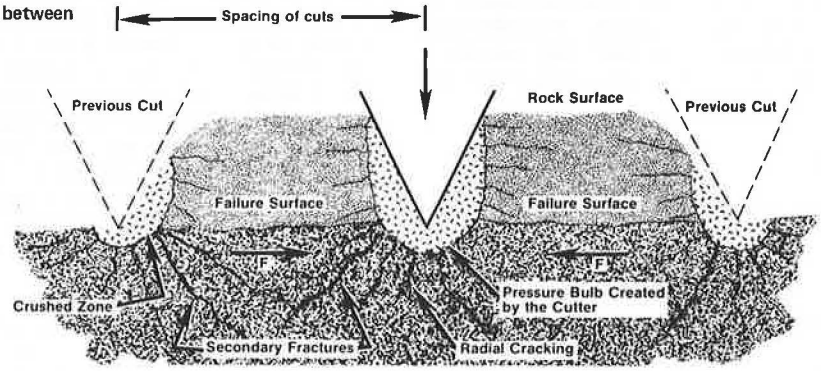

Figure 7. Geometry of disc penetration.

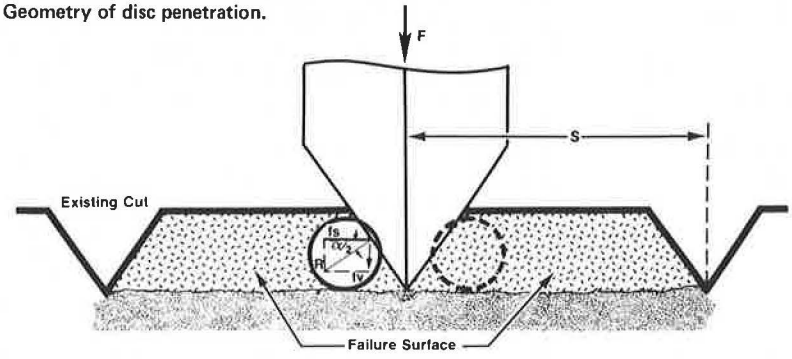

where

τ = rock unconfined shear strength (cohesion) and
SA = area of failure surface.

At the instant of chip formation, the failure surface will have a nearly rectangular configuration with a length that approaches the chord length (Figure 5) and a width approximately equal to the spacing of the cuts minus the width of the crushed zone. Thus, the area of the failure surface is $SA = R\phi(s - 2p \tan\alpha/2)$, which results in the following expression for side force:

$$f_s = \tau R\phi(s - 2p \tan\alpha/2) \quad (4)$$

Assuming there is no cutter-rock friction, the resultant is perpendicular to the side of the cutter edge. Therefore, we can write $f_v = f_s \times \tan\alpha/2$ or $f_v = \tau R\phi(s - 2p \tan\alpha/2)\tan\alpha/2$ since $F_2 = 2f_v$; then

$$F_2 = 2\tau R\phi(s - 2p \tan\alpha/2) \tan\alpha/2 \quad (5)$$

where F_2 is the vertical force required to shear the rock on both sides of the cutter. If there is a previous cut on only one side of the cutter, the preceding analysis and results still hold true because of a required balance of forces on the cutter edge. Having determined the two parts of the predictor equation, one then only needs to combine these two effects (Equations 4 and 5) to arrive at an equation for the total vertical force on the cutter. Thus, $VF = F_1 + F_2$ or

$$VF = [CR^2(\phi - \sin\phi\cos\phi) + 2\tau R\phi(s - 2p \tan\alpha/2)] \tan\alpha/2 \quad (6)$$

As presented, Equation 6 will provide a theoretical estimate of cutter thrust for given levels of penetration, spacing, cutter geometry, and required rock properties. However, it may be desirable, as it would be in field boring practice, to calculate the cutter penetration for a given value of cutter thrust. This can be accomplished by rearranging the equation so that the penetration is the unknown parameter, but such a process is difficult because angle ϕ is a function of penetration. It is feasible, however, to simplify the equation by inserting reasonable approximations for the cutter-rock contact area and angle ϕ, which gives

$$VF = D^{1/2} p^{3/2}[4/3C + 2\tau(s/p - 2 \tan\alpha/2)] \tan\alpha/2 \quad (7)$$

The results provided by Equation 7 were found to be in excellent agreement with those from the exact solution (Equation 6) with a maximum deviation of around 2 percent for the most likely levels of pertinent variables.

Rearranging Equation 7 gives

$$(4/3C - 4\tau \tan\alpha/2)p^{3/2} + 2\tau s p^{1/2} - (VF/D^{1/2} \tan\alpha/2) = 0 \quad (8)$$

which can then be solved for penetration by using various methods given in the literature.

The rolling (tractive) force on the cutter can now be obtained by multiplying the developed vertical force equation (Equation 7) by a constant that reflects the geometrical relation of these two force components. This constant (3) is commonly referred to as the cutting coefficient ($C\bar{C}$) and is found to be

$$CC = (1 - \cos\phi)^2/(\phi - \sin\phi\cos\phi) \quad (9)$$

where $\phi = \cos^{-1}[(R - p)/R]$.

Since rolling force (RF) is defined as $RF = VF \times CC$, inserting the predetermined values of VF and CC provides the following analytical expression for the rolling force:

$$RF = [Cp^2 + 4\tau\phi(s - 2p \tan\alpha/2)/D(\phi - \sin\phi\cos\phi)] \tan\alpha/2 \quad (10)$$

To summarize the results of the foregoing theoretical analysis, the following equations were derived for predicting the vertical and rolling forces on a disc roller cutter (because the equations were formulated in U.S. customary units of measurement, no SI equivalents are given):

$$VF = D^{1/2} p^{3/2}[4/3C + 2\tau(s/p - 2\tan\alpha/2)] \tan\alpha/2 \quad (11)$$

and

$$RF = [Cp^2 + 4\tau\phi(s - 2p \tan\alpha/2)/D(\phi - \sin\phi\cos\phi)] \tan\alpha/2 \quad (12)$$

where

VF = vertical force on the cutter (lbf);
RF = rolling force on the cutter (lbf);
C = rock uniaxial compressive strength (lbf/in^2);
τ = rock unconfined shear strength (cohesion, lbf/in^2);
D = cutter diameter (in);
α = cutter included edge angle (deg);
s = spacing of cuts (in);
p = cutter penetration (in); and
$\phi = \cos^{-1}[(R - p)/R]$ where R is the cutter radius (in).

The foregoing analysis and subsequently developed predictor equations expressed the force-spacing behavior with a linear equation of a certain intercept and slope. As discussed earlier, laboratory cutting results with disc roller cutters showed a linear increase in forces with increasing spacings up to an optimum value, and thereafter the increase in force followed more of a curvilinear trend. Thus, from a theoretical viewpoint, the developed equations characterized the force behavior over the spacing values below the optimum. Although the rock failure mechanism for spacings beyond the optimum is generally understood and confirmed by laboratory observations, no attempt was made to modify the developed equations to describe the force behavior in this region because (a) the problem appears to be complicated and probably needs a separate, in-depth study and (b) force behavior in this region does not depart appreciably from linear trend, especially up to maximum spacing values [about 7.5 cm (3 in)] commonly used on hard-rock-boring machines. Thus, the developed prediction equations are assumed to apply to spacings beyond the optimum as well.

The developed predictor equations are meant to be used in estimating forces on sharp disc cutters. Since most tunnel-boring machines operate with cutters in some stage of dullness, the developed equations should be modified to consider the effect of wear on cutter performance. Before any modification, the wear surface to be analyzed should be defined. In this study, a toroidal wear surface was chosen to describe the geometry of worn disc cutters based on a survey of patterns of cutter wear in the field and discussions with manufacturers of cutters. Assuming a toroidal wear surface, the equations developed for sharp disc cutters were then modified to incorporate the presence of a wear surface along the cutter edge, providing a new set of equations for estimating the forces on dull disc cutters. Because of the complexity and length of the resulting equations, those equations are not presented in this paper. The equations and a detailed description of the steps

followed in their derivation are given elsewhere (3).

LABORATORY EQUIPMENT, INSTRUMENTATION, AND TESTING PROCEDURE

The laboratory testing for this investigation was carried out by using a large, stiff, linear rock-cutting machine. This equipment has been described in full elsewhere (1, 2, 3). The instrumentation included a triaxial load cell capable of resolving the load on the cutter into its three mutually perpendicular components and time-based digital integrators for recording forces.

The average values of the three force components (vertical, rolling, and side) were measured, and peak readings were taken. Occasionally, XYY′ plotters were introduced into the bridge circuits to provide analog copies of cutter forces and to allow visual observation of their behavior and interdependence.

The rock types tested were samples of St. Cloud gray granodiorite [trade name Charcoal Gray Granite (CG)], Holston limestone [trade name Tennessee Marble (TM)],

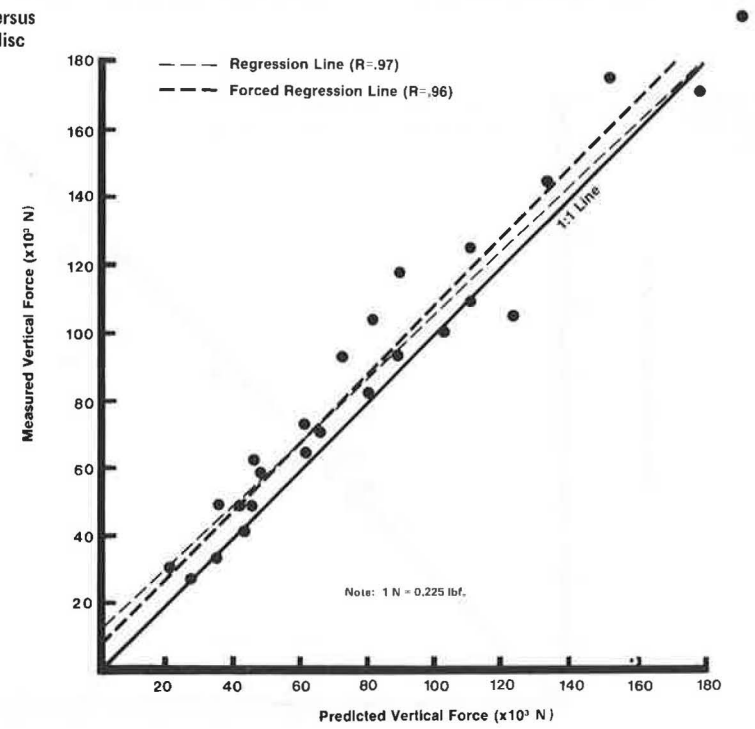

Figure 8. Predicted vertical forces versus vertical forces measured with sharp disc cutters in Colorado Red Granite.

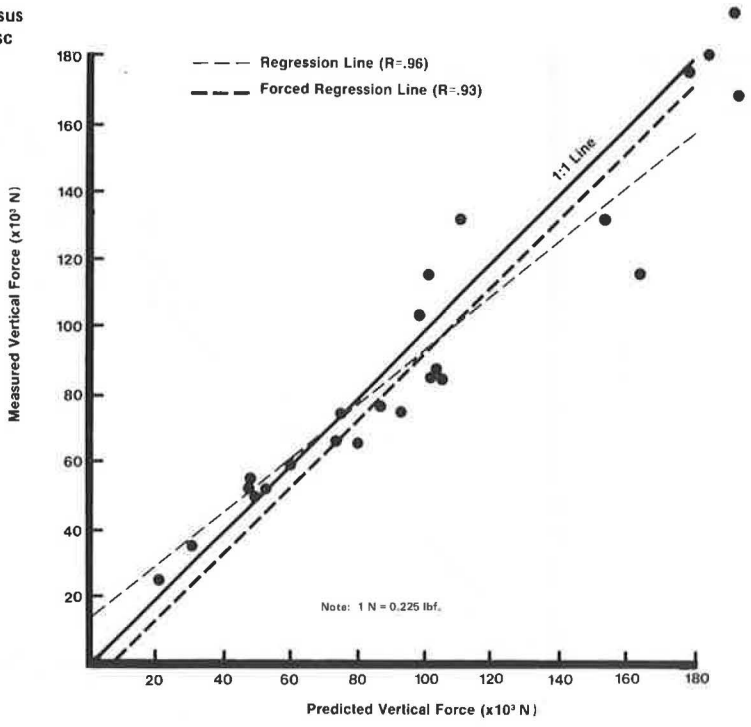

Figure 9. Predicted vertical forces versus vertical forces measured with sharp disc cutters in Charcoal Gray Granite.

and orthoclase-bladed porphyritic granite of the Colorado red granite type [trade name Colorado Red Granite (RG)].

The testing procedure involved setting the disc at the required level of penetration and then traversing it over the rock surface and measuring the forces that act on the cutter. Each test consisted of making several passes over the rock surface; each pass contained several cuts taken at a fixed spacing. The test started with a smooth rock surface. Data for the first two or three passes were discarded, and these passes were used to condition the rock to create a rock surface similar to that found on a tunnel boring face.

The entire laboratory testing was carried out at a cutting velocity of 25 cm/s (10 in/s). This choice was based on the experimental results reported by Ozdemir (2) since cutting velocity was found not to affect cutter forces in the range above 12.5 to 25 cm/s (5 to 10 in/s).

LABORATORY CUTTING RESULTS

A very ambitious laboratory testing program was carried out with both sharp and artificially dulled disc cutters. All of these tests were performed according to designed experimental plans to permit the application of various statistical procedures to cutting results. For tests with sharp disc cutters, Latin square experimental

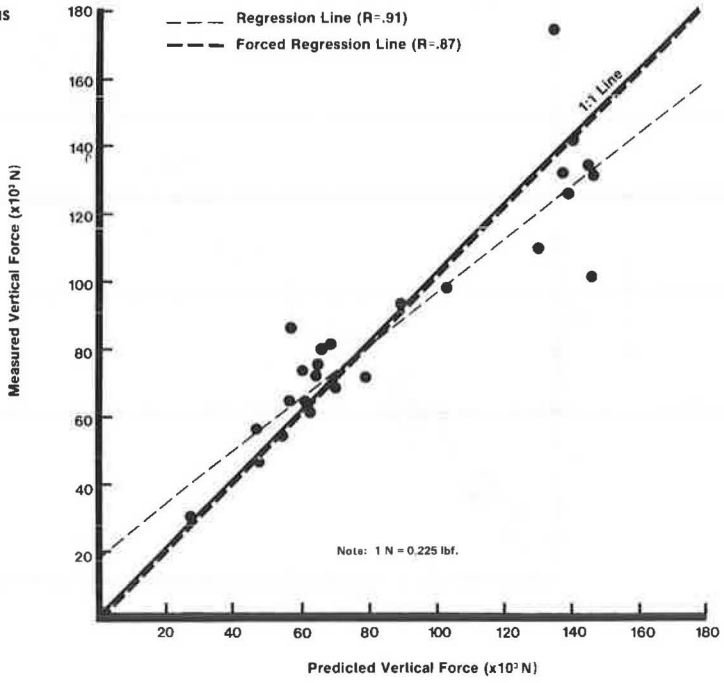

Figure 10. Predicted vertical forces versus vertical forces measured with dull disc cutters in Colorado Red Granite.

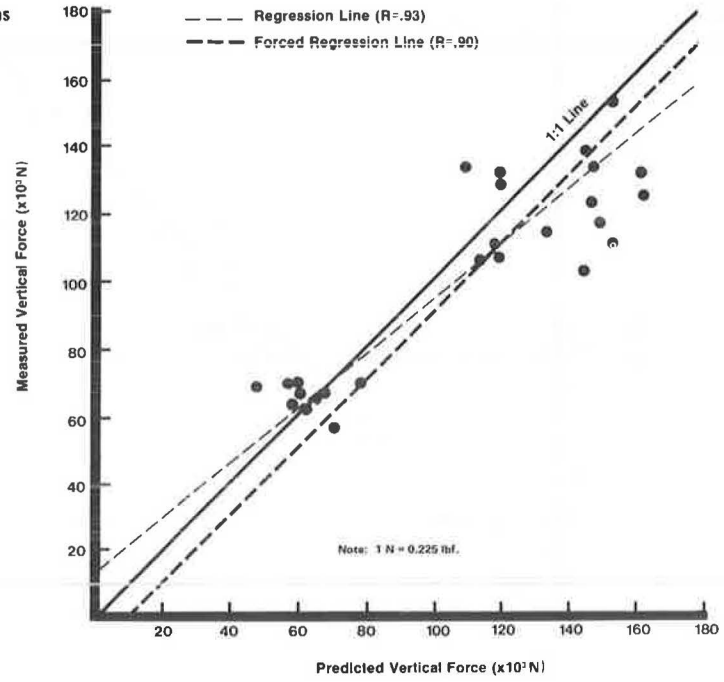

Figure 11. Predicted vertical forces versus vertical forces measured with dull disc cutters in Charcoal Gray Granite.

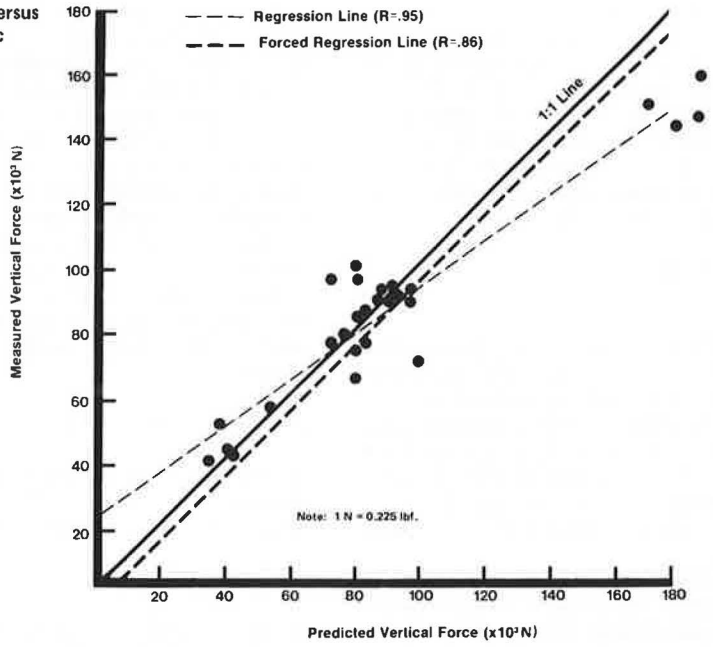

Figure 12. Predicted vertical forces versus vertical forces measured with dull disc cutters in Tennessee Marble.

Table 1. Comparison of predicted and measured penetration rates for tunnel-boring machine in use in Chicago.

Station	Machine Thrust Pressure (kPa)	Machine Thrust (kN)	Rate of Penetration (m/h)	
			Measured	Predicted
269+41	13 793	6703	1.69	1.59
269+41	17 241	8379	2.33	2.22
266+27	18 620	9050	2.36	2.48
258+73	18 275	8880	2.27	2.42

Notes: 1 kPa = 0.145 lbf/in^2; 1 kN = 225 lbf; 1 m = 3.3 ft.
Average rock unconfined compressive strength during tests = 81 896 kPa (11 875 lbf/in^2), average rock tensile strength during tests = 9724 kPa (1410 lbf/in^2), and estimated rock shear strength (cohesion) during tests = 13 103 kPa (1900 lbf/in^2).

plans were constructed and used for cutting each type of rock; each plan included the following variables and their respective levels (1 cm = 0.39 in and 1 mm = 0.039 in):

Variable	Level
Cutter edge angle (α), °	60, 75, 90, 105, 120
Cutter diameter (D), cm	20, 25, 30, 35, 40
Cutter penetration (p), mm	1.25, 2.5, 3.75, 5.0, 6.25
Spacing of cuts (s), cm	2.5, 3.75, 5.0, 6.25, 7.5

The cutting results obtained from testing many planned combinations of the above levels of the variables were analyzed to determine the relative significance of each variable in affecting cutter forces and also to establish empirical relations between each variable and the cutter forces. Penetration, spacing, and edge angle, in that order, were found to affect cutter forces significantly whereas cutter diameter was shown to be a variable of minor significance.

In tests that used artificially dulled disc cutters, the following variables and their levels were investigated:

Variable	Level
Cutter edge angle, °	60, 75, 90
Cutter wear (measured as tip loss w), mm	1.56, 3.90, 6.25
Cutter penetration, mm	1.25, 2.5, 3.75
Spacing of cuts, cm	2.5, 5.0, 7.5
Rock type	RG, CG, TM

In these tests, a partial factorial design that required a total of 81 laboratory tests was constructed and used. The results showed the pertinent variables to affect the dull cutter forces in much the same way that they affect sharp-disc cutter forces. That is, the presence of wear surface along the cutter edge did not seem to affect the characteristic behavior of disc cutter forces at increasing levels of the variables investigated. It was also found that the degree to which cutter wear affects cutter forces depends on the spacing of cuts and becomes smaller with increasing spacing. It was concluded that cutter wear would have a small effect on boring performance for the spacing values most commonly used on tunnel-boring machines equipped with disc roller cutters [about 7.5 cm (3 in)]. Cutter wear, however, was found to reduce cutting efficiency considerably when cuts were spaced close to each other.

COMPARISON OF EXPERIMENTAL AND THEORETICAL RESULTS

By using the developed predictor equations (Equations 7 and 10), theoretical force values were calculated and compared with those measured in laboratory tests performed with sharp and artificially dulled disc cutters in three rock types. The goal of successfully predicting the vertical force on the cutter was given the most attention because it is the vertical force on the cutter that determines how much the cutter can penetrate a given type of rock at a given cut spacing.

To observe visually the degree of correlation, the theoretical vertical force values are plotted against the measured ones in Figures 8 through 12. At first glance, these figures indicate good agreement between the measured and predicted vertical forces. To assign a form of statistical confidence to the degree of correlation, two separate regression analyses—standard and forced—were performed. The former is a well-known regression technique that uses the least-squares analysis method. The latter constitutes the regression line, which has an imposed slope of one. That is, the slope was taken as one, and thereafter the intercepts and the correlation coefficients were determined for each set of data by regression analysis. As seen in these figures, the correlation coefficients for all rock types tested are high enough to confirm the validity of the developed equa-

tions for both sharp and dull cutters.

For rolling forces, again the predicted and the measured values agreed very well, but the correlation coefficients were lower than they were for the vertical forces. It was suggested that ignorance of the cutter bearing friction in the development of the rolling force equation and the enormous sensitivity of rolling force to cutter penetration were responsible for the observed deviation of the predicted and measured values.

PREDICTION OF FIELD BORING PERFORMANCE

The field boring data supplied by Jarva, Inc., from one of their machines currently in operation in Chicago provided an excellent opportunity to verify the developed predictor equations for their applicability to predictions of field boring performance. Since the Chicago machine is boring through a relatively homogeneous and competent dolomitic limestone formation with very little jointing, the field data were considered ideal for comparison with the predicted values.

Theoretical advance rates were calculated by using a computer program that incorporated the developed predictor equations and was specifically written for use in predictions of field boring performance. The calculated advance rates and actual rates measured in the field are given in Table 1. The predicted rate of penetrations is clearly very close to those measured. This initial success in predicting field boring performance does not, of course, mean that the equations can be universally applied to cases of tunnel boring. To arrive at such a conclusion, more field data from different machines operating in different rock formations must be collected and compared with predicted data.

SUMMARY AND CONCLUSIONS

The developed predictor equations successfully predicted the forces acting on disc roller cutters in laboratory studies of borability with sharp and artificially dulled disc cutters. Moreover, they closely predicted the field rate of penetration of a Jarva tunnel-boring machine currently operating in dolomitic limestone in Chicago.

It is obvious that more field boring data must be collected and compared with the predicted values before the equations can be considered universal. In addition to parameters of machine design and operation, these data should also include any existing geological features in order to understand their effect on the predicted values.

Future work on this project will concentrate on collecting and procuring more distinct field boring data. The theoretical analysis performed for disc roller cutters will also be extended to include other commonly used rolling cutters such as disc-button and multikerf cutters.

ACKNOWLEDGMENTS

We wish to express sincere appreciation to the National Science Foundation for their financial support and to Jarva, Inc., for supplying the field data.

REFERENCES

1. R. J. Miller. Laboratory Analysis of Small and Large Scale Cuttings of Rock for Improvement of Tunnel Boreability Prediction and Machine Design. Colorado School of Mines, Golden, PhD thesis T1629, 1974.
2. L. Ozdemir. A Laboratory and Field Investigation of Tunnel Boreability. Colorado School of Mines, Golden, MSc thesis T1755, 1975.
3. L. Ozdemir, R. J. Miller, and F. D. Wang. Mechanical Tunnel Boring—Prediction and Machine Design. Colorado School of Mines, Golden, Annual Rept. to National Science Foundation, 1977.

Notice: The Transportation Research Board does not endorse products or manufacturers. Trade names appear in this report because they are considered essential to its object.

Soft-Ground Tunneling by Ground Freezing: A Case History

John S. Jones, Law Engineering Testing Company, Washington, D.C.
Ralph E. Brown, Law Engineering Testing Company, Atlanta

A brief introduction to artificial ground freezing for temporary excavation retention during construction is presented. The major aspects that affect the suitability of ground freezing in a particular project are discussed. To illustrate the applicability of artificial ground freezing, a case history in Washington, D.C., is presented. The project consisted of a circular 3.8-m (12.5-ft) diameter sewer tunnel approximately 33.5 m (110 ft) in length that passed 2.7 m (8.9 ft) beneath four sets of railroad tracks. The design process, including the frozen-soil laboratory testing program and the computer modeling, is presented. An instrumentation program was used during construction to monitor the performance of the project. The instrumentation consisted of thermocouples to monitor ground temperatures and elevation monuments to monitor ground movement during construction.

Temporary ground freezing is one of the more promising techniques for soft-ground tunneling. Ground freezing is particularly suitable where more conventional systems such as grouting or compressed air are unfeasible since ground freezing is effective in any soil that contains some pore water. Stratification and variations in permeability have little effect on freezing but can seriously affect the success of grouting. Fine sands and silts can be successfully frozen but are difficult if not impossible to grout because of their low permeabilities. Freezing eliminates the hazards of using compressed air, such as blowouts and dangers associated with working under high pressures.

The purpose of this paper is to provide an insight into

the applicability of temporary frozen-earth support systems for tunnels. The paper presents a brief introduction to ground freezing for temporary construction as well as the major factors that affect the suitability of ground freezing. These considerations are then illustrated by a tunneling case history in which ground freezing was used to support loads imposed by trains passing directly over a tunnel.

PROCESS OF GROUND FREEZING

The basic concept in ground freezing is the removal of heat from the ground so that the pore water freezes and acts as a bonding agent (8, 19, 21). The heat removal is accomplished by using coolants that circulate through pipes embedded in the zone of ground to be frozen. Currently, the most commonly used and least expensive freezing method is the Poetsch process, which was developed in Germany approximately 100 years ago. This system consists of a refrigeration plant (ammonia or Freon) used to cool a secondary coolant (usually calcium chloride brine) that is circulated through the freeze pipes embedded in the soil.

Various alternative freezing systems are also available, including a primary Freon plant with an in situ evaporator, a reliquefaction plant with an in situ second stage, and expendable refrigerant systems that use liquefied nitrogen or carbon dioxide (8, 21). These alternative methods generally offer a much lower freezing temperature and faster freezing time but are currently more expensive than the Poetsch process.

The design of any freezing system requires a thorough knowledge of the mechanics of the freezing process and its effects on the soil. Some of the major considerations involved in designing a freezing system include thermal considerations, associated ground movements, strength of the frozen soil, and the cost of the freezing system. Each of these considerations is discussed below.

Thermal Considerations

A detailed discussion of the thermal design of a freezing system is beyond the scope of this paper. Therefore, only a brief overview is presented. Closed-form heat transfer solutions have been developed for very simple geometries (17). These solutions are based on two-dimensional heat conduction theory, which assumes isothermal boundary conditions at the freeze pipes and in the surrounding soil at some large distance from the pipes. The finite element method offers an alternative approach for cases of unusual geometry and complex soil stratigraphy (16).

Shuster (21) has presented a graph that shows the effect of the size and spacing of the freeze pipes on typical times required to freeze a zone of soil by various types of freezing methods (Figure 1). Additional factors that affect the time required to freeze a zone of soil include the thermal properties of the soil and coolant and the rate of groundwater flow (21). The freezing time is directly proportional to the energy to be removed from the ground and inversely proportional to the required freezing temperature. The thermal energy requirements are also related to the water content of the soil. As a rough rule of thumb, the energy requirement in kilojoules per cubic meter of soil frozen is approximately 2200 to 2800 times the water content in percentage (21).

Available literature (3, 5, 21) indicates that most of the problems and the rare failures associated with ground freezing have been related to high rates of groundwater flow. Soil cannot be frozen if the groundwater flow introduces more energy into the zone to be frozen than is being removed by the freezing system. The maximum rate of groundwater flow that can be tolerated in using the Poetsch process is approximately 0.01 to 0.02 cm/s (0.0039 to 0.0078 in/s) (2, 17, 21).

Ground Movements

Potential ground movements associated with artificial ground freezing come from three sources: frost expansion during the freezing period, stress relief during the excavation, or consolidation during the thawing period.

Ground movements associated with frost expansion are the result of two phenomena (25). The first is the expansion of the pore water during the phase change from water to ice. The volume change during the phase change is about 9 percent; therefore, the maximum expansion is 9 percent of the pore-water volume if all of the pore water freezes and there is no drainage. If the soil can drain at the same rate at which the freezing front progresses, such as in a free-draining sand, no frost heave can occur. The second potential cause of heave is pore-water migration and ice segregation at the freezing front or in the frozen zone. This will not result in ground movement if the confining pressure is greater than the pressure developed by the freezing soil-water system. Williams (25) has developed equations for estimating when the second phenomenon will result in frost heaving. These equations are dependent on the pressures in the ice and in the water and the surface tension and radius of the ice-water interface. Figure 2 shows a graphical representation of Williams' work developed by Shuster (21). Although the figure is not precise, it does illustrate that the more fine-grained the soil is, the higher is the frost expansion pressure that is developed. However, as Figure 2 also shows, the rate of frost expansion also decreases in the types of clayey soils that experience large expansion pressures. The combined pressure curve in Figure 2 represents the maximum pressure that can be developed if a source of water is available. In clayey soils, the pressures are also influenced by temperature—i.e., they are higher for colder temperatures (10).

The second cause of ground movement, stress relaxation during excavation, is common to any excavation.

The third cause of movement is thaw consolidation. Tsytovich (22) has presented equations for calculating the time rate and magnitude of thaw consolidation. Endo (4) has observed that the amount of settlement attributable to thaw consolidation appears to be about 20 percent larger than the amount of heaving during the freezing period. This additional settlement has also been observed by various other investigators (13, 14).

Strength

Frozen soil behaves viscoplastically in that it creeps under stress. The strength and deformation of frozen soils depend on both the internal friction between soil particles and the cohesion. The internal friction component depends on ice content; grain size arrangement, distribution, and shape; and the number of grain-to-grain contacts (20). Sayles (20) has shown that the angle of internal friction of frozen Ottawa sand, after overcoming the initial peak strength, is very nearly that of unfrozen Ottawa sand. The cohesion can be attributed to (a) molecular forces of attraction between particles, (b) physical or chemical cementation of particles, and (c) particle cementation by ice formation in the soil voids (20, 24).

The behavior of frozen soil depends strongly on time, temperature, and stress level. Sayles (19) has presented the following concept of the behavior of frozen

soil under stress. When a load is applied to a frozen mass, stress concentrations occur between the soil particles at their points of contact, and this results in melting of the ice. Differential water surface tensions are produced that result in the unfrozen water migrating to regions of lower stress at which the water freezes. As a result of the melting of the ice and movement of the water, a breakdown of the ice and structural bonds occurs with plastic deformation of the pore ice and a readjustment in the soil particle arrangement, which results in the time-dependent deformation phenomenon of creep. As deformation occurs, there is a denser packing of the soil particles that results in a gain in strength attributable to an increase in internal friction between grains. At the same time, there is also a weakening in cohesion and a possible increase in the amount of unfrozen water. If the applied stress is less than the long-term strength of the frozen soil, the weakening process is offset by the strengthening. If the applied stress exceeds the long-term strength, where the strengthening process does not compensate for the weakening process, the rate of deformation increases with time. Structural failure of the frozen mass eventually results. The load-deformation curve for frozen soils is similar to the classical creep curve for metals (19).

The ultimate compressive and tensile strength of frozen soil depends strongly on the freezing temperature. Both compressive and tensile strengths increase with de-

Figure 1. Generalized relation between size and spacing of freeze pipe and required freezing time.

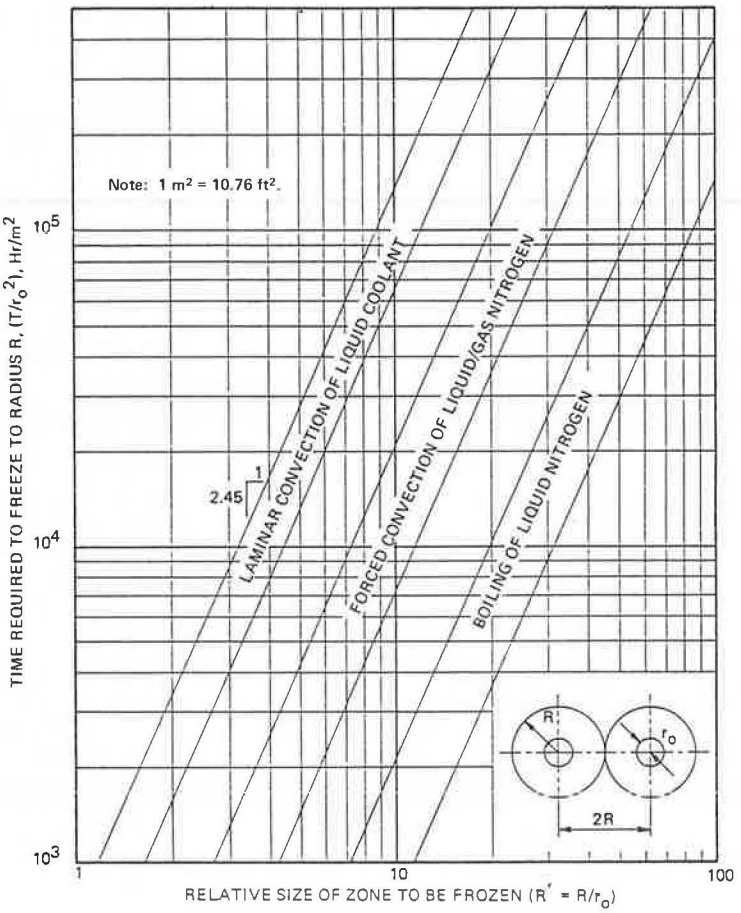

Figure 2. Typical frost expansion pressures and rates as a function of permeability.

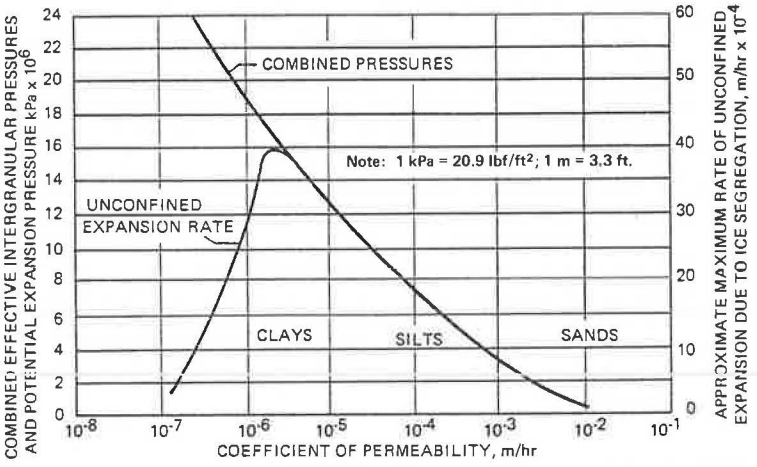

creasing temperature. The strength of frozen soil is also a function of the moisture content of the soil. The strength increases with increasing moisture content up to complete saturation.

Vialov (23) has developed equations to describe the creep of frozen soil by using the theory of hereditary creep. Sayles (18, 19) has proposed the use of equations based on strain rate. Rein (16) has proposed the use of two separate equations that define an approximate bilinear stress-strain curve that discounts a continuous stress-strain function over the entire stress range. A detailed discussion of these relations is beyond the scope of this paper.

Cost

Because so many variables influence the cost of a freezing system, it is impossible to assign a cost per cubic meter of material to be frozen. The major items that affect the cost of the Poetsch process include ground conditions, spacing of freeze pipe, the available time for freezing, and the length of time the system has to be maintained. Typical costs associated with freezing are about $\$60/m^2$ ($\$5.60/ft^2$) of frozen surface area to install a single row of freeze pipes and around $\$2$/week/$m^2$ ($\$0.18$/week/$ft^2$) of frozen surface area to maintain the system. Therefore, the length of time the system has to be maintained has a strong influence on the total cost of freezing.

In comparing the cost of a freezing system with that of more conventional systems, one also has to consider the potential cost savings that may be realized by eliminating the necessity for dewatering, compressed air, and the like. Although the freezing process often appears expensive in direct comparison with other methods, our experience indicates that many freezing systems have been less expensive than more conventional systems as a result of time and cost savings in the overall project. This has been particularly true when the contractor was able to complete the freezing portion of the project within a relatively short time period and minimize the energy costs associated with freezing.

STUDY PROJECT

To illustrate the applicability of the freezing method, a case study is presented in which ground freezing was evaluated as temporary support for a tunnel that was to pass beneath multisets of railroad tracks. The railroad company involved in the project specified that the tunnel be designed to support a Cooper E-80 engine loading on two adjacent sets of track above the tunnel. The requirement resulted in a line load of 152 kN/m (10 400 lb/ft) for each track or a distributed stress of 61 kPa (1270 lbf/ft^2).

The project consisted of a circular sewer tunnel 3.8 m (12.5 ft) in diameter in Washington, D.C. The tunnel was approximately 33.5 m (110 ft) in length and passed 2.7 m (8.9 ft) beneath four sets of railroad tracks. Figure 3 shows a plan view of the study project.

The subsurface conditions, shown in Figure 4, consisted of clayey sand, sand, and gravel with varying amounts of clay and silt to a depth of 7.6 m (25 ft). Standard penetration resistances in the material varied from 7 to more than 115 blows/m (2 to more than 50 blows/ft) with an average value of 66 (20). The average moisture content for the clayey sand material was about 34 percent. Beneath this material was a thick stratum of silt. The average standard penetration resistance in this stratum was 13 blows/m (4 blows/ft). Typical moisture contents in this lower stratum were in the range of 60 to 80 percent. The gradation characteristics of representative samples of the two materials are given below. D_{90}, D_{60}, D_{30}, and D_{10} are the grain-size diameters at 90, 60, 30, and 10 percent of the sample passing respectively (1 mm = 0.039 in):

Type of Material	Gradation (mm)			
	D_{90}	D_{60}	D_{30}	D_{10}
Clayey sand	0.7	0.2	0.008	-
Silt	0.03	0.003	-	-

DESIGN ASPECTS OF STUDY CASE

Design of a frozen tunnel requires an economic balancing of freezing temperature and time, configuration of freeze pipe, and frozen soil thickness plus verification that freezing will not damage adjacent structures or underground utilities. These factors are all interrelated and depend on such factors as the configuration and depth of the tunnel, subsurface conditions, and loading conditions. For example, as the design temperature is lowered, the strength of the frozen soil increases, thus allowing use of a thinner frozen soil zone. However, the cost of the freezing system or the freezing time increases as the design temperature decreases. As Figure 1 shows, the smaller the spacing of the freeze pipe is, the faster the soil can be frozen; however, the cost also increases as the spacing of the freeze pipe decreases. Therefore, experience and judgment are very important in obtaining an economical and safe freezing system.

Selection of a freezing temperature is an important consideration in the design process for a frozen-soil tunnel. Typical brine temperatures for commercial refrigeration plants are around -25°C to -40°C (-13°F to -40°F). A temperature of -5°C to -15°C (23°F to 5°F) can normally be attained throughout the zone to be frozen at reasonable freezing times and freeze-pipe spacings. Based on previous experience, the thermal properties of the soils, and judgments, a design temperature of -10° C (14°F) was selected for the Washington tunnel.

The configuration of the freeze pipe is a very important design consideration. The two major types of freezing configurations are (a) a circular or elliptical frozen zone in which the freeze pipes are placed horizontally around the perimeter of the tunnel and (b) an arch-shaped configuration in which the freeze pipes are placed vertically or inclined from the ground surface. The first configuration is shown in Figure 5. The freezing system must prevent bottom heave; this can be accomplished by using either configuration. Because of the relatively small diameter and length of the Washington tunnel and since access was available from the ends of the tunnel, horizontal placement of the freeze pipes was selected.

A third consideration is the thickness of the frozen soil, which has to be sufficient to provide an adequate safety factor against structural failure or excessive deformation. The selection of the soil thickness is highly dependent on the loading conditions and freezing temperature. The selected thickness must be verified by stress analyses (discussed in a later section). A 1-m (3.3-ft) thick zone of frozen soil was selected for the Washington tunnel.

The potential for frost heave and subsequent damage to adjacent structures or underground utilities also has to be considered in the design of the tunnel system. A method for analyzing the potential for frost heave has already been presented. An evaluation of the potential for frost heave at the study site indicated that approximately 5 to 13 cm (2 to 5 in) of heave could be expected—the larger amount at the south end of the tunnel where the soft silt stratum was at the bottom. Most of the anticipated heave was expected to occur as a result of ex-

pansion of the pore water in the soft silt stratum during the phase change from water to ice. It was decided that the expected amount of frost heave could be tolerated without causing damage.

The next step in the design process was to develop a laboratory test program to simulate the field behavior of the in situ frozen soils and to determine the stress and deformation states for the frozen tunnel configuration selected.

Figure 3. Plan view of Washington, D.C., tunnel.

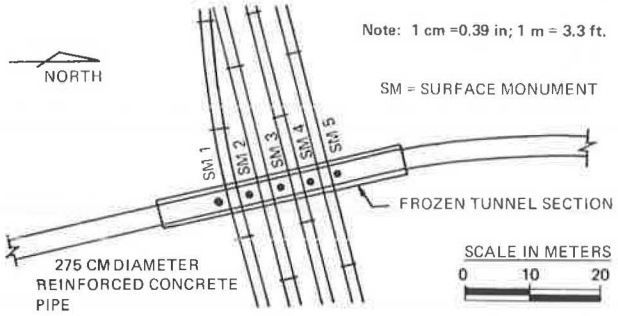

LABORATORY TESTING PROGRAM

The laboratory testing program was designed to determine the strength and deformation characteristics of the frozen soil under the specified design loading and in situ conditions. Design of the testing program consisted of selecting the type of strength tests and test temperatures, considering undisturbed versus remolded samples, and evaluating the necessity of tensile testing.

The specified design criteria required that the frozen tunnels support large-magnitude static loads until the permanent tunnel liners were installed. Therefore, long-term triaxial creep tests were conducted to obtain strength and deformation parameters for the analyses.

A freezing temperature of -10°C (14°F) was used in the testing program to simulate the average freezing temperature in the field. Since high-quality, undisturbed samples of the fill soils were impossible to obtain, remolded samples were used in the laboratory testing program. The use of remolded samples was considered acceptable since the study soils, with the exception of the soft silts near the bottom of the tunnel, did not have a sensitive structure.

Since the laboratory testing program was intended to allow an evaluation of the field behavior of the frozen soil, it was necessary to decide whether tensile stresses would occur in the field and, if so, whether tensile testing would be necessary. Our experience and the avail-

Figure 4. Subsurface conditions at tunnel section.

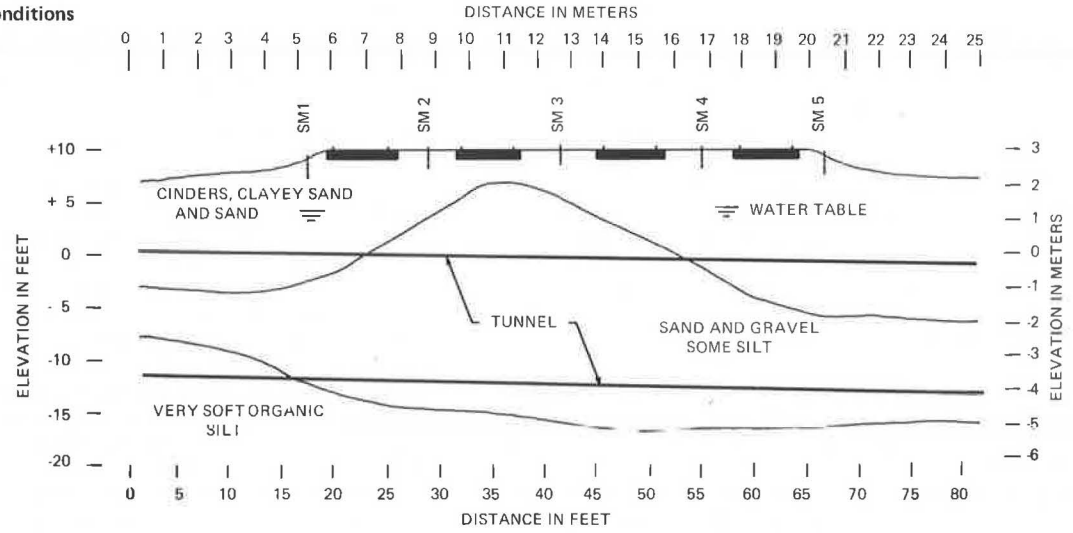

Figure 5. Frozen-soil tunnel using horizontal freeze pipes.

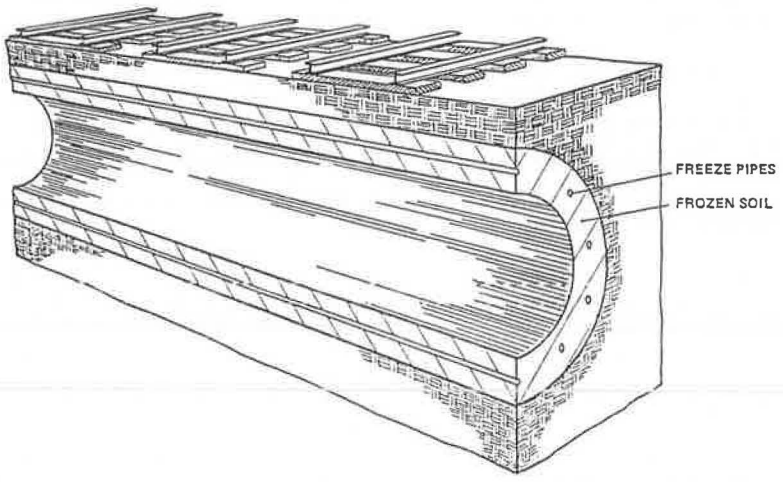

able literature both indicated that only nominal tensile stresses could be expected in the smaller tunnels. The available literature (9, 19, 22) indicated that the frozen soil would have tensile strengths in excess of the anticipated stresses. It was therefore decided not to conduct tensile tests.

Since only the very bottom of the tunnel passed through the organic silt, the strength of the frozen fill material would provide the major support for the tunnel. It was therefore not considered necessary to test the strength of the frozen silt.

Preparation of Samples

The samples were uniaxially frozen to a temperature of -10°C (14°F). Uniaxial freezing was used to simulate actual field freezing behavior since the in situ soil freezes in a radial direction emanating from the freeze pipes. A temperature of approximately 1°C (33.8°F) was maintained around and at the top of the uniaxial freezing chamber while the bottom of the chamber was maintained at the freezing temperature. The freezing chamber was sufficiently rigid to prevent radial expansion. Water was supplied to the samples since they were obtained below the water table. After a minimum freezing period of 24 h, each sample was ejected from the freezing chamber and inspected for formation of ice lenses. No ice lenses were observed during the testing program, however. Each sample was then placed in the triaxial cell after a rubber membrane was placed around the sample. The process of transferring the samples from the uniaxial freezing chamber to the triaxial cell was performed in a cold room at a temperature of approximately -10°C (14°F).

The remolded samples were formed in a split lucite mold at a predetermined water content. The split mold was designed to fit directly into the controlled freezing chamber to allow uniaxial freezing. A moisture content of 34 percent was used for the clayey sand fill in the Washington tunnel. The samples were uniformly compacted to average field densities in five equal layers. The compaction was performed with a 2.5-cm (1-in) diameter tamper. The surface of each layer was scarified before placement of an additional layer. The samples were then frozen in the uniaxial freezing chamber to the design temperature for a minimum period of 24 h. After that time, the sample was ejected from the mold, the rubber membrane was placed around the sample, and the sample was placed in the triaxial cell.

Equipment

A schematic of one of the triaxial cells is shown in Figure 6. The freezing unit used to cool the sample consists of a primary Freon refrigeration plant that cools a 190-L (50-gal) bath of agitated ethylene glycol. The ethylene glycol is pumped through the copper coils surrounding the sample as shown in Figure 6. The ethylene glycol in the coils cools the antifreeze that is used as the triaxial chamber fluid. To maintain a uniform temperature throughout the sample, the antifreeze is agitated by a motorized propeller. In addition, the samples are isolated from the base pedestal and top cap by lucite discs. The temperature throughout the system is monitored by copper-constantan thermocouples. The temperature was regulated to ±0.4°C (±32.7°F).

Procedure and Results

Static creep tests were performed on remolded samples of the clayey sand material, which would be expected to have the lowest strength and deformation properties of the fill material. Figure 7 shows a plot of the reciprocal of the applied axial stress versus the recorded time to failure. Figure 8 shows the stress-strain curves obtained for various loading times.

SUMMARY OF FROZEN SOIL PROPERTIES

The frozen soil parameters and the unfrozen soil properties selected for use in the analyses are given below (1 kPa = 20.9 lbf/ft^2 and 1 kg/m^3 = 0.062 lb/ft^3):

	Clayey Sand and Sand		Silt	
Parameter	Frozen	Unfrozen	Frozen	Unfrozen
Modulus of elasticity, kPa	95 760	28 728	-	4788
Unit weight γ, kg/m^3	1 857	1 857	-	1440
Poisson's ratio μ	0.3	0.3	-	0.45
At-rest earth pressure coefficient K_o	0.54	0.54	0.35	0.38
Angle of internal friction ϕ, °	0	20	-	0
Cohesion C, kPa	814	0	-	24

The slope of the stress-strain curve for the frozen soil for various loading times indicated the material could be modeled by hyperbolic functions. However, our previous experience and the available literature indicated the stresses in a 1-m (3.3-ft) thick zone of frozen soil would be in the linear portion of the stress-strain curve and would be nominal in the tensile range. The moduli were therefore selected for stress levels of 50 percent of the ultimate stress.

STRESS ANALYSES

The tunnel investigated in this study is transverse to the direction of train travel. To obtain an accurate determination of the stress and deformation states in the frozen soil, a three-dimensional analysis was considered. Because of economic constraints, however, it was decided to use conservative two-dimensional models.

Stress analyses were conducted in which all the tracks were assumed to be fully loaded with Copper E-80 engines. Since the ratio of the tunnel diameter to the available loading distance along the longitudinal axis of the tunnel was small, the train load could be approximated by a large area load. Therefore, a large area load that was infinite along the longitudinal axis of the tunnel was applied at the ground surface to simulate the train loading.

As discussed previously, linear elastic stress-strain moduli were used in the finite element analyses to model the behavior of the frozen soil. A plane strain finite element model was used to calculate tunnel stresses and deflections. The maximum calculated shearing stress in the frozen zone was 337 kPa (7040 lbf/ft^2); the corresponding normal stress in compression was 370 kPa (7730 lbf/ft^2). The maximum shearing stress occurred at the springline. The calculated levels of stress in the Washington tunnel were considered to be well within acceptable ranges. The maximum tensile principal stress, which occurred at the crown, was 262 kPa (5470 lbf/ft^2). The maximum shear stress at the crown was 154 kPa (3220 lbf/ft^2).

A factor of safety of two was maintained on the shearing stresses. The maximum calculated tensile stress of 154 kPa (3220 lbf/ft^2) was considered to be within an acceptable range. Haynes (9) has reported uniaxial tensile strengths greater than 2500 kPa (52 250 lbf/ft^2) for frozen Fairbanks silt at -9.5°C (14.9°F) tested at very slow strain rates.

Figure 6. Frozen soil triaxial cell.

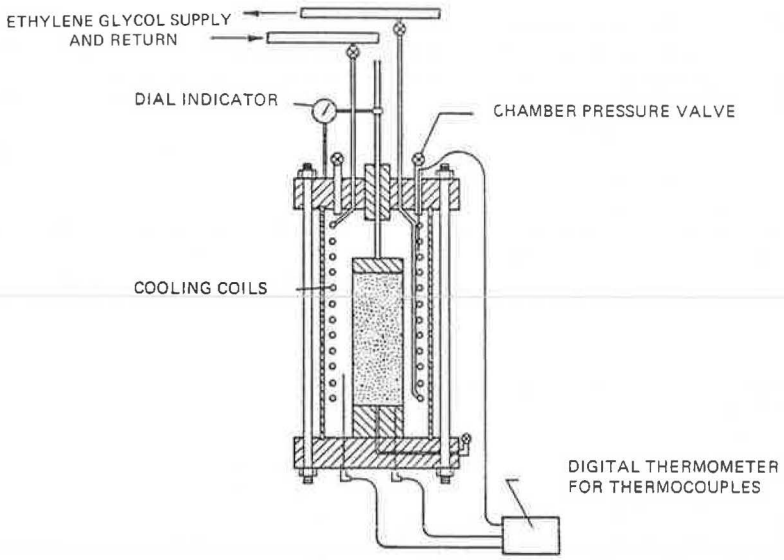

Figure 7. Triaxial test results.

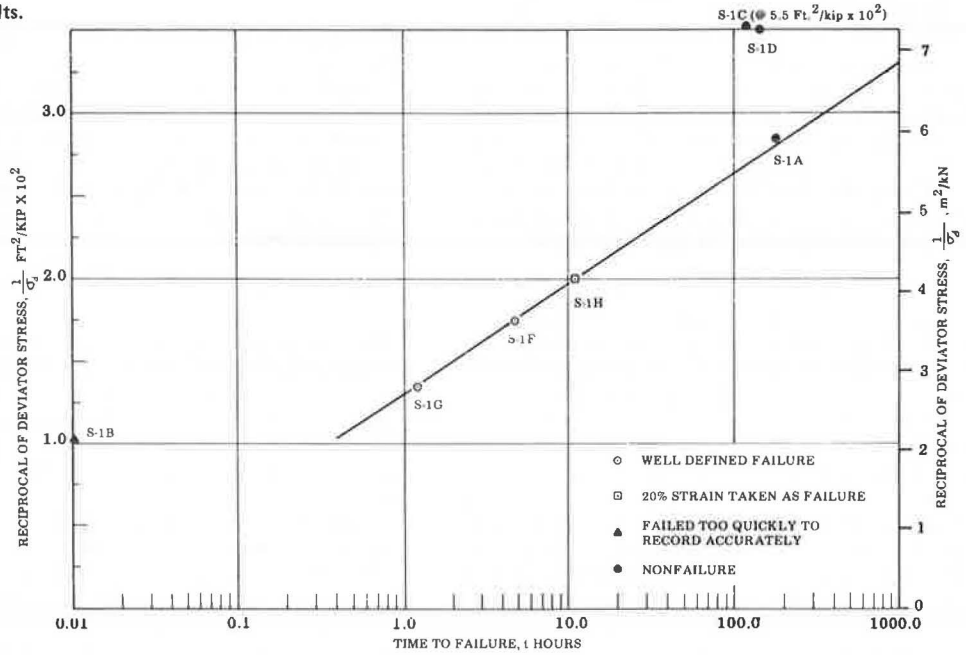

Figure 8. Stress-strain curves for clayey sand.

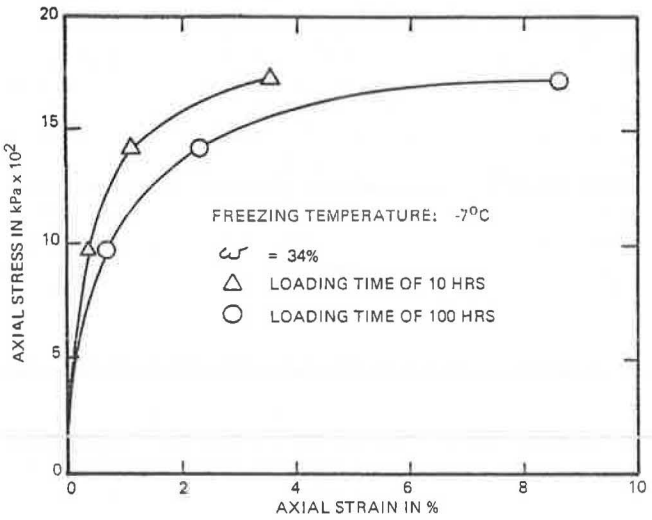

Although the calculated stresses indicated that a frozen zone of 0.9 m (3 ft) would be sufficient for structural support, the governing agencies required the thickness of the frozen zone to be 1.5 m (5 ft) to add an additional safety factor.

FIELD PERFORMANCE AND EVALUATION

Steel pipes 9 cm (3.5 in) in diameter and spaced approximately 0.9 m (3 ft) on center were used as the refrigeration pipes. To ensure closure of the freeze wall during a reasonable time period, it was necessary to have fairly accurately placed pipes or, if not, to know the deviation of the pipes. The pipes were driven from two cofferdams placed at each end of the tunnel. Placement of the pipes was first attempted by use of an air-actuated "down-hole" device that pulled the freeze pipes behind it. It was extremely difficult to maintain accurate alignment with this self-drilling device; therefore, it was decided to abandon this system in favor of horizontally driving the pipes. To improve the alignment of each

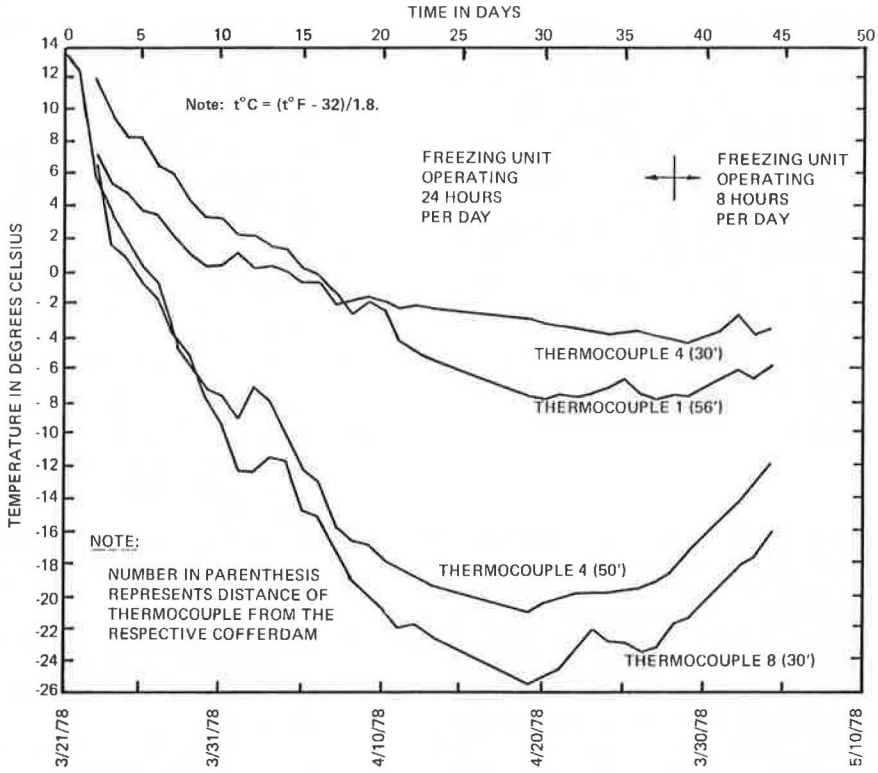

Figure 9. Readings of ground temperature over time.

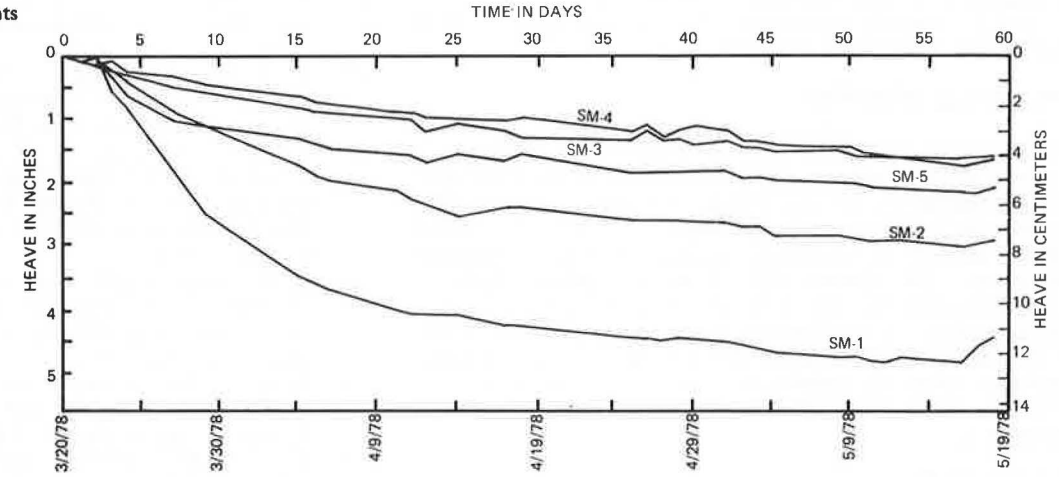

Figure 10. Heave measurements over time.

pipe, the freeze pipes were not driven from one cofferdam completely through to the other cofferdam. Instead, the pipes were driven only halfway through the tunnel distance with a 1.5-m (5-ft) overlap midway along the tunnel. The location of each freeze pipe was determined by use of a borehole deflectometer. In several instances the deflectometer revealed significant deviations of the pipe. In the areas where large deviations occurred, a second freeze pipe was installed to ensure that the required freeze zone would freeze within a reasonable time period.

Freezing was begun on March 21, 1978. Twelve thermocouples were used to record the temperature of the soil to be frozen. Figure 9 shows a time history of ground temperatures at selected locations throughout the period of freezing. Thermocouple 1 was located in a horizontal monitoring pipe installed from the north access shaft and was positioned at the eight o'clock position (southwest quadrant) in the zone to be frozen. Thermocouple 4 was in a horizontal monitoring pipe installed from the north access shaft and was positioned at the six o'clock sector. Thermocouple 1 was in a horizontal monitoring pipe installed from the south access shaft and was positioned in the three o'clock sector of the tunnel. The readings indicated that an average temperature of less than -10°C (14°F) (the design temperature) was attained in the planned frozen zone.

Mining operations were initiated on April 21, 1978, 1 month after the freezing plant was turned on. However, based on the temperature measurements, mining operations could have begun earlier than after the 1-month freezing period. Because of the extended waiting period, the inside section of the tunnel—and not just the 1.5-m (5-ft) thick annular ring as planned—was frozen. Before April 28, 1978, the freezing unit operated continuously. After that date, the freezing plant was operated on a maintenance mode, which required operation only 8 h/d. Mining operations were completed on May 22, 1978; how-

ever, the freezing unit was turned off on May 16, 1978.

Heave measurements were obtained throughout the course of the freezing operations. In addition to measuring the elevations of the railroad tracks, five permanent settlement monuments were embedded in the ground surface. The locations of the monuments are shown in Figure 3. Figure 10 shows a record of heave measurements. As expected, the major portion of heave occurred during the phase change of the pore water to ice and mainly in the soft silt material. Also as expected, the greatest amount of heave occurred at the south end of the tunnel because a greater thickness of soft silt was frozen at that end.

Unfortunately, there is currently no acceptable method for directly measuring stress in frozen soil. Therefore, there was no verification that the calculated stresses in the frozen zone were correct.

CONCLUSIONS

The design of a frozen soil lining for temporary support of a tunnel beneath mainline railroad tracks in Washington, D.C., illustrates the basic decisions that must be made during the design process for an artificially frozen ground-support system. Instrumentation data in the form of temperature readings and measurements of ground movement were obtained and presented for the study project. Although it was not possible to obtain direct data on stresses in the frozen soil, the instrumentation data provided verification of several of the design decisions. Based on this case history study and the instrumentation data obtained during the actual construction of the tunnel, ground freezing offers a viable system for use in soft-ground tunneling.

ACKNOWLEDGMENTS

The freezing project described in this paper was performed by Terrafreeze Corporation of Lorton, Virginia. Law Engineering Testing Company served as design consultant to Terrafreeze Corporation. The tunnel is owned by the District of Columbia Department of Environmental Services. The authors wish to express special appreciation to John Shuster of Terrafreeze Corporation and William Kelly of the District of Columbia Department of Environmental Services for their invaluable cooperation and assistance throughout the course of the project. Permission to publish the results of this project is appreciated.

REFERENCES

1. B. Braun and A. Macchi. Ground Freezing Techniques at Salerno. Tunnels and Tunneling Magazine, March 1974.
2. J. A. Carega and E. R. Mayer. Frozen Soil: A Material to Solve Problems in the Construction Industry. Third Inter-American Conference on Materials Technology, Mexico, 1972, pp. 57-64.
3. D. R. Ellis and J. McConnell. The Use of the Freezing Process in the Construction of a Pumping Station and Storm-Water Overflow at Fleetwood, Lancashire. Proc., Institute of Civil Engineering, London, Feb. 1959.
4. K. Endo. Artificial Soil Freezing Method for Subway Construction. Japan Society of Civil Engineers, 1969.
5. High Gorge Dam, Skagit River, Washington. Engineering News-Record, New York, March 7, 1957, and Jan. 22, 1959.
6. Novel Approach to Tunneling. Engineering News-Record, New York, July 16, 1959.
7. C. P. Gail. Tunnel Driving Using Subsurface Freezing. Civil Engineering, ASCE, Vol. 42, No. 5, 1972, pp. 37-40.
8. P. T. Goldberg and others. Lateral Support Systems and Underpinning: Volume 3—Construction Methods. Federal Highway Administration, U.S. Department of Transportation, Rept. FHWA-RD-75-130, 1975.
9. F. D. Haynes. Tensile Strength of Ice Under Triaxial Stresses. U.S. Army Cold Regions Research and Engineering Laboratory, Hanover, NH, Res. Rept. 312, 1973.
10. A. Hoekstra and others. Frost-Heaving Pressure. U.S. Army Cold Regions Research and Engineering Laboratory, Hanover, NH, Res. Rept. 51, 1959.
11. J. S. Jones and R. E. Brown. Temporary Tunnel Support by Artificial Ground Freezing. Journal of Geotechnical Division, ASCE, Vol. 104, No. GT 10, Oct. 1978.
12. G. J. Low. Soil Freezing to Reconstruct a Railway Tunnel. Journal of Construction Division, ASCE, Vol. 86, No. CO3, Proc. Paper 2639, Nov. 1960, pp. 1-12.
13. N. R. Morgenstern and L. C. Smith. Thaw Consolidation Tests on Remoulded Clays. Canadian Geotechnical Journal, Vol. 10, No. 1, 1973, pp. 25-40.
14. J. F. Nixon and N. R. Morgenstern. The Residual Stress in Thawing Soils. Canadian Geotechnical Journal, Vol. 10, 1973, pp. 571-580.
15. H. G. Poulos and E. H. Davis. Elastic Solutions for Soil and Rock Mechanics. Wiley, New York, 1974.
16. R. G. Rein, Jr., and others. Creep of Sand-Ice System. Journal of Geotechnical Engineering Division, ASCE, Vol. 101, No. GT2, Feb. 1975.
17. F. J. Sanger and C. W. Kaplar. Plastic-Deformation of Frozen Soils. International Permafrost Conference, Purdue Univ., 1963; Proc., National Academy of Sciences and National Research Council, 1966.
18. F. H. Sayles and D. Haines. Creep of Frozen Silt and Clay. U.S. Army Cold Regions Research and Engineering Laboratory, Hanover, NH, Technical Rept. 252, July 1974.
19. F. H. Sayles. Creep of Frozen Sands. U.S. Army Cold Regions Research and Engineering Laboratory, Hanover, NH, Technical Rept. 190, 1968.
20. F. H. Sayles. Triaxial Strain Rate Tests and Triaxial Creep Tests on Frozen Ottawa Sand. U.S. Army Cold Regions Research and Engineering Laboratory, Hanover, NH, Technical Rept. 253, Aug. 1974.
21. J. A. Shuster. Controlled Freezing for Temporary Ground Support. First North American Rapid Excavation and Tunneling Conference, Chicago, June 1972.
22. N. A. Tsytovich. The Mechanics of Frozen Ground. McGraw-Hill, New York, 1975.
23. S. S. Vyalov. Rheological Properties and Bearing Capacity of Frozen Soils. U.S. Army Cold Regions Research and Engineering Laboratory, Hanover, NH, Translation 74, 1965.
24. S. S. Vyalov and S. Tsytovich. Cohesion of Frozen Soil. Doklady Akademiia Nauk, Vol. 104, No. 4, 1955, pp. 527-529.
25. P. J. Williams. Ice Distribution in Permafrost Profiles. Canadian Journal of Earth Sciences, Vol. 5, No. 12, Dec. 1968.

Practical Design of Concrete Diaphragm Walls

Jerome S. B. Iffland, Iffland Kavanagh Waterbury, New York City

Diaphragm walls constructed by the slurry trench method achieve their greatest economy when it is possible to use them as part of the permanent underground structure. To use these support-of-excavation structures as permanent components of a structure, engineers must be assured of their compatibility with structures built in an open excavation. There should be consistent reliability in applied loads, levels of stress, watertightness, durability, and performance. It is suggested that the use of diaphragm walls of precast concrete panels can provide reliable strength and durability and that use of a cement bentonite grout on the backside of the diaphragm wall to displace excess slurry can meet waterproofing requirements. It is recommended that plastic analysis be combined with ultimate strength methods in the design of these walls to resolve the problem presented by the complicated residual stress patterns generated in the diaphragm wall by the construction processes of excavation; installation, prestressing, and removal of braces; and backfilling. In addition, use of a built-in hinge in the diaphragm wall at the lowest brace facilitates control of residual moments. This approach can satisfy the need for reliability in stress levels in the structure. A structure so designed and constructed will be compatible with one built in an open excavation.

A large share of both the theoretical and the experimental research currently available on the subject of diaphragm walls constructed by the slurry trench method is associated with construction methods and problems, trench stability, design of slurry, ground movements and loss of adjacent ground, and the design of these walls as temporary support-of-excavation structures. Little attention has been paid to the problems of the structural engineer when diaphragm walls are incorporated in a permanent underground structure. When these temporary support-of-excavation structures are to be permanent, the engineer is concerned with designing these walls for consistent loads, stress levels, watertightness, and durability and overall structural compatibility with the rest of the permanent structure. Criteria for the performance of temporary structures are generally not satisfactory for the performance of permanent structures.

This paper discusses some of the problems that arise when diaphragm walls are incorporated in permanent underground structures and suggests design approaches and construction details to resolve these problems. Included is a discussion of soil-structure interaction, soil properties, temporary and permanent loading conditions, effects of construction excavation and bracing procedures and techniques, the advantages of precast concrete walls over cast-in-place concrete walls, methods of establishing continuity between the diaphragm wall and the remaining portions of the permanent structure, concrete durability and quality, and watertightness. Based on the discussion and the conclusions drawn, a design synthesis for incorporation of diaphragm walls in permanent underground structures is recommended. The design philosophy is presented from the point of view of the structural engineer rather than from that of the geotechnical engineer.

NOTATION

The following symbols are used in this paper:

c = cohesion intercept,
K_o = coefficent of at-rest lateral earth pressure,
ϕ = internal angle of friction,
γ = unit weight of soil,
H = height (depth) of excavation,
N = standard penetration resistance,
K_A = coefficient of active earth pressure,
d = depth to water table,
S_u = undrained shear strength,
q = surcharge load, and
K = modulus of subgrade reaction (spring constant).

ASSESSMENT OF DESIGN PROBLEMS AND ASSUMPTIONS

A number of problems must be resolved by the structural engineer in designing permanent diaphragm walls. Perhaps the fundamental problem is the fact that the stresses within the wall are continually changing during the construction process. These stresses are subject to the vagaries of both the excavation and bracing techniques used and the removal of bracing and the backfilling process. Typical movement of a braced wall installation during excavation and the resulting stresses are shown in Figure 1. Similar movements (and stresses) occur during removal of bracing and backfilling. The problem is further complicated by the fact that the designer has almost no control over these procedures. For consistent performance of structures that do not incorporate temporary components in the permanent structure, the residual stresses that arise from the construction process must be considered in the analysis.

Another major problem is the quality of the construction. Although slurry walls are acceptable in many cases, they have been known to have extremely rough and out-of-alignment surfaces as well as large sand pockets, understrength concrete, or other structural defects. Once they are built, corrective measures are not practical. The structural engineer must consider the real possibility of such defects in a design. Other problems arise—i.e., waterproofing the diaphragm wall and connecting it to the remainder of the structure to be built within the excavation. Assumptions, design procedures, and construction techniques to be used in resolving these problems are considered.

Soil-Structure Interaction

Before an assessment of soil properties or earth pressures can be made, a decision on the use of a mathematical model of soil-structure interaction to implement the basic design approach must be made. Use of such a model will affect the type of soil information needed and assumptions concerning earth pressure loading.

The state of the art of mathematical modeling of the mechanical behavior of soil masses is sufficiently advanced to give serious consideration to the use of such a soil-structure interaction model for solution of the problem of designing diaphragm walls. The complexity of the problem and the availability of finite element techniques and computer technology suggest such an approach. Wong (14) has developed one such solution by using finite element techniques. The ca-

pabilities of this solution have been extended by Jaworski (10) and also by Clough and Tsui (2). The solution must incorporate a soil constitutive model. Developing constitutive equations to represent the mechanical properties of the soil mass is the main problem in soil-structure interaction solutions. Considerable attention was devoted to the subject during the Second International Conference on Numerical Methods in Geomechanics held at the Virginia Polytechnic Institute and State University (3). Additional valuable information on the subject has been made available in an American Society for Testing and Materials (ASTM) symposium on concrete pipe and the soil-structure system (1) and by Gudehus (7).

Currently, the following deficiencies can exist in such solutions:

1. Our ability to furnish appropriate material properties and boundary conditions of the soil mass is limited compared with our ability to formulate mathematical models and solve theoretical problems.
2. Existing solutions can be unrealistically sensitive to changes in the physical parameters that define the problem.
3. Existing solutions can be plagued by gross inaccuracies because of the truncation of matrixes and round-off errors.
4. Existing solutions have given reasonable results for the distribution of earth pressure behind diaphragm walls but poor results for displacements and the corresponding stresses they produce.

It is concluded, therefore, that, although they are a powerful tool, finite element solutions are not yet practical for solving design problems of this type. Soils are extremely complicated materials, and their mechanical behavior is governed by very complex factors. Sophisticated solutions that incorporate finite element methods may not be more realistic than solutions obtained by using good engineering judgment. The results could also be grossly in error and misleading.

Soil Properties

Soil mechanics has been aptly described as an art rather than a science. This definition is inherent in the nature of soil. It is usually a heterogeneous material, sometimes artificially deposited, subjected to varying degrees of consolidation, surcharge loads, and pore-water pressure, and all of these conditions are subject to considerable variation from one point in the ground to another. Even the best available methods for determining the parameters that define soil properties give results that might vary 100 percent from actual conditions. When the variations of properties from point to point are considered, assessment of average soil properties for design purposes becomes an art and not a science. The soil mechanics engineer rightfully uses science and all the modern means of testing and analysis in evaluation. However, these results must be judiciously applied in view of the overall nature of the complex heterogeneous soil mass. The nature of the problem suggests avoiding complexity and using simple assumptions.

It is suggested that the assumptions used for soil properties by Wickham and Tiedemann (13) generally be used in designing diaphragm walls. They used an average angle of internal friction ϕ and zero for the soil cohesion c. Most soils encountered will have some cohesion, but use of an equivalent ϕ—even if c = 0 for clays—is proposed as a conservative assumption in many cases. Soil loading conditions as well as the unit soil weight γ, undrained shear strength S_u, standard penetration resistance N, and the knowledge of surcharges and the existence and levels of groundwater are to be determined from these parameters. Even if a value of c is used, the number of parameters that define the soil properties is relatively small and can be obtained from reasonably reliable and simple testing procedures.

Loading Conditions

Assumptions for earth pressure and its distribution should be consistent with those used for the parameters that define the soil properties. Field measurements of earth pressure behind braced retaining structures show considerable variation. Actual performance cannot be correlated with sophisticated assumptions, and there is little justification for their use. Earth pressure and its variation are materially affected by the method of excavation, the sequence of construction, and the installation and the possible prestressing of bracing. The engineer does not have control over or even postdesign knowledge of many of these factors.

Therefore, as in the case of soil parameters that define the properties of the soil, simplifying assumptions are warranted in establishing design earth pressures on diaphragm walls. Goldberg, Jaworski, and Gordon (5) have made a comprehensive study of earth

Figure 1. Typical movement of braced walls during stages of excavation.

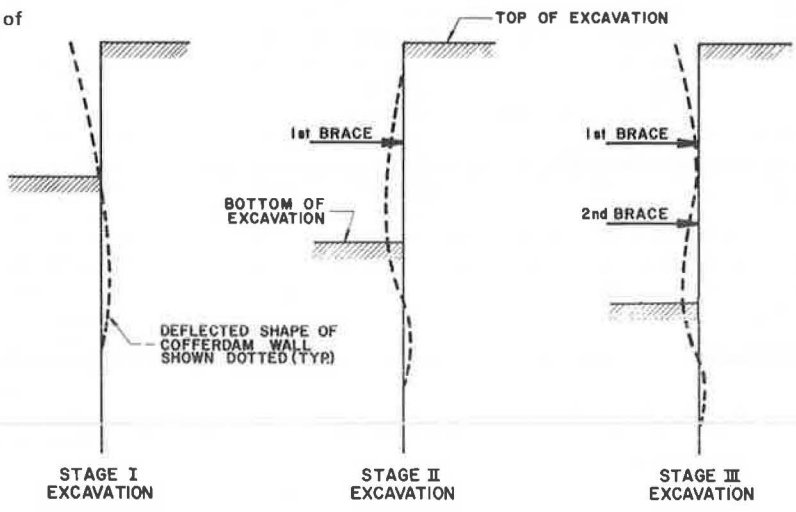

pressures on lateral support systems. Their recommendations are shown in Figure 2, where they have taken the first three cases from Terzaghi and Peck (12). These pressure diagrams were developed from empirical data for flexible walls. Goldberg, Jaworski, and Gordon (5) have shown that higher pressures develop behind stiffer diaphragm walls. However, this was a theoretical study and, at the present time, some (6), but not sufficient, empirical data are available for pressures behind braced diaphragm walls to justify any significant change from the pressure diagrams shown in Figure 2. For practical purposes, the temporary earth pressure to be used in design can be taken as a constant uniform load, as shown in Figure 3. The hydrostatic water pressure and any surcharge loads must be added to this. Prestressing of the braces is recommended as a mandatory requirement for stability considerations.

Figure 2. Design diagrams of earth pressure for internally braced, flexible walls (hydrostatic pressure not shown).

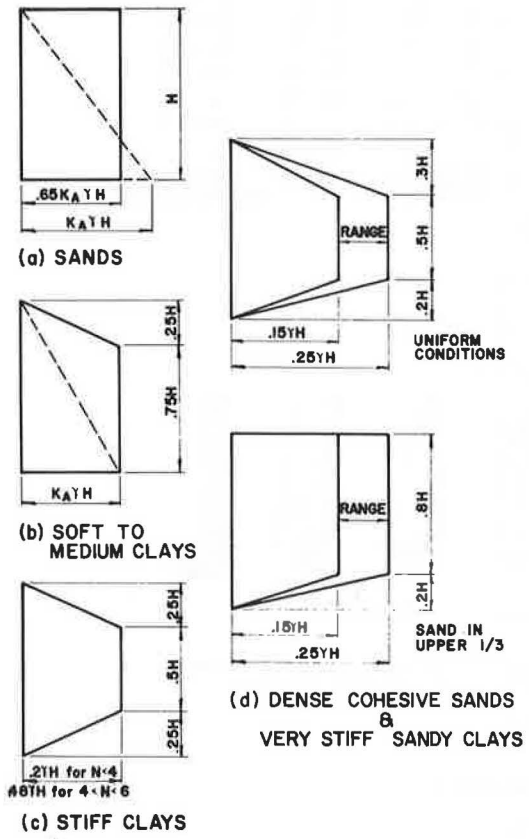

Figure 3. Loading conditions for braced wall.

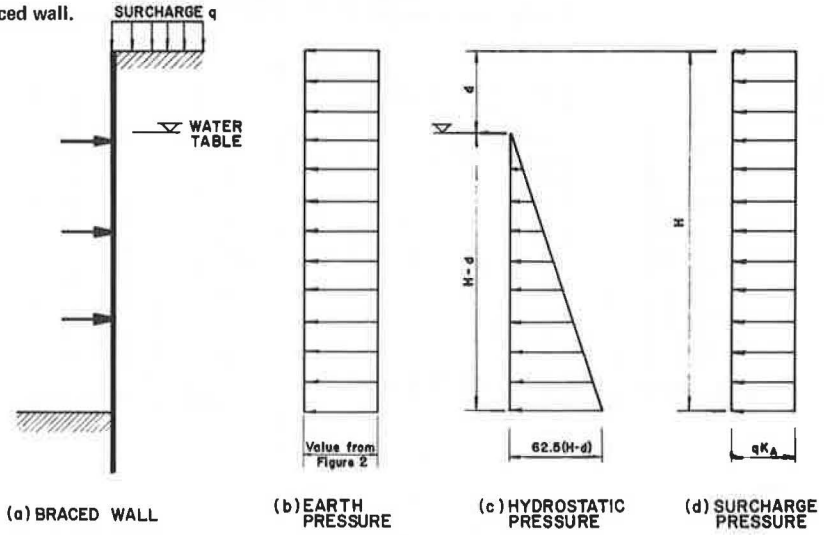

The hydrostatic water pressure and any surcharge loads must be added to this. Prestressing of the braces is recommended as a mandatory requirement for stability considerations.

Figure 3 defines the recommended loading conditions on a braced diaphragm wall. Once the wall is incorporated into the permanent structure, earth pressures change with time. For buried structures, at-rest pressures are recommended (6). There is also always the distinct possibility of unbalanced asymmetrical earth pressures on the adjacent sides of an underground structure since these pressures do not necessarily develop equally. The unbalanced load is taken by friction along the bottom of the structure. One-half at-rest pressures acting on one side, without consideration of the temporary bracing loading conditions, and full at-rest pressure action on the other side are recommended. Any change in water levels during and after construction must also be considered.

These loading conditions on the permanent structure are shown in Figure 4. Figure 4 shows that the diaphragm wall must be designed for the loads shown in Figure 3 plus the increment of at-rest pressure that results from incorporation of the wall into the permanent structure. The loads on the remainder of the permanent structure and its interaction with the diaphragm wall will also cause additional stresses in the diaphragm wall. Some continuity at the junctures must be provided, or the permanent structure will be unstable.

Additional loads on the permanent structure are the roof loads and the base reaction. To accommodate both external and internal continuity conditions, some sort of soil-structure interaction at the base is required. A finite number of individual springs that corresponds to the number of discrete elements used in the structural analysis is used. The soil modulus or stiffness of these springs is varied to obtain an overall pressure pattern consistent with observed behavior. An example of this approach is shown in Figure 5 for a station design in the Washington, D.C., subway system. The shape of the pressure diagram was established from principles of soil mechanics. The subgrade modulus was varied as shown in the figure to obtain the shapes desired.

This approach is used in Figure 6 to show the loading on the diaphragm wall before backfilling operations.

Figure 4. Loading conditions on permanent structure.

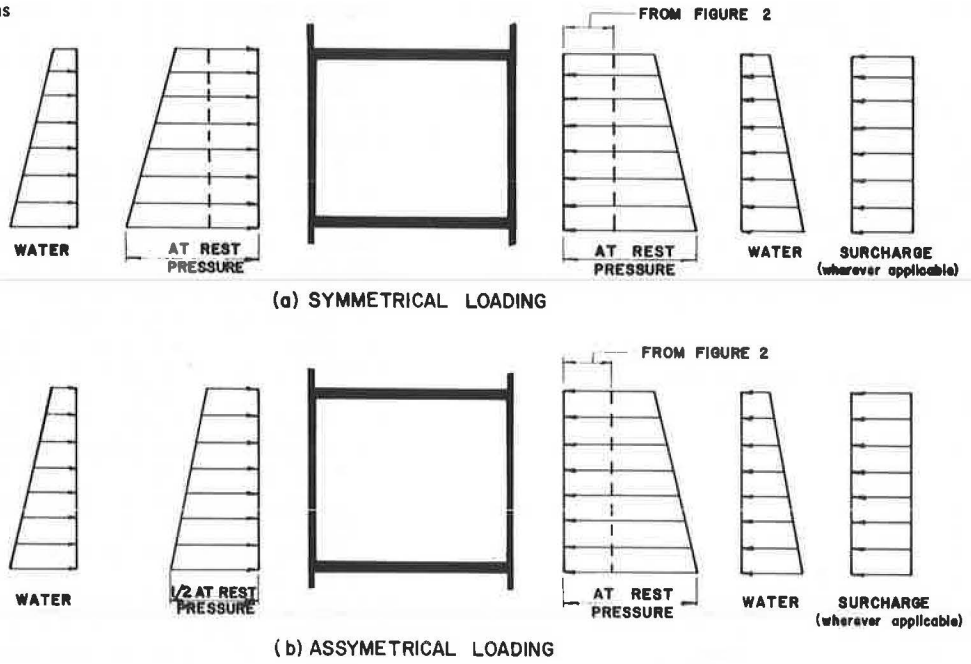

Figure 5. Station arch in Washington, D.C., subway system: long-term design loads.

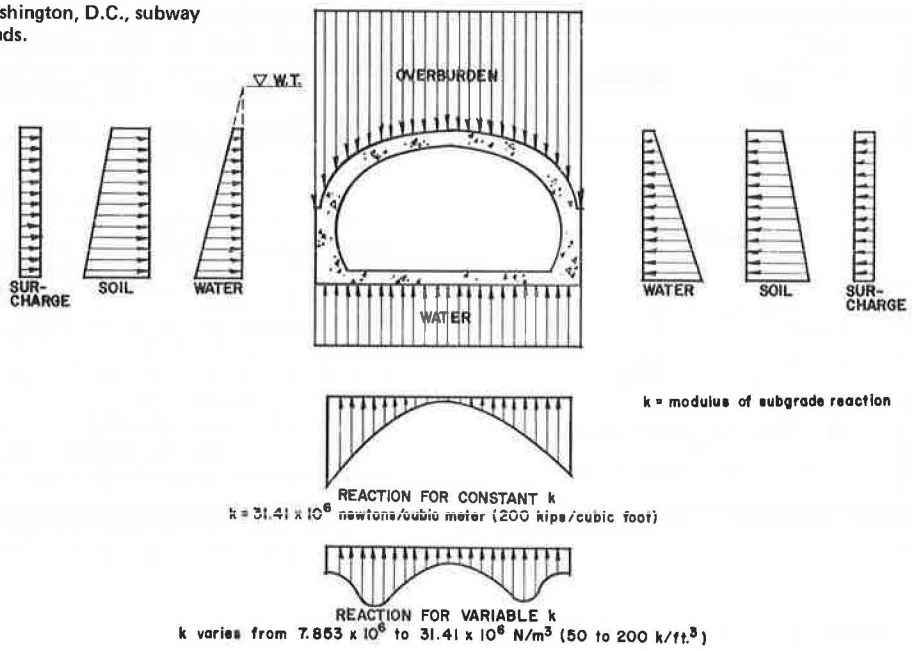

Figure 6. Diaphragm-wall loading condition before backfilling operations.

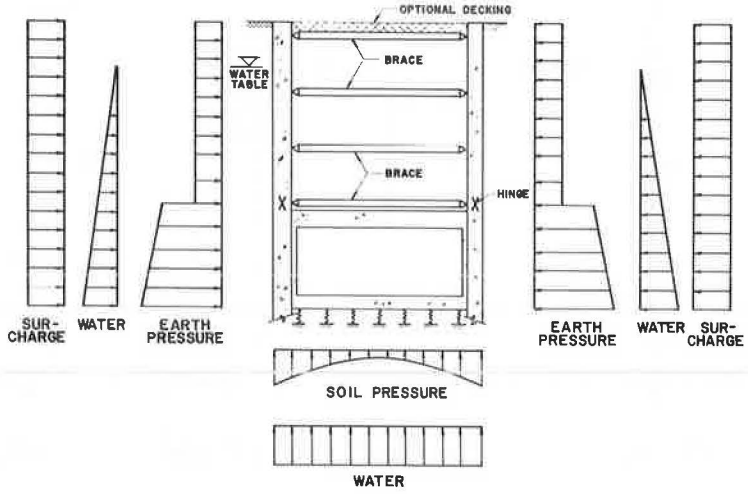

Figure 7. Final loading condition for permanent structure.

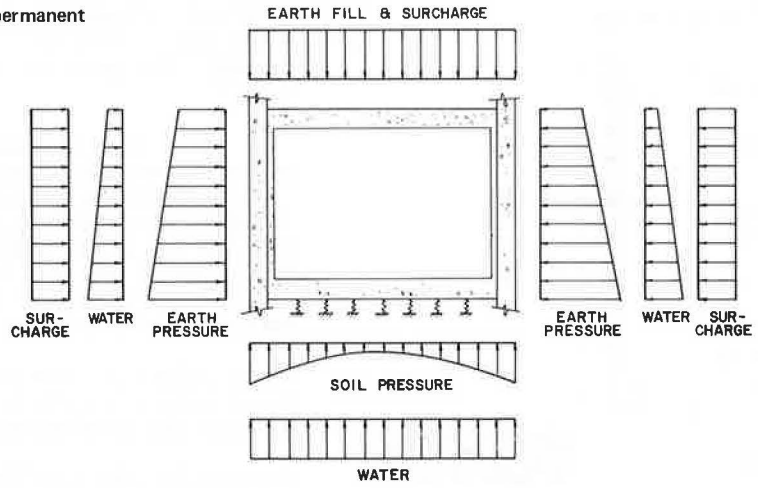

Figure 8. Effect of support movement in plastic analysis.

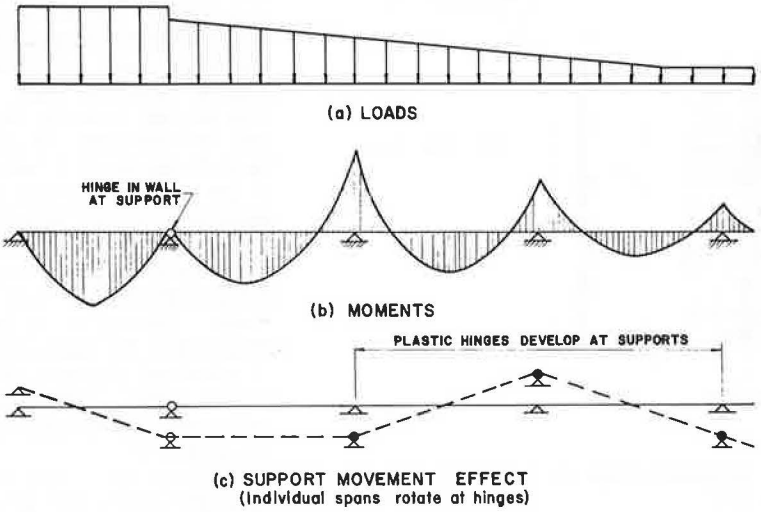

Figure 9. Detail of full hinge.

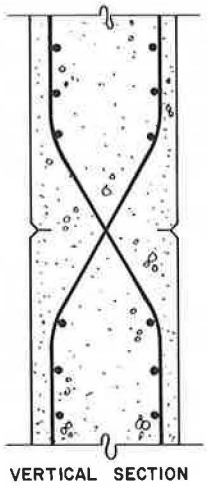

Note that the surcharge on each side of the structure can be different. Another loading condition, which is not shown, would be the asymmetrical earth-loading condition previously discussed. Active earth pressures could be used at this stage of the loading. However, because the lower portion of the diaphragm wall will eventually be subjected to at-rest pressures, these pressures are used in the design since it is questionable how long it takes for them to develop.

Finally, backfilling and removal of the bracing take place, and the final loading condition is shown in Figure 7. The asymmetrical condition and any water table changes related to the construction process or future conditions must also be investigated.

Plastic Analysis

What has been neglected so far in the synthesis of the problem is the movements and stresses that take place in the diaphragm wall as braces are prestressed, unstressed, relocated, wedged, adjusted, loosened, and finally removed. It is also one of the reasons for introduction of hinges in the diaphragm walls at the lower brace indicated in Figure 6.

The designer has only nominal control over the movements and the associated stresses that take place during the installation and removal of braces. The spacing can be specified, and other criteria, such as the amount of prestressing in the cross braces, can be prescribed. Traditionally, however, their design and installation are the prerogative of the contractor. Even if a rigidly specified procedure is mandated, field conditions usually develop in such a way as to invalidate conformity. To overcome this difficulty, plastic analysis of the bracing system is advocated. This

Figure 10. Detail of continuity requirements.

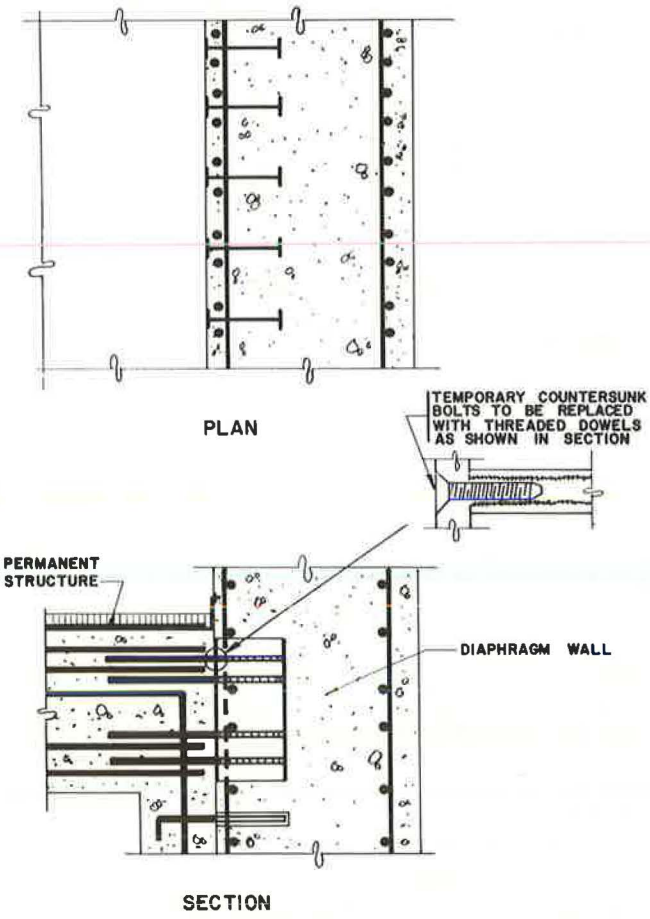

method of analysis offers the following advantages over an elastic analysis (11):

1. In-and-out movement of one or more of the supports before loading does not affect the collapse load.
2. In-and-out movement of one or more of the supports during or after loading does not affect the collapse load.
3. The presence of initial residual stresses has no influence on the collapse load.
4. The collapse load is independent of the previous history of loading.

For these reasons, the use of plastic analysis eliminates the problems introduced by support movement, whatever the cause. This principle is shown in Figure 8.

Plastic analysis and design are not currently accepted by U.S. codes and specifications. However, this approach is now under study for braced structures that include the diaphragm wall. Plastic analysis and design are currently acceptable in many European standards including those of the British Standards Institute (8). Furlong (4) presents a plastic design methodology based on limit design concepts for reinforced concrete that can be used in proportioning the diaphragm wall. The method uses limit values for coefficients of maximum moments in simple beams and is compatible with concrete design in the United States. The detailed procedure suggested by Furlong is not repeated here.

Although the diaphragm wall is designed so that plastic hinges can form at all points of support by the braces, it is suggested that an actual full hinge be detailed in the diaphragm walls at points of support of the lowest brace. This hinge is designed to transmit zero moment. The purpose of this full-hinge design is twofold:

1. It will prevent transmittal of wall diaphragm moments into the permanent structure.
2. It facilitates disconnecting the diaphragm wall, which is not part of the permanent structure, from the permanent structure before backfilling. This permits the diaphragm wall to be (a) left in place after it is disconnected or (b) removed without any effect on the permanent structure.

The use of a precast concrete diaphragm wall, which is discussed below, facilitates detailing these full hinges. A method that provides this hinge is shown in Figure 9.

Concrete Durability and Quality

The problem of concrete durability and quality, including geometrical alignment, can be solved by using precast concrete diaphragm walls. Precast concrete segments placed in a slurry trench to construct a diaphragm-wall system have been used successfully in the past (9, 13). The precast concrete diaphragm wall can vary in size and configuration. It includes tongue-and-groove continuous panels or T-beam and panel combinations. Some of the systems are patented. The procedure of wall excavation is similar to that for the cast-in-place slurry wall system. The grout slurry is an important component of the system since the precast concrete units do not completely fill the trench as do cast-in-place slurry walls. The setting of the grout, which is equal in strength to the surrounding soil, ensures elimination of voids and filling of all irregularities in the trench, thus stabilizing the position of the precast concrete units and also minimizing potential settlement of the adjacent soil.

Besides being assured of satisfactory and acceptable concrete quality and wall alignment, the use of a precast concrete diaphragm wall permits accurate installation of dowels, keys, recesses, bearing plates, and other details for the required continuity connections to the permanent structure built within the excavation. The full-hinge detail suggested in the previous section can also be satisfactorily detailed. The various aspects of precast concrete diaphragm walls are discussed in detail by Wickham and Tiedemann (13). Several applications have been reported in detail (9).

Watertightness

Use of a precast concrete diaphragm wall also facilitates the problem of obtaining a watertight wall. Bentonite waterproofing systems have proved to be effective if properly installed. In the precast concrete diaphragm wall system, the bentonite slurry used during excavation of the trench and remaining on both sides of the panels after the panels have been installed can be displaced and replaced by a combination portland cement-bentonite grout that eventually sets up to solidify the excavation. This grout can be satisfactorily designed to provide the appropriate watertightness on the rear face where any thickness can be prescribed. The grout on the front face is held to a minimum and can be subsequently removed if the precast concrete panels are pretreated with an appropriate bond breaker. Patented grouts are available for this use. Other acceptable formulations can also be derived if desired.

Continuity Requirements

As stated before, the diaphragm wall must be made to act continuously with the cast-in-place remainder of the permanent underground structure. Full continuity is neither needed nor necessarily desired. Use of precast concrete panels for the diaphragm wall also facilitates providing for these continuity details. One such detail is shown in Figure 10. The pertinent features of this detail are the following:

1. Use of an embedded wide-flange structural steel section permits maximum bond development and distribution of stress concentrations with the reinforced concrete. It also permits a flush surface that does not interfere with forming or with subsequent erection.
2. The embedded steel units can be staggered between vertical reinforcing steel. This facilitates fabrication of the precast panel.
3. The flush steel surface permits alternate welded connection details if the threaded inserts for the horizontal dowel connections shown are not desired.
4. Flexible flashing is continuously attached to the continuous steel T-insert in the diaphragm wall and lapped with membrane waterproofing on the roof to provide a watertight joint.

A similar detail is required at the concrete-box base slab where the degree of continuity will be much more than that required at the concrete-box roof slab. Development of full continuity at both points is possible if desired.

SUMMARY OF DESIGN SYNTHESIS

Based on the foregoing reasoning and related discussion, the suggested design synthesis for diaphragm walls to be incorporated into permanent underground structures may be summarized as follows:

1. Do not use an overall soil-structure model for design.
2. Determine average soil properties from basic soil parameters obtained from simple tests.
3. Use a constant, uniform design earth pressure loading on the braced diaphragm wall before the construction of the permanent underground structure. Add hydrostatic and surcharge loads when they are applicable.
4. Use plastic analysis and design for proportioning the diaphragm wall. Design the wall with a full hinge detailed at the lowest brace just above the permanent underground structure. Provide embedded flush inserts for future partial continuity connections and waterproofing details to the permanent underground structure.
5. Specify construction of the diaphragm wall by use of precast concrete panels and the like in a slurry-constructed trench in which excess slurry is displaced by a cement-bentonite grout for waterproofing requirements. Specify prestressing of the braces of the diaphragm walls.
6. After construction of the permanent underground structure, design this structure for the added increment of at-rest earth pressures by considering both the symmetrical and the asymmetrical cases. In this analysis, consider the structure to be supported on individual springs of varying magnitudes as required to simulate desired soil-bearing pressure distributions.
7. Specify construction of the required continuity connection and waterproofing details between the diaphragm wall and the permanent underground structure. Specify full separation of the diaphragm walls at the point of the full hinge before backfilling and removal of bracing.
8. Design the permanent underground structure for the additional backfill and overlying surcharge loads. Consider both symmetrical and asymmetrical cases, groundwater variations, and surcharges where applicable. Consider the structure supported on individual springs to simulate desired bearing pressure.

Under proper conditions—usually adjacent to heavy structures that would otherwise require substantial underpinning—braced diaphragm walls incorporated into the permanent structure can provide an economical solution for underground construction.

REFERENCES

1. M. Bealey and J. D. Lemons, eds. Concrete Pipe and the Soil-Structure System. Symposium presented at 79th Annual Meeting, ASTM, Chicago, June 27-July 2, 1976, ASTM Technical Publ. 630, Sept. 1977, 136 pp.
2. G. S. Clough and Y. Tsui. Performance of Tied-Back Walls in Clay. Journal of Geotechnical Engineering Division, Proc., ASCE, Vol. 100, No. GT 12, Paper 11028, Dec. 1974, pp. 1259-1273.
3. C. D. Desai, ed. Numerical Methods in Geomechanics. ASCE, New York, Vols. 1, 2, and 3, June 1976.
4. R. W. Furlong. Plastic Design for Reinforced Concrete Frames. ASCE National Structural Engineering Meeting, Cincinnati, Meeting Preprint 2214, April 22-26, 1974, 13 pp.
5. D. T. Goldberg, W. E. Jaworski, and M. D. Gordon. Lateral Support Systems and Underpinning: Volume 2—Design Fundamentals. Offices of Research and Development, Federal Highway Administration, Rept. FHWA-RD-76-129, April 1976; NTIS, Springfield, VA, PB 257 211.
6. J. P. Gould. Lateral Pressures on Rigid Permanent Structures. Specialty Conference on Lateral Stresses in Ground and Design of Earth Retaining Structures, Soil Mechanics and Foundations Division, ASCE, June 22-24, 1970, pp. 219-269.
7. H. Gudehus, ed. Finite Elements in Geomechanics. Wiley, New York, 1977, 573 pp.
8. B. P. Hughes. Limit State Theory for Reinforced Concrete Design. Van Nostrand, New York, 2nd Ed., 1976, 697 pp.
9. Diaphragm Walls and Anchorages. Proc., Institute of Civil Engineers Conference, London, Sept. 18-20, 1974, 223 pp.
10. W. E. Jaworski. An Evaluation of the Performance of a Braced Excavation. MIT, Cambridge, June 1973.
11. B. G. Neal. The Plastic Methods of Structural Analysis. Chapman and Hall, London, 1965, 358 pp.
12. K. Terzaghi and R. B. Peck. Soil Mechanics in Engineering Practice. Wiley, New York, 1968.
13. G. E. Wickham and H. R. Tiedemann. Cut-and-Cover Tunneling: Volume 1—Construction Methods, Design, and Activity Variations. Offices of Research and Development, Federal Highway Administration, Rept. FHWA-RD-76-28, May 1976; NTIS, Springfield, VA, PB 257 014.
14. I. H. Wong. Analysis of Braced Excavations. MIT, Cambridge, ScD thesis, 1971.

Theory of Roof Bolting

Donald J. Dodds, Foundation Sciences, Inc.,
Portland, Oregon

There is currently an unfulfilled need in the field of rock mechanics for a rational, easily used system of rock bolt design. During the late 1950s and early 1960s, Panek and Lang performed independent studies on the nature of rock bolt behavior. Panek, working with bolt action in flat, laminated mine roof strata, attributed support to both suspension and friction and concluded that reinforcement by friction is a complex function of mine geometry, bolt spacing, and load. Lang, working with bolted gravel beams, developed essentially the same conclusions and, in effect, generalized Panek's work. By taking these two theories a step further, it is shown that rock support is a function of the rock bolt's power to enforce mechanical continuity on the rock. By using equations from two-hinged arch theory, it is possible to relate load directly to beam strength with the parameters of conventional structural analysis—load, strength, and beam geometry. Tables can thus be prepared that compare beam thicknesses and an offset dimension with span length. An example of such a table is included in the paper.

Most determinations of rock bolt length are made by some old timer in the field squinting at the exposed rock, spitting, and saying, "Twelve feet ought to do it" and "Put one there and there." This has given way a little, under pressure from modern rock mechanics, to the more sophisticated and expensive method of running a few tests on the depth of the field of influence around the opening (a rather nebulous term) combined with at least 48 h of central processor time on a finite element model before anybody spits and says 3.6 m (12 ft) ought to do it. However, rock mechanics, having progressed far enough to be able to convince people of the need for these expensive tests, has the responsibility now to produce a rational, easily used method by which these data can produce a specific length and spacing of rock bolt. The intention of this paper is to provide modifications to current theory that it is hoped will move rock bolt design toward this end.

CURRENT THEORIES OF ROOF BOLTING

Many important studies have been performed by the U.S. Bureau of Mines, particularly the work of Panek on the analysis of roof support (1, 2, 3, 4, 5). He considered bolt action in flat, laminated strata commonly found in the roofs of many mines. Panek attributes support to two mechanisms: suspension and friction.

The suspension effect "refers to the transfer of part of the weight of the weaker or thinner strata to one or more thick strata, which occurs when strata with differing tendencies to deflect are constrained to have equal deflection" (5). Suspension effects are heavily dependent on the geometry and mechanical properties of the bolted section.

The strengthening is then caused by the tying of the thicker, thereby stronger, beds to the thinner, weaker beds—the gain in strength being proportional to the cube of the bed thickness. During these analyses, no strengthening was allowed for any partial bonding between beds that would produce a composite beam effect. This was handled under the mechanism of friction.

The friction effect "refers to reduction of bending in a stratified roof due to clamping action of tensioned bolts, which compress the strata, thereby creating frictional resistance to displacement along planes of stratification" (5).

Panek concluded from essentially empirical data that reinforcement by friction is a complex function of mine geometry, bolt spacing, and bolt load. The latter is usually taken to be the maximum force the bolt can sustain over the design life of the bolt. Panek combined these effects into the concept of a reinforcement factor that is defined as follows:

$$RF = \text{maximum bending stress, unbolted roof} \div \text{maximum bending stress, bolted roof} \quad (1)$$

To simplify the computations necessary to design a support system, Panek prepared the chart shown in Figure 1 (since the chart was prepared in U.S. customary units, no SI equivalents are given).

In practice, using the design method requires knowledge of the number of beds to be bolted, their thicknesses, and their moduli to arrive at any strength value better than an educated guess. For this reason, the design method was not well received by the industry.

Concurrently with Panek, Lang was also conducting several studies of bolt behavior (6, 7, 8). The emphasis was on heavily fractured ground rather than laminated mine roofs, and an extensive analysis of bolting patterns across various types of joints was presented. Particularly important, however, for the understanding of bolt behavior was a series of photoelastic studies that determined the effects of bolt spacing and length. It was found that bolts spaced closely enough produced a zone of uniform compression within the back and were much more effective at supporting the roof. The thickness of the beam of compressed rock was approximately the bolt length minus the spacing.

By summarizing these two theories, it can be seen that Panek's theory is a special case of Lang's more general theme, and that support depends on the following factors: interlayer movements (continuity) and suspension, end fixity of the beam, end restraint, and end shear. The most important of these seems to be the continuity or interlayer movement. The enforcement of continuity, or prevention of interlayer movement, can be analyzed by looking at interlayer stresses. The most apparent stress is the direct stress applied by the bolt to the rock beam. This stress would produce an increase in normal force that would translate into a frictional force along the bedding. The stress F, mobilized to prevent interjoint movements in this situation, is then

$$F = P \tan \phi \quad (2)$$

where P is the normal stress and ϕ is the friction angle. Though this approach is commonly used, the additional strength supplied in a real case is quite low. Since the layer movement is over the entire cross section of the beam, the bolt load should be transferred into a stress and frictional force should be a frictional stress. A 1.2- by 1.2-m (4- by 4-ft) pattern and 9100 kg (20 000 lb) of bolt load yield a normal load increase of approximately 89 kPa (13 lbf/in^2). This increase in normal force will add only 89 to 103 kPa (13 to 15 lbf/in^2) increased friction strength at best to enforce continuity. The actual amount, of course, depends on the value of the tangent of friction along the laminated surfaces and could be much less.

Analysis of a fixed-end beam 5.5 m (18 ft) long, 1.2 m (4 ft) wide, and 1.8 m (6 ft) high loaded uniformly at 689 kPa (100 lbf/in^2) yields a maximum horizontal shear

stress near the rib of 1552 kPa (225 lbf/in^2) and an extreme fiber stress of 2965.5 kPa (430 lbf/in^2) at the midspan of the beam. Clearly, the resistance of 89 kPa (13 lbf/in^2) caused by the increase in friction attributable to roof bolting is of little value in overcoming these forces in maintaining continuity. Roof bolts, however, are a proven method of support. Another mechanism, then, must be invoked to explain their action.

It is possible that this mechanism could be attributed to the interlocking of beds along their contacts. Einstein, Bauhn, and Mirschfeld (9) performed theoretical and laboratory studies on friction in jointed rock masses and reported, "It is conceivable that ... on a microscopic scale and for rough surfaces, interlocking will be the dominant characteristic (governing friction)." Normal rock found in cavern roofs rarely presents the smooth planar laminations used in model studies. Even in horizontally laminated roofs, the material encountered in practice tends to separate along weak, nearly horizontal bedding planes until (a) a weak vertical flaw is encountered or (b) bedding plane A-A becomes stronger than bedding plane B-B, and the separation moves to the weaker bed. The result is a series of nearly parallel flat surfaces with short, steep connections. A typical lamination interface may look like that shown in Figure 2.

The strength of this laminated beam depends on the lack of relative motion between the laminations. In order for relative movement to take place between two rock units in contact along an interlocking surface,

1. The shear stress on the plane A-A or B-B (Figure 2), whichever is stronger, must be overcome;
2. The tensile strength in the rock on vertical plane C-C (Figure 2) between the two irregularities must be overcome; or
3. The projecting portions of each unit must ride up and over one another.

In the average rock, shear strength and tensile strength are of the same order of magnitude as the shear and fiber stresses calculated above, i.e., 1379 to 3448 kPa (200 to 500 lbf/in^2). However, the normal sagging associated with an opening provides assistance to the mechanism of unlocking. Opening of joints and bedding surfaces by gravity allows the laminations to move relative to one another and act as N independent beams with a resulting loss in strength by a factor of N. The rock bolts oppose this action and mechanically enforce continuity on the roof beam.

The amount of force required to open the bedding surface depends on the geometry of the interlocking projects. Einstein, Bauhn, and Mirschfeld found that "In ... gypsum models with a single joint inclined at 30° to the major principal stress, failure occurs by sliding along the joint for all applied confining stresses between 0 and 1500 psi. In the models with a joint inclination of 60°, failure occurs only by fracture through intact material" (9). In the above condition, the joint inclination is almost entirely above 60°; most are nearly vertical. Therefore, it would appear that, if dilation can be prevented, the full shear strength of the rock can be mobilized along the nonsheared joint surfaces.

As shown in Figure 3, the tangential stress f along the joint caused by the lateral stress τ, which tends to cause overriding, is

$$f = \tau \sin \theta \qquad (3)$$

The tangential strength F along the joint caused by the bolting required to prevent overriding is

$$F = \sigma \sin \theta \qquad (4)$$

Under normal bolting practices, where σ = 103 kPa (15 lbf/in^2) and τ = 3103 kPa (450 lbf/in^2), to obtain a balance between these two stresses would require that the controlling joints be nearly vertical or one or two degrees from vertical. It should also be noted that this is an inverse chain effect in that the strongest link must be overcome before general failure occurs.

Figure 1. Roof-bolt design chart for friction effect.

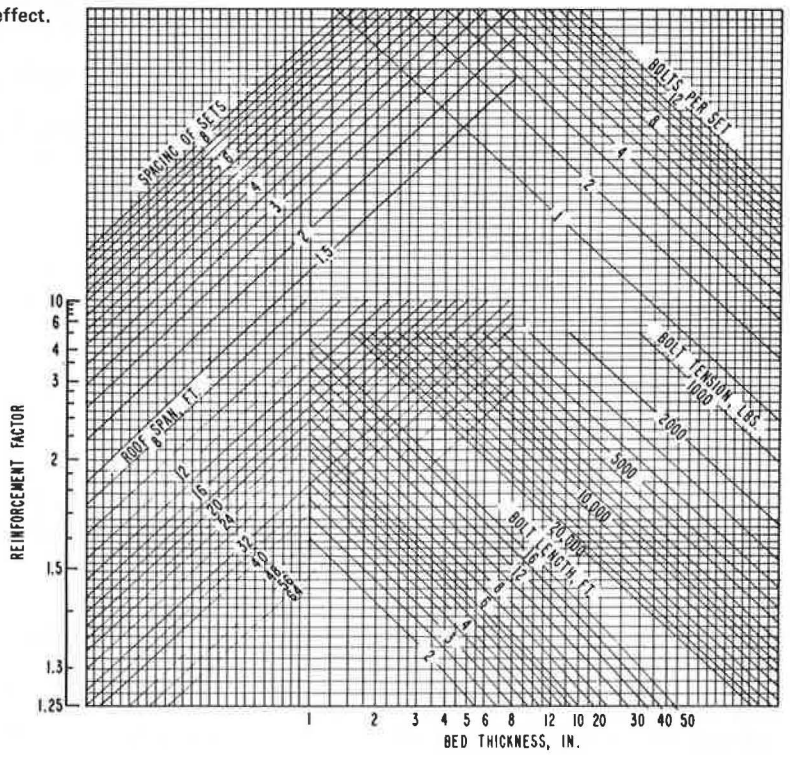

Figure 2. Typical laminated rock formation showing probable bedding point.

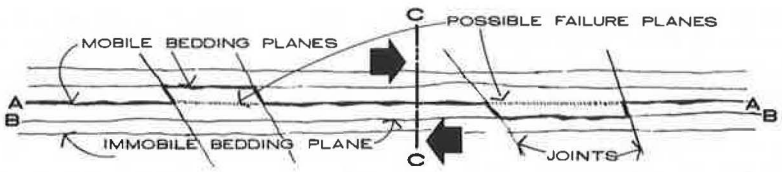

Figure 3. Stresses along joint asperity.

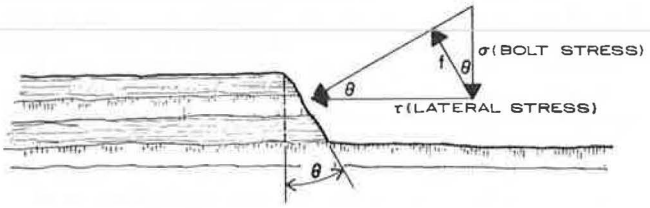

Figure 4. Stress beam produced by pattern bolting.

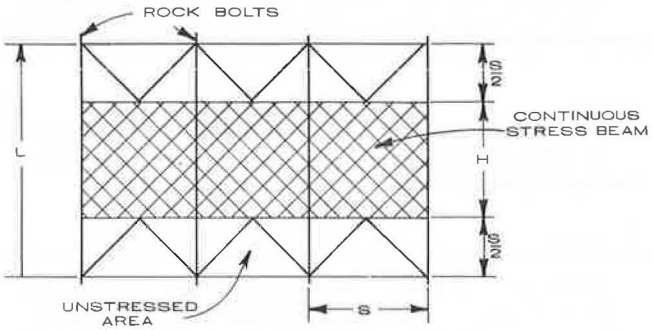

Figure 5. General stress condition in fixed-end, two-hinged arch.

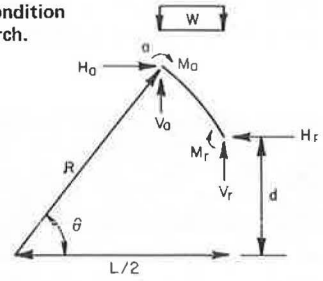

The existence of these joints is based on direct observations; that they act in this manner is only theorized. This hypothesis could explain, however, that the obvious mechanical advantages gained by roof bolting are attributed to restriction of movement along joints or by providing continuity through mechanical means. Not much is known about this mechanism—in particular, how much tension is required to produce continuity—but the study of rock bolts made by Lang for other purposes was of sufficient detail to shed some light on how bolt tension may affect beam strength.

The data were obtained by loading a rock-bolted 1.2-m (4-ft) cube of crushed rock. The cube was supported laterally and instrumented to measure deflection and lateral pressure. This experiment showed that competent structures could be formed from completely incoherent, suitably bolted masses of gravel and that the mass exhibited elastic and plastic (strain-hardening) properties similar to those of intact rock masses. By using the data gathered in these tests, it can be further shown that an increase in bolt tension, which increases bolt-induced continuity, decreases beam deflection (Figure 4).

Lang also concluded elsewhere in his report that beam strength remains relatively constant until a threshold level is reached, and then failure occurs rapidly.

These two findings support the hypothesis that, regardless of the orientation of joints, cracks, or bedding planes, as long as the rock is laterally confined the rock bolts support by enforcing mechanical continuity and allow the rock to support itself with its own inherent properties. The beam produced by the interference of the individual bolt stress patterns is shown in Figure 4.

If this be the case, neglecting all the rock except for the cross-hatched area, a simple, conservative, conventional analysis can be performed on the remaining rectangular section by assuming that the material is held continuous by the rock bolts throughout this zone. Of the many conventional methods of analysis available, the one that seems to be most adaptable to the actual situation is the two-hinged analysis. If this beam is assumed to be a two-hinged arch separate from the surrounding rock material and is assumed to be loaded with a uniform vertical loading, the general stress condition in this arch stress beam would be as shown in Figure 5. Real loading conditions other than this assumption generally produce errors on the side of safety.

$$H_R = K_1 WL = \{ [\int(Mmds/EI) + \int(Vvds/AG) + \int(Nn/AE)ds] \div [\int(M^2 ds/EI) + \int(v^2 ds/AG) + \int(n^2 ds/AE)] \} \quad (5)$$

where

$M = (W/2)[(L^2/4) - R^2 \cos^2 \theta]$,
$m = 1(R \sin \theta - d)$,
$ds = rd\theta$,
$V = (wl/2) \cos^2 \theta$,
$v = \cos \theta$,
$N = (wl/2) \cos \theta \sin \theta$,
$n = -\sin \theta$, and
$G = \frac{2}{5} E$.

This produces

$$K_1 = (WL/2A)\{ [L^2/4t^2(3NJ^2 - 2)(\pi/2 \tan^{-1} N) - 3I^2 + 4] + 6/J^2 \} \div \{ [L^2/4t^2(2N^2 + J^2)(\pi/2 - \tan^{-1} N) - 3N] + 7/2(\pi/2 - \tan^{-1} N) - 3/2N \} \quad (6)$$

where

$N = 2d/L$ and
$J = 2t/L$.

These values will allow expressions to be written for beam stress by using the familiar equation

$$a = (M_a C/I) \pm (N_a/A) \quad (7)$$

The sum of the moments around a produces

$$M_a = V_r(L/2 - R \cos \theta) - W/2(L/2 - R \cos \theta)^2 - H_r(R \sin \theta - d) - M_r \quad (8)$$

Substituting $V_r = WL/2$ and reducing lead to

Figure 6. Relation between beam strength and in situ load.

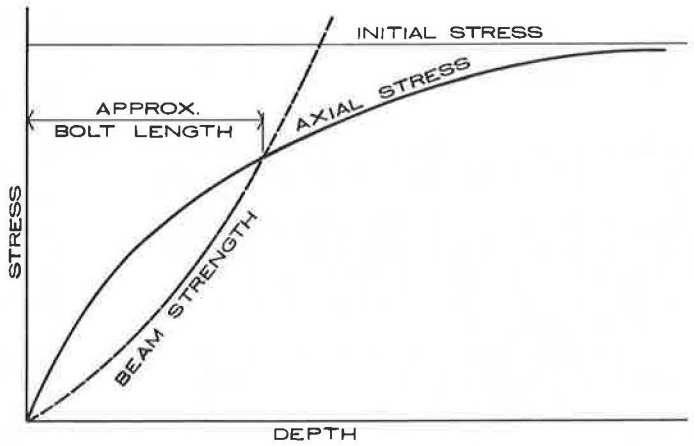

$$M_a = W/2(L^2/4 - R^2\cos^2\theta) - H_r(R\sin\theta - d) - M_r \quad (9)$$

If we let $H_r = K_1WL$ and $M_r = K_2WL^2$, then the equation reduces to

$$M_a = W/2(L^2/4 - R^2\cos^2\theta) - 2K_1WL(R\sin\theta - d) - 2K_2WL^2 \quad (10)$$

The normal and shear stresses at point a can be written

$$N_a = H_a\sin\theta - V\cos\theta \quad (11)$$

Substituting $H_a = H_r = K_1WL$ and $V_a = V_r - W_2L)(1 - \cos\theta)$ produces

$$N_a = K_1WL\sin\theta - W(L/2 - R\cos\theta)\cos\theta + WL/2\cos\theta \quad (12)$$

If, for the purpose of illustration, it is assumed that end rotation is allowed (hinged arch), K_2 is equal to zero and K_1 can be found by assuming the controlling condition to be at midspan where θ equals 90°:

$$\sigma_{90} = 3(WL^2/4t^2)K_3K_1(WL/t) \quad (13)$$

where

$$K_2 = 1 - 4K_1(1 + N^2)^{1/2} - N \text{ and}$$
$$\sigma_{90} = 3(K_3W/J^2) \pm 2K_1(W/J)$$
$$= W(3K_3 \pm 2K_1J)/J^2$$
$$= K_4W.$$

This equation then relates load directly to beam strength not only in a simple manner but in a manner commonly used by structural engineers. The upper boundary on the beam load would be a vertically applied uniform load equal in magnitude to the in situ stress level. However, this is, in many instances, ultraconservative because the in situ load is really the radial load, which varies from zero at the surface to the in situ level, a depth according to the following relation:

$$\sigma_{90} = \tfrac{1}{2}S_v[1 - (a^2/r^2)] + \tfrac{1}{2}S_v[1 - 4(a^2/r^2) + 3(a^4/r^4)] \quad (14)$$

where

S_v = vertical applied stress,
a = L/2, and
r = distance from hole center.

If this load were plotted with depth, as shown in Figure 6, it would commence at zero and increase concavely downward; if strength plus depth were plotted on the same axis, it would commence at zero and increase concavely upward. The point at which the curves intersect is the design depth. These concepts may be used to modify the load portion of the K_4 value. Tables can then be prepared based on the two dimensionless ratios of beam thickness to span length (t/L) and offset dimension d shown in Figure 6 over the span length (d/L). The table below was prepared in this way:

	d/L				
t/L	0.00	0.30	0.60	0.90	1.20
0.10	0.10	2.15	2.34	2.44	2.71
0.11	2.10	2.21	2.28	2.38	2.67
0.12	2.02	2.12	2.18	2.29	2.59
0.13	1.92	2.01	2.07	2.17	2.49
0.14	1.81	1.90	1.95	2.05	2.37
0.15	1.70	1.78	1.82	1.92	2.24
0.16	1.59	1.66	1.70	1.79	2.12
0.17	1.49	1.35	1.59	1.67	1.99
0.18	1.39	1.44	1.47	1.55	1.87
0.19	1.29	1.34	1.37	1.44	1.75
0.20	1.20	1.24	1.27	1.34	1.64
0.21	1.11	1.15	1.17	1.24	1.53
0.22	1.03	1.07	1.09	1.15	1.43
0.23	0.95	0.99	1.01	1.07	1.33
0.24	0.88	0.91	0.93	0.99	1.24
0.25	0.82	0.84	0.86	0.91	1.16
0.26	0.75	0.78	0.79	0.84	1.07
0.27	0.69	0.71	0.73	0.78	1.00
0.28	0.64	0.66	0.67	0.72	0.92
0.29	0.58	0.60	0.61	0.66	0.85
0.30	0.53	0.55	0.56	0.60	0.78
0.31	0.48	0.50	0.51	0.55	0.72
0.32	0.44	0.45	0.46	0.50	0.65

This form of table is simple and easy to use. If the geometry of the openings is known, then the table is entered in the column with the appropriate d/L ratio, searched for the correct beam strength to load ratio, and exited with the proper beam thickness to span ratio. For example, a beam with a d/L ratio of zero, a beam strength of 4138 kPa (600 lbf/in^2), and an undisturbed stress level of 3448 kPa (500 lbf/in^2) would produce a beam thickness ratio of approximately 0.20. If the cavern span were 15.2 m (50 ft), it would require a beam thickness of 3 m (10 ft), or a 4.3-m (14-ft) bolt on a 1.2-m (4-ft) spacing would provide adequate protection.

The value of this method lives or dies on what the rock beam strength really is under bending stresses. I believe that, if research were done in this area, significant advancements could be made in placing rock-bolt design on a firm analytical footing. The 4138-kPa (600-lbf/in^2) bending strength seems to be a conservative number. If research did indeed show this to be the case, current rock bolt practice is specifying bolt lengths that are grossly overdesigned. This would explain the lack of failures in properly placed and grouted, tensioned rock bolt systems.

CONCLUSIONS

There appear to be four major conclusions in this research:

1. Roof support by rock bolting is a function of the power of the rock bolts to enforce mechanical continuity on the rock.
2. A study should be made to determine the effect of bolt tension on beam stability and the threshold tension required to produce continuity and to identify any other important variable in predicting levels of mechanically induced continuity.
3. A study should be made to determine realistic values of rock beam strength to enable the use of K_4 tables and reduce the apparently high rock-bolt safety factors.
4. Laboratory or field tests should be developed to predict rock beam strength.

REFERENCES

1. L. A. Panek. Analysis of Roof Bolting Systems Based on Model Studies. Mining Engineering, Vol. 7, No. 10, 1955, pp. 954-957.
2. L. A. Panek. Anchorage Characteristics of Bolts. Mining Congress Journal, Vol. 43, No. 11, Nov. 1957, pp. 62-64.
3. L. A. Panek. The Combined Effects of Friction and Suspension in Bolting Bedded Mine Roof. U.S. Bureau of Mines, Rept., Invoice 6139, 1962.
4. L. A. Panek. The Effects of Suspension in Bolting Bedded Mine Roof. U.S. Bureau of Mines, Rept., Invoice 6138, 1962.
5. L. A. Panek. Design for Bolting Stratified Roof. Trans., Society of Manufacturing Engineers and American Institute of Mining, Metallurgical and Petroleum Engineers, Vol. 229, 1964.
6. T. A. Lang. Underground Experience in the Snowy Mountains—Australia. Second Protective Construction Symposium, Rand Corp., Santa Monica, CA, 1959.
7. T. A. Lang. Theory and Practice of Rock Bolting. Trans., American Institute of Mining, Metallurgical and Petroleum Engineers, Vol. 220, 1961, pp. 333-348.
8. T. A. Lang. Notes on Rock Mechanics and Engineering for Rock Construction. Univ. of California, Berkeley, class notes, 1962-1963.
9. H. Einstein, R. Bauhn, and R. Mirschfeld. Mechanics of Jointed Rock. Office of High Speed Ground Transportation, U.S. Department of Transportation, 1970.